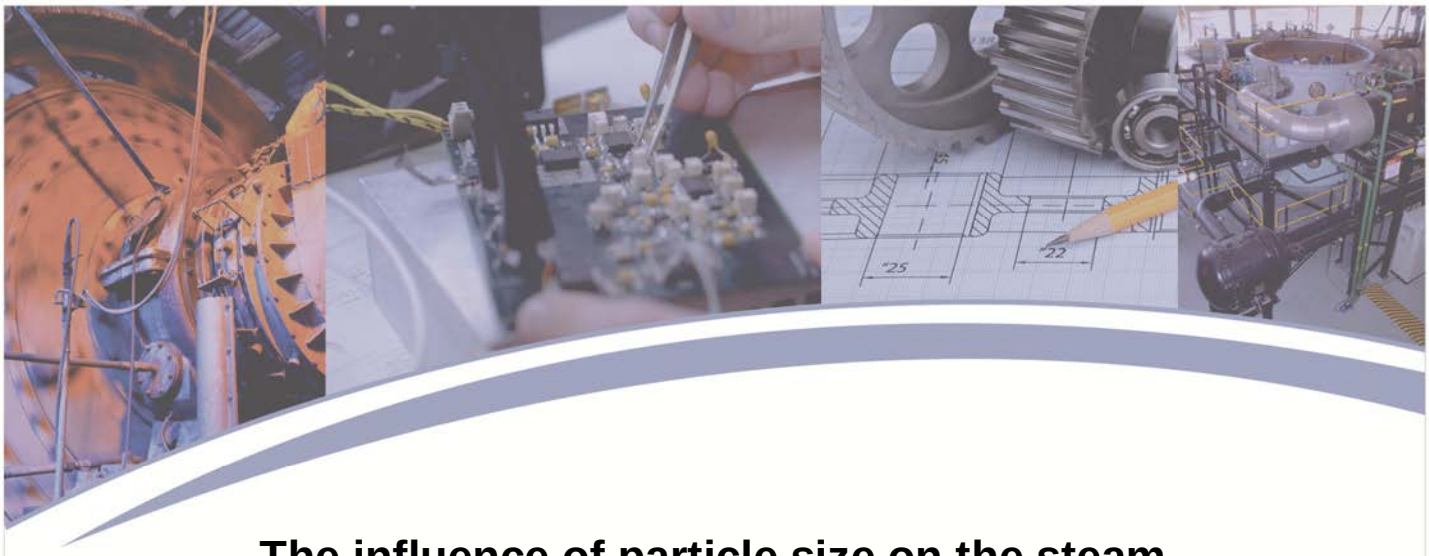

The influence of particle size on the steam gasification kinetics of coal

School of Chemical and Minerals Engineering

Gert Hendrik Coetzee

Dissertation submitted in fulfilment of the requirements for the degree Masters in Chemical Engineering at the Potchefstroom campus of the North-West University, South Africa

Supervisor: Prof. H.W.J.P. Neomagus
Co-supervisors: Prof. J.R. Bunt, Prof. R.C. Everson

November 2011

NORTH-WEST UNIVERSITY
YUNIBESITI YA BOKONE-BOPHIRIMA
NOORDWES-UNIVERSITEIT

Declaration

I, Gert Hendrik Coetzee, hereby declare that the dissertation entitled: **"The influence of particle size on the steam gasification kinetics of coal"**, submitted in fulfilment of the requirements for a Masters degree in Chemical Engineering (M. Eng.) at the North-West University, is my own work, unless specified otherwise, and that this dissertation has not been submitted for an equivalent or higher qualification at any other tertiary institution.

Signed at Potchefstroom, on the ..... day of ....., 2011.

_____

Gert Hendrik Coetzee

Acknowledgement

I would like to thank and acknowlede the following people, without whom I would not have been able to complete this dissertation.

- I would firstly like to thank my Heavenly Father for the guidance, support and wisdom He has given on me during this investigation.
- A special thanks to Professor Hein Neomagus, Professor John Bunt and Professor Raymond Everson for their guidance and support as well as the long technical discussions during Tuesday meetings.
- Sasol Hub and Spoke initiative for partial funding of this study.
- Mr. Jan Kroeze and Mr. Adrian Brock for their technical assistance.
- My family for the love and support received for the duration of this study.
- Ms Sansha Nel, for her love and support.

Abstract

Steam gasification has been extensively researched in order to optimise and efficiently utilise coal. Reactivity on powdered coal has received considerable attention, however, due to equipment limitation large coal particle research has not progressed to the same extent. The lack of knowledge regarding the steam gasification reactivity of large coal particles is the main motivation of this study.

A South African Highveld seam 4 coal was used in this investigation. Conventional coal characterisation was conducted on a representative sample of the run-of-mine coal sample. The results obtained for the conventional analysis are typical for what is found in literature for a South African Highveld seam 4 coal.

The run-of-mine coal was sieved into particle size fractions for easy hand selection of large coal particles. The single coal particles were hand selected on size and shape and afterwards a density cut (1400 – 1500 kg/m^3) was used as the final selection criterium. The particles, selected according to size, shape and density, were used for the petrographic analysis, char pore structure analysis and reactivity experiments.

The petrographic analysis of the raw coal particles was conducted on 5 and 30 mm particles. Both samples are clasified as inertinite rich bitiminous, medium rank C coal. The maceral concentartion varied with particle size. The char pore structure of the 5, 10, 20 and 30 mm coal particles were also studied. It was observed that an increase in the particle size decreased the char porosity, reduced pore diameter and increased surface area (BET surface area for gas adsorption and pore area for mercury porosimetry).

Steam gasification reactivity experiments using 5, 10, 20 and 30 mm coal particles at gasification temperature ranging from 775 to 900 °C were conducted. The ash produced after gasification was studied to determine the degree of fragmentation. A large degree of fragmentation was observed for the 30 mm coal particles when compared to the other (smaller) coal particles.

To quantitatively determine the influence of particle size on the reactivity of coal, the validity of powdered reactivity models were tested on the reactivity results of large coal particles. Fundamental models, like the homogenous, shrinking core and random pore models, were found to fit most of the experiments, but the fitted constants lacked a chemical / physical

meaning. The semi-empirical Wen model accurately predicts the experimental carbon loss and was used for modelling.

The initial reactivities obtained from the Wen model were used to quantatively determine the influence of temperature and particle size on the steam gasification kinetics. The activation energy obtained from the Arrhenius plots for the 5, 10, 20 and 30 mm particles are 165, 145, 150 and 143 kJ/mol, respectively.

In order to determine the influence of particle size on the reactivity of coal the initial reactivity obtained from the Wen model was normalised using the 30 mm coal particle reactivity. This showed that a six fold decrease in particle size resulted in a twofold increase in steam gasification reactivity. Also, no significant difference in reactivity is observed for the 20 and 30 mm coal particles and it is proposed that the large degree of fragmentation of the 30 mm particle is responsible for this phenomenon. The increase in reactivity observed with a decrease in particle size is proposed to be a combination of different conversion mechanisms as well as a combination of several different factors (fragmentation, petrographic composition and char pore structure) which are dependent on coal particle size.

Opsomming

Stoomvergassing reaktiwiteit is voorheen al breedvoerig bestudeer met die doel om steenkool omskaklingsprosesse te optimaliseer, en steenkool as energiebron so effektief as moontlik te benut. Tot dusver was die fokus hoofsaaklik op die navorsing van die reaktiwiteit van steenkoolpoeiers, en toerustingbeperkings het navorsing met groot steenkoolpartikels verhoed. Die tekort aan kennis rakende stoomvergassing van groot steenkoolpartikels is die motiverende faktor van dié studie.

'n Suid-Afrikaanse Hoëveld steenkool (laag 4) was gebruik vir die studie. Konvensionele steenkoolkarakterisering was gedoen op a verteenwoordigende monster van die oorspronklike steenkoolmonster. Die resultate wat ingesamel was in noue ooreenstemming met gepubliseerde resultate, en is tiperend van Hoëveld laag 4 steenkool.

Die oorspronklikesteenkool monster was gesif volgens partikel grootte fraksies, om handseleksie van groot steenkoolpartikels te vergemaklik. Die dimensies en vorm van die geselekteerde partikels was volgens digtheid gesorteer, met 'n digtheidsvariansie tussen 1400 en 1500 kg/m^3. Die geselekteerde partikels was gebruik vir petrografiese analise, kool porie-struktuur-analise en reaktiwiteit eksperimente.

Die petrografiese analise was op die rou 5 mm en 30 mm partikels uitgevoer. Albei die monsters is geklassifiseer as inertiniet-ryke, bitumineuse, medium rang-C steenkool. Dit was gevind dat 'n toename in partikel grootte geassosieer kan word met 'n toename in vitriniet inhoud. Die koolporie-struktuur-analise op die 5, 10, 20 en 30 mm partikels het aangetoon dat die mikro-porie struktuur van die kool toeneem met 'n toename in partikel grootte.

Stoomreaktiwiteiteksperimente was uitgevoer met die 5, 10, 20 en 30 mm partikels, by vergassingstemperature tussen 775 en 900 °C. Dit was gevind dat 20 mm die termiese stabiele partikel grootte is. 'n Groot mate van fragmentasie was geobserweer vir die 30 mm partikels. Resultate het kwalitatief bewys dat 'n toename in partikel grootte lei tot 'n afname in steenkoolreaktiwiteit.

Met die doel om die invloed van partikel grootte op steenkoolreaktiwiteit kwantitatief te bepaal, was die toepaslikheid van poeierreaktiwiteitmodelle op die reaktiwiteit van groot steenkool partikels bestudeer. Dit was gevind dat die fundamentele modelle wat getoets

was, nl. die homogene model, krimpende kern model en die “random pore” model, die eksperimentele koolstof-verlies akkuraat kon voorspel. Dit was ook gevind dat die Wen model die eksperimentele koolstof-verlies akkuraat kon voorspel, en nadat die passingsparameters krities geëvalueer was, was daar bepaal dat hierdie model die reaktiwiteit van die groot steenkoolpartikels akkuraat beskryf.

Die aanvanklike reaktiwiteite wat verkry was deur die passing van die Wen model, was gebruik om die invloed van temperatuur en partikel grootte op die stoom vergassingskinetika kwalitatief te bepaal. Die aktiveringsenergie wat verkry is van die Arrhenius grafieke vir die 5, 10, 20 en 30 mm partikels, is 165, 145, 150 en 143 kJ/mol, onderskeidelik. Die hoë aktiveringsenergie van die 5 mm steenkoolpartikels kan moontlik toegeskryf word aan die hoë inertiniet inhoud.

Die invloed van partikel grootte op die steenkoolreaktiwiteit was bepaal deur die aanvanklike reaktiwiteite, wat verkry was deur die passing van die Wen model, te normaliseer in terme van die 30 mm partikel se reaktiwiteit. Dit het bewys dat ‘n sesvoudige toename in partikel grootte ‘n halfering in die stoomvergassingsreaktiwiteit van die steenkool tot gevolg het. Dit was ook gevind dat daar geen noemenswaardige verskil is tussen die reaktiwiteit van die 20 mm en 30 mm partikels nie, en hierdie verskynsel kan toegeskryf word aan die hoë graad van fragmentasie. Die toename in reaktiwiteit wat geobserweer word vir ‘n afname in partikel grootte kan moontlik toegeskryf word aan die meganisme van die reaktiwiteitsmodel, asook ‘n kombinasie van verskeie ander faktore (fragmentasie, petrografiese komposisie en koolporie-struktuur), wat almal afhanklik is van die partikel grootte.

Table of Content

List of Figures

List of Tables

List of Symbols

Symbol	Description	Units
b	Solid stoichiometry	-
C_{Ag}	Steam concentration at solid interface	mol/m^3
D_e	Effective ash diffusion coefficient	m^2/s
d_p	Particle diameter	mm
ΔH_{298K}	Enthalpy of reaction	kJ/mol
K_{CO}	Adsorption constant for CO	Pa^{-1}
K_{CO2}	Adsorption constant for CO_2	Pa^{-1}
K_{H2}	Adsorption constant for H_2	Pa^{-1}
K_{H2O}	Adsorption constant for H_2O	Pa^{-1}
k	Reaction rate constant	s^{-1}
k_0	Reaction rate constant	s^{-1}
k_1	Reaction rate constant (steam)	s^{-1}
k_2	Hydrogen inhibition constant	s^{-1}
$k_{30,T}$	Average reactivity constant of the 30 mm particle size at T temperature	s^{-1}
k_g	Mass transfer coefficient	m/s
$k_{i,T}$	Average reactivity constant of i^{th} particle size at T temperature	s^{-1}
k_r	Reaction rate constant	s^{-1}
L_0	Total pore length per unit volume	m/m^3
m	Order of solid reaction	-
m_0	Starting weight	g
m_1	Weight of particle	g
m_2	Weight of submerged particle and plunger	g
m_i	i^{th} mass data point	g
m_p	Weight of submerged plunger	g
N	Amount of data points	-
n	Order of hydrogen inhibition	-
n_{ash}	Normalised value for the ash	-
n_g	Gasification starting normalised value	-
n_i	i^{th} normalised data point	-
P_{CO}	Carbon monoxide partial pressure	Pa
P_{CO2}	Carbon dioxide partial pressure	Pa
P_{H2}	Hydrogen partial pressure	Pa
P_{H2O}	Steam partial pressure	Pa
R	Particle radius	m
r_C	Rate of carbon conversion	Dependent on model
r_p	Equivalent spherical radius	mm
r_s	Reaction rate	m/s
t_{90}	Time required for 90% conversion	s
t_{model}	Time predicted by the model	s
S_0	Initial surface area	m^2/m^3
X_i	Carbon conversion	-
$X_{experimental}$	Experimental carbon conversion	-
ε_0	Initial porosity	%
ρ_b	Solid density	mol/m^3
ρ_P	Particle density	kg/m^3
ψ	Structural parameter	-

Chapter 1: Introduction

Coal is not only one of the most important and abundant sources of energy, it is also the fastest growing energy source in the world (WCI, 2009). According to WCI (2009), South Africa is the fifth largest producer of coal and has the seventh largest coal reserve globally. The abundant coal resources of South Africa allow the utilisation of coal to such an extent that sufficient amounts of electricity and chemicals are supplied, in order to support the increasing demand for energy.

Coal is utilised in the industry mainly to produce energy and chemicals (Miller, 2005). 39% of the world's electricity is generated using coal, while indirect coal liquefaction is growing in popularity as the price of oil increases (WCI, 2009). The technologies used for energy and chemical production differ significantly. Power generation technologies are designed to optimise the energy (heat) converted into power, whereas petrochemical technologies optimise the amount of valuable chemicals produced from coal (Demirbas, 2009).

The industrial coal conversion technologies, mostly used for power generation, are pulverised fuel and fluidised bed technologies (Spliethoff, 2010). According to the WCI (2009), 97% of South Africa's electricity is produced using pulverised fuel technology. The particle size range used is <74 µm, with increased research and optimisation suggesting technology development for a <20 µm particle size range (Miller and David, 2008; Xiumin *et al.*, 2002).

There are mainly three gasification technologies used to produce higher value chemicals from coal *i.e* pulverised fuel, fluidised bed and moving-bed gasification (Miller, 2005). Pulverised fuel and fluidised bed gasification technologies are mostly used in integrated gasification combined cycle (IGCC) power plants (Spliethoff, 2010). Particle sizes used for pulverised fuel and fluidised bed gasification are <100 µm and <10 mm, respectively (Higman and van der Burgt, 2008; Hanson *et al.*, 2002). The moving-bed technology is the oldest process used to produce water gas. There are two moving bed processes used industrially worldwide. The first is the Sasol® FDBD™ and the second is the British Gas/Lurgi slagging gasifier (Higman and van der Burgt, 2008). The feed size for a moving-bed gasifier can be as large as 100 mm, according to Higman and van den Burgt (2008).

Pilot-scale reactors are used to determine the validity of coal feedstock for coal conversion processes. In order to optimise coal conversion technologies, fundamental studies are

conducted on the behaviour of coal. Bench-scale equipment such as fluidised beds (Hanson *et al.*, 2002; Ye *et al.*, 1998), TGA's (Lu and Do, 1992; Everson *et al.*, 2006), drop tube reactors (Du *et al.*, 2010; Barranco *et al.*, 2003) and bed reactors (including fixed, packed and moving bed) (Huang and Watkinson, 1996; Zhuo *et al.*, 2000) are used for fundamental studies. The influence of factors such as gasification conditions, chemical and structural transformations, and coal physical properties on the reactivity of coal, are investigated in fundamental studies (Molina and Mondragon, 1998).

Fundamental studies on the gasification of coal using CO_2 (Fu and Wang, 2001; Kajitani *et al.*, 2006; Kwon *et al.*, 1987; Zhang *et al.*, 2006) and steam (Schmal *et al.*, 1983; Mühlen *et al.*, 1985; Ginter *et al.*, 1993; Peng *et al.*, 1995; Zhang *et al.*, 2006) were conducted with powdered coal, using thermogravimetric analysers and packed beds. Combustion and gasification experiments using powdered South African coal have also recently received considerable attention *i.e.* Cai *et al.* (1998), Sekine *et al.* (2006), Everson *et al.* (2008), Everson *et al.* (2011) and Hattingh *et al.* (2011). However, mainly due to equipment limitations, steam gasification has received less attention. The steam gasification reaction is of utmost importance in the petrochemical industry, and is considered as the starting point for converting coal into higher value chemicals (Van Heek and Mühlen, 1900). Due to the variation in particle sizes used for the various gasification technologies (ranging from powders to 100 mm particles), it is important to study the influence of particle size on the reactivity of coal. The influence of large coal particles was investigated by Hanson *et al.* (1992), Ye *et al.* (1998) and Huang and Watkinson (1996). However, particle sizes smaller than 4.1 mm were used for these studies. The experimental methodology of each study is shown in Table 1.1.

Table 1.1: Experimental methodology for steam gasification research on large coal particles.

	Equipment	Particle size Range (mm)	Carbon conversion calculation
Hanson *et al.* (1992)	Fluidised bed	$0.5<d_p<2.8$	Outlet gas composition
Ye *et al.* (1998)	Fluidised bed	$0.8<d_p<4.1$	Proximate analysis
Huang and Watkinson (1996)	Stirred bed reactor	$0.8<d_p<3.0$	Outlet gas composition
Oberholzer (2009)	TGA	5 mm	Mass loss (TGA)

The aim of this study is to investigate lump coal particles larger than 5 mm (up to 30 mm), to determine the effect of coal particle size on the steam gasification reactivity of a typical South African coal. Thermogravimetric analysis is used to reduce the influence of gas flow hydrodynamics, temperature variations and secondary reactions, which are observed in coal beds and fluidised bed reactors.

1.1 Objectives of this investigation

- To investigate the steam gasification reactivity with respect to temperature and particle size.
- To evaluate the influence of particle size on the petrographic and char structural properties of lump coal.
- To evaluate the validity of powdered coal mathematical models on the prediction of large particle steam gasification kinetics.

1.2 Scope of this dissertation

The coal that will be used is a South African Highveld seam 4, medium rank-C, bituminous coal. Conventional characterisation analyses will be conducted on a representative sample of the bulk raw coal. The coal particle sizes used are 5, 10, 20 and 30 mm lump coal particles. The larger coal particles (20 and 30 mm) will be handpicked (based on size and shape) and screened on a density cut (using mercury submersion density analysis), to increase homogeneity of the large coal particles. The screened particles will be used for the char pore structure analysis, petrographic analysis and reactivity experiments. The influence of particle size on the char structure (charred at 900 °C) and petrographic composition will also be investigated. An in-house manufactured large particle TGA will be used to study the reactivity of lump coal, at temperatures ranging between 775 and 900 ˚C and a steam concentration of 80 mol%. The ash obtained from the gasification experiments (at 900 °C) will also be studied to determine the influence of the particle size on fragmentation.

The dissertation is sub-divided into 7 chapters, and the outline of each chapter is discussed:

- The introduction, as provided in this chapter, discusses coal utilisation and technologies, particle size research and project motivation.
- A detailed literature survey regarding steam gasification, which consists of the coal gasification overview, gas-solid reactions, steam gasification mechanisms, factors affecting steam gasification and coal reactivity studies, is presented in Chapter 2. In the coal reactivity section the emphasis is placed on particle size influences on the steam gasification reactivity of coal.
- The aim, objectives and scope of this investigation is outlined in Chapter 3.
- Chapter 4 contains the coal preparation and characterisation, as well as a discussion regarding the coal characterisation results.

- Chapter 5 contains the experimental methodology followed for the steam reactivity experiments, and the experimental result obtained are presented and discussed.
- An extensive evaluation of the results obtained from various reaction models are given in Chapter 6.
- Chapter 7 provides the conclusions and recommendations made based on the experimental results obtained during this study.

Chapter 2: Literature review

The engineering complexities of coal gasification are discussed in this chapter. A brief overview of the history of coal gasification is given in Section 2.1 and heterogeneous gas-solid reactions are described in Section 2.2. The mechanism of steam gasification is discussed in Section 2.3. Factors affecting the reactivity of steam gasification are explained in Section 2.4, while Section 2.5 contains a discussion regarding the influence of particle size on the reactivity of coal.

2.1 Coal gasification overview

Gasification is defined as a process where carbonaceous material is converted into combustible gases (i.e. CH_4 or syngas). The carbonaceous materials include coal, crude oil, biomass and natural gas. The first gasification process was created in 1792 by the Scottish engineer, Murdoch, for illumination purposes (Rezaiyan and Cheremisinoff, 2005). Since then the gasification process has been extensively researched and developed to produce different products with increasing economical potential.

The first known gasification product was illumination gas, otherwise known as coal gas or town gas. Town gas was produced during devolatilisation, where combustible gases were released as the coal heats to high temperatures (Rezaiyan and Cheremisinoff, 2005). The gas was used to illuminate streets, houses and as a spatial heating source. The economical downside of this process was that only around 20 wt% of the coal was utilised. Therefore, it was important to develop a chemical process to exploit the remaining carbonaceous material in the coal (Schobert, 1991).

Steam gasification is one of the processes used to utilise the remaining carbonaceous material in the coal, after devolatilisation. The carbonaceous material is partially oxidised with humidified air to produce hydrogen and carbon monoxide. The gas products formed during steam gasification became known as producer or water gas (Higman and van der Burgt, 2008). The producer gas contains hydrogen, carbon monoxide, carbon dioxide and nitrogen, and was used for illumination, and spatial and industrial heating. In the 1920s, Franz Fischer and Hans Tropsch developed a process to efficiently convert the carbon monoxide and hydrogen produced during gasification, into liquid fuels (Schobert, 1991).

The development and importance of coal gasification have drastically fluctuated during the past few centuries. The importance is heavily dependent on the price and availability of other fossil fuels, as well as renewable resources. The actual importance of coal as fossil fuel was first realised in the iron production sector. Iron production in England was reduced from 180 000 tons (in 1620) to 18 000 tons (in 1720) per year due to the depletion of wood, and coal was seen as a suitable replacement. In the 1950s, coal was seen as an alternative raw material for the production of ammonia, to supply the exponential growth observed in the fertiliser market. The oil crisis in the early 1970s led to an ever-increasing awareness of the use of alternative fuels, and the production of liquid fuel via the Fischer-Tropsch process became increasingly important (Higman and van der Burgt, 2008). An increasing demand for liquid fuel has also lead to extensive research in order to understand and optimise existing coal gasification technologies. The most important chemical reactions associated with the coal gasification process, are presented by Equations 2.1-2.6 (Higman and van der Burgt, 2008) :

$$\frac{1}{2}O_2 + C \rightarrow CO \qquad \Delta H_{298K} = -111 \ \frac{kJ}{mol} \qquad \text{Eq 2.1}$$

$$\frac{1}{2}O_2 + CO \rightarrow CO_2 \qquad \Delta H_{298K} = -283 \ \frac{kJ}{mol} \qquad \text{Eq 2.2}$$

$$CO_2 + C \rightarrow 2CO \qquad \Delta H_{298K} = 172 \ \frac{kJ}{mol} \qquad \text{Eq 2.3}$$

$$H_2O + C \rightarrow CO + H_2 \qquad \Delta H_{298K} = 131 \ \frac{kJ}{mol} \qquad \text{Eq 2.4}$$

$$2H_2 + C \rightarrow CH_4 \qquad \Delta H_{298K} = -75 \ \frac{kJ}{mol} \qquad \text{Eq 2.5}$$

$$CO + H_2O \rightarrow CO_2 + H_2, \quad \Delta H_{298K} = -41 \ \frac{kJ}{mol} \qquad \text{Eq 2.6}$$

The combustion reactions (Equation 2.1 and 2.2) are highly exothermic and are very important in generating the energy required to drive the endothermic reactions in a gasifier. The Boudourd reaction (Equation 2.3) is endothermic and is very slow in the absence of a catalyst (Liu *et al.*, 2010). The Water-gas (Equation 2.4) reaction is also an endothermic reaction and it is the primary reaction required to produce syngas (Rezaiyan and Cheremisinoff, 2005). The water-gas reaction is faster than the Boudourd reaction and slower than the combustion reactions (Liu *et al.*, 2010). The methanation reaction (Equation 2.5) is extremely slow at atmospheric pressure. However, a significant increase in methane production is observed with an increase in operating pressure (Liu *et al.*, 2010). The Water-

gas shift reaction (Equation 2.6) is used to manipulate the CO and H_2 ratio in syngas. Equation 2.6 is a gas phase reaction and is usually in thermodynamic equilibrium at gasification temperatures (Liu *et al.*, 2010).

2.2 Gas-solid reactions

Gas-solid reactions are defined as heterogeneous reactions, which take place when gas comes into contact with a solid (Denbich and Turner, 1971). Lapidus & Amundson (1977) further defined the solid as a porous material, in order to accurately describe the industrial applications of coal conversion processes. In general, gas-solid reactions can be given as:

$$aA(g) + bB(s) \leftrightarrow \text{products} \qquad \text{Eq 2.7}$$

Due to the multiple phases present in a gas-solid reaction, it is important to describe the transfer of species between the different phases. For the description of the overall reaction kinetics, Yagi and Kunii (1955) developed a three elemental step reaction model to include the movement of compounds between the gas and the solid phase. Figure 2.1 illustrates the boundary layer (gas film) for gas-solid reactions.

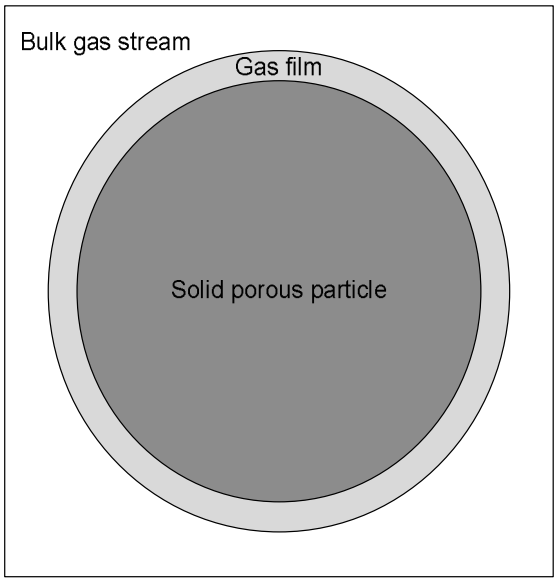

Figure 2.1: Boundary layer for gas-solid reaction adapted from Yagi & Kunii (1955).

A gas film boundary layer exists between the solid particle and bulk gas stream. The gas film boundary layer is defined as the thin film layer around an object where vast velocity changes are observed. The steps, as developed by Yagi & Kunni (1955), are:

- Mass transfer of the reaction gas from the bulk gas stream through the gas film, to the surface of the solid particle
- Diffusion of the reaction gas through the pores of the particle.
- Chemical reaction between the gas and solid at the surface of the particle.
- Diffusion of the product gas through the pores of the porous particle.
- Mass transfer of the product gas from the surface of the particle, through the gas film, to the bulk gas stream.

Using the above mentioned reaction model it was found that there are three elemental steps influencing the overall reaction kinetics of gas-solid reactions. These steps are external mass transfer, internal diffusion and chemical reaction. During steady-state operation, the rate of all three elemental steps is equal. However, the rate of one elemental step will limit the rate of the other elemental steps, hence, the rate-limiting or rate-controlling step (Denbigh, 1966). According to Wicke (1955) and Walker *et al.* (1959), the rate-limiting step is strongly dependent on temperature, as shown in Figure 2.2:

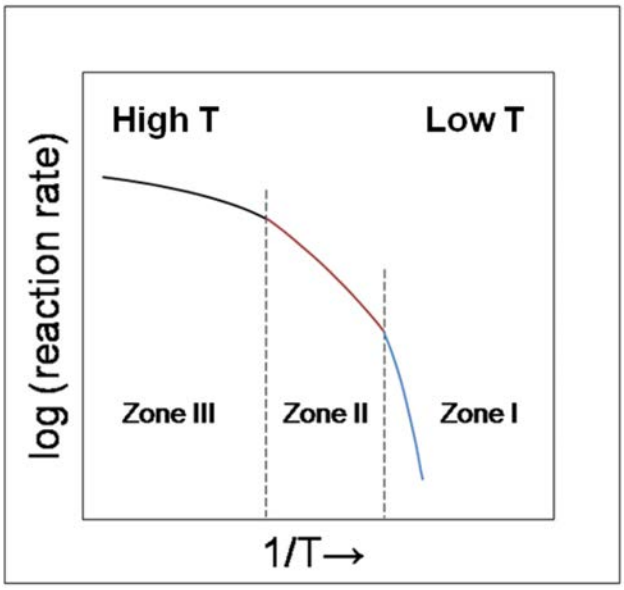

Figure 2.2: Temperature dependence of the regime change for gasification of coal, adapted from Walker *et al.* (1959).

From Figure 2.2 it is clearly observed that an increase in the reaction temperature results in an increase in the reaction rate. It can also be seen that the reaction rate versus temperature profile can be divided into three regimes, according to the various gradients. The change in gradient is due to the change in rate limiting step as the temperature is increased (Walker *et al.*, 1959). At lower temperatures, an increase in the temperature

strongly increases the reaction rate. The rate-limiting step in Zone I is known as the chemical-reaction control regime, while Zone II is known as the internal diffusion control regime. The internal diffusion control regime also results in an increased reaction rate with an increase in gasification temperature. However, the reaction rate is less dependent on gasification temperature. Zone III is known as the mass transfer control regime, which is the least influenced by temperature (Walker *et al.*, 1959).

2.3 Steam gasification mechanism

Since steam gasification is a heterogeneous (gas-solid) reaction, all gasification mechanisms are classified as complex surface reaction mechanisms (Masel, 1996). The steam gasification mechanisms were first derived using pure carbon (graphite) and steam and afterwards the applicable mathematical models were tested on coal. Due to the high carbon content of coal, it is possible to use graphite as an analogue for coal. However, aliphatic carbons and mineral matter present in coal are not found in graphite, and may influence the proposed reaction mechanisms (Sunggyu *et al.*, 2007). Numerous studies have shown that different reaction mechanisms are followed for catalytic steam gasification, due to alkali earth metals present in the coal (Domazetis *et al.*, 2008; Wang *et al.*, 2009; Mims and Pabst, 1983).

2.3.1 Steam gasification mechanisms

The first steam gasification mechanism developed consists of two stages, and is based on the Rideal-Eley mechanism. The first stage in this mechanism is the reaction of gas molecules and surface atoms by direct collision, while the second stage involves desorption of the products from the surface (Kolasinski, 2008). The two-step mechanism derived for the application of steam gasification is shown in Equation 2.8 (stage 1) and 2.9 (stage 2) (Srivastava *et al.*, 2007):

$$C_{fas} + H_2O \rightarrow C(O) + H_2 \qquad \text{Eq 2.8}$$

$$C(O) \rightarrow CO \qquad \text{Eq 2.9}$$

Equation 2.8 describes the dissociation of water at a free active carbon site (C_{fas}), producing hydrogen and an oxidised surface complex (C(O)). The oxidised surface complex contains the oxygen (from the dissociation of water) reacted onto the free active carbon (Fushimi *et al.*, 2011). The carbon monoxide is desorbed from the surface complex, producing a new

free active carbon site. This mechanism was revised by Langmuir and further modified by Hinshelwood to derive the Langmuir-Hinshelwood gasification mechanism. The Langmuir-Hinshelwood mechanism is a three-stage mechanism, which includes the adsorption of the reactant gas onto the solid particle, the reaction between the solid and adsorbed reagent and lastly desorption of the product gases from the solid particle (Srivastava *et al.*, 2007). The three-step mechanism derived for the application of steam gasification is shown in Equation 2.10 to 2.13 taken from Sheth *et al.* (2003).

$$H_2O(g) \rightarrow H_2O(ad) \qquad \text{Eq 2.10}$$

$$C_{fas} + H_2O(ad) \rightarrow C(O) + H_2(ad) \qquad \text{Eq 2.11}$$

$$H_2(ad) \rightarrow H_2(g) \qquad \text{Eq 2.12}$$

$$C(O) \rightarrow CO(g) \qquad \text{Eq 2.13}$$

Equation 2.10 signifies the adsorption of steam to the carbon surface. The next step (Equation 2.11) is the reaction between adsorbed water and a free active carbon site. The water dissociates and produces hydrogen and an oxidised surface complex, which is still adsorbed onto the carbon surface. The last step in the mechanism is desorption of the product gases, hydrogen and carbon monoxide, to produce a free active carbon site. The Langmuir-Hinshelwood mechanism can be expressed as the following rate equation for the steam gasification of coal (see Equation 2.14) (Sheth *et al.*, 2003).

$$-r_C = \frac{k_1 P_{H_2 0}}{1 + K_{H_2O} P_{H_2O}} \qquad \text{Eq 2.14}$$

Studies conducted on coal (Bayarsaikhan *et al.*, 2006; Sheth *et al.*, 2003; Karimi *et al*., 2011) and biomass (Fushimi *et al.*, 2011; Klose and Wolki, 2005) show that the rate equation derived from the Langmuir-Hinshelwood mechanism adequately describes the reactivity of carbonaceous material.

2.3.2 Hydrogen inhibition mechanisms

It was established that the Langmuir-Hinshelwood rate equation, as given in Equation 2.14, could not accurately predict carbon consumption at high hydrogen (Bayarsaikhan *et al.*, 2006; Matsuoka *et al.*, 2009) and carbon monoxide concentrations (Everson *et al.*, 2006; Huang *et al.*, 2010). The deviation is due to the inhibitory effect of hydrogen and carbon monoxide. Carbon monoxide inhibition has a greater influence on CO_2-gasification when compared to steam gasification (Chen *et al.*, 1993).

Studies on the inhibition of hydrogen adsorption on the rate of steam gasification have resulted in three mechanisms. The first mechanism proposed for hydrogen inhibition is a two-stage mechanism describing the adsorption and desorption of hydrogen (reversible process). The mechanism proposed is known as the associative hydrogen adsorption mechanism, and is shown in Equation 2.15 (Bayarsaikhan *et al.*, 2006).

$$C_{fas} + H_2(g) \leftrightarrow C(H_2) \qquad \text{Eq 2.15}$$

$$C_{fas} + \frac{1}{2}H_2(g) \leftrightarrow C(H) \qquad \text{Eq 2.16}$$

$$C(O) + H_2(g) \leftrightarrow C_{fas} + H_2O \qquad \text{Eq 2.17}$$

The hydrogen is adsorbed onto a free active carbons site, consequently inhibiting the reaction between a water molecule and free active carbon site (Equation 2.15). A dissociative hydrogen adsorption mechanism (Equation 2.16) and reverse oxygen exchange mechanism (Equation 2.17) is also proposed (Lussier *et al.*, 1998). There is still no consensus on which mechanism describes the hydrogen inhibition process. Lussier *et al.* (1998) determined that at low hydrogen concentrations the dissociative hydrogen adsorption mechanism describes the hydrogen inhibition rate. However, at elevated pressures the reverse oxygen exchange mechanism describes the inhibition rate accurately. Bayarsaikhan *et al.* (2006) determined that the dissociative hydrogen adsorption mechanism is valid for the entire range of gasification conditions (varying hydrogen concentrations, as well as elevated pressure). All three the proposed mechanisms resulted in the following Langmuir-Hinshelwood rate equation (Sunggyu *et al.*, 2007).

$$-r_C = \frac{k_1 P_{H_2 0}}{1 + K_{H_2O} P_{H_2O} + K_{H_2} P_{H_2}^n} \qquad \text{Eq. 2.18}$$

The steam gasification Langmuir-Hinshelwood rate equation for the consumption of carbon with hydrogen inhibiting effects were validated by numerous studies (Bayarsaikhan *et al.*, 2006; Everson *et al.*, 2006; Matsuoka *et al.*, 2009; Lussier *et al.*, 1998; Fushimi *et al.*, 2011) and holds irrespective of the hydrogen inhibiting mechanism proposed (Sunggyu *et al.*, 2007).

2.3.3 Multi-gas gasification

The combined gasification of carbon dioxide and steam was studied by Mühlen *et al.* (1985), and it was concluded that there are two mechanisms which describe the multi-gas gasification of coal. The first mechanism (Equation 2.19) assumes that the CO_2 and H_2O reactions occur at the same active site (competitive), while the second mechanism (Equation 2.20) assumes that the reactions occur at different active sites (non-competitive). The mechanisms used to describe the separate reaction of carbon-steam and carbon-carbon reactions are assumed to be valid for the multi-gas gasification of coal. An in-depth study on the CO_2 gasification mechanism and Langmuir-Hinshelwood rate equation was done by Chen *et al.* (1993), Liu *et al.* (2000) and Kapteijn *et al.* (1992). The following Langmuir-Hinshelwood rate equation derived by Mühlen *et al.* (1985) for the different multi-gas gasification mechanisms, are given in Equation 2.19 (competitive) and 2.20 (non-competitive):

$$-r_C = \frac{k_1 P_{H_2 0} + k_2 P_{CO_2}}{1 + K_{H_2O} P_{H_2O} + K_{H_2} P_{H_2}^n + K_{CO} P_{CO} + K_{CO_2} P_{CO_2}} \qquad \text{Eq 2.19}$$

$$-r_C = \frac{k_1 P_{H_2 0}}{1 + K_{H_2O} P_{H_2O} + K_{H_2} P_{H_2}^n} + \frac{k_2 P_{CO_2}}{1 + K_{CO} P_{CO} + K_{CO_2} P_{CO_2}} \qquad \text{Eq 2.20}$$

Studies conducted by Everson *et al.* (2006) and Huang *et al.* (2010) show that at atmospheric pressure, the non-competitive (Equation 2.20) reaction mechanism and Langmuir-Hinshelwood rate equation adequately describe the reactivity of steam and CO_2 combined gasification of coal.

2.4 Factors affecting steam gasification

Molina and Mondragon (1998) and Miura *et al.* (1989) conducted an overview of steam gasification research and found that devolatilisation, fragmentation, coal and char structure, petrographic composition and chemical constituents greatly influence the reactivity of steam gasification. Therefore, the factors influencing the steam gasification of coal (Section 2.4) are subdivided into 5 sections, according to the above-mentioned factors.

2.4.1 Devolatilisation

During the heating of coal, volatiles are released to produce a remaining residue solid known as char. The volatile matter released during devolatilisation contains gases (CO, CO_2, hydrogen, methane and other sulphur and nitrogen containing gases) and tars (defined as volatiles condensable at room temperature). During the heating of coal, the particle undergoes complex chemical and physical transformations to produce the char (Yu *et al.*, 2007). The changes in chemical and physical properties influence the reactivity of the parent coal for the duration of the gasification process (Solomon and Fletcher, 1994). The devolatilisation process is dependent on temperature, heating rate and particle size (Yu *et al.*, 2007). A discussion regarding the influence of various devolatilisation conditions on the steam gasification reactivity of char follows.

Temperature

The devolatilisation temperature has an influence on the physical and chemical properties of the char. Numerous studies have concluded that an increase in pyrolysis temperature results in an increase in volatile matter release, and consequently an increase in chemical property change (Tamhankar *et al.*, 1984; Tyler and Schafer, 1980; Scaroni *et al.*, 1981; Yeasmin *et al.*, 78). It was also found that the maximum volatile release rate is obtained at temperatures between 400 and 600 ˚C (de la Puente *et al.*, 1998; Alonso *et al.*, 1999).

The release of volatiles has an effect on the physical char properties, as well as the reactivity of the char. A study conducted by Wu *et al.* (2006) on Yanzhou coal, found that an increase in devolatilisation temperature resulted in a decrease in steam gasification reactivity. The devolatilisation temperature was varied between 900 and 1200 ˚C. Studies conducted on the influence of devolatilisation temperature on CO_2 gasification (Devi and Kannan, 2000; Van der Merwe, 2010) and combustion (Alonso *et al.*, 1999) resulted in the same conclusion.

Heating rate

An increase in heating rate is found to increase the reactivity of coal (Mermouda *et al.*, 2006; Cetin *et al.*, 2004). The increase in reactivity is due to the increased surface area and feeder pores formed during volatile release. Cai *et al.* (1996) studied the influence of devolatilisation heating rate (up to 5000 $K.s^{-1}$) on the reactivity of coal. Five different coals were studied and it was determined that the heating rate (up to 1000 K/s) increases the coal

reactivity. Higher heating rates (> 1000 K/s) also increase the reactivity, but the enhancing effect is less significant.

Particle size

An increase in particle size results in the devolatilisation mechanism changing from chemical reaction controlled to predominantly heat transfer controlled (Stubington *et al.*, 1991). Due to the devolatilisation mechanism, the particle size has a considerable effect on the devolatilisation process. The coal particle size influences the degree of fragmentation (discussed in Section 2.4.2), particle temperature gradient, particle heating rate, devolatilisation rate and time (Stubington and Sasongko, 1998; Sasongko and Stubington, 1996; Bunt and Waanders, 2008; Dacombe *et al.*, 1999).

2.4.2 Fragmentation

Fragmentation is defined as the breaking of a single coal particle into two or more pieces during coal gasification (Bunt and Waanders, 2008). Fragmentation of coal particles can lead to health and safety risks due to an increase in fly ash (Seames, 2003; Yan *et al.*, 2002), fouling in the plant (Card and Jones, 1995), unstable reactor conditions and elutriation of un-reacted carbon (Bunt and Waanders, 2008).

The studies conducted on coal fragmentation at high temperatures have concluded that three different coal fragmentation mechanisms are responsible for the breakage.

- Primary fragmentation
- Secondary fragmentation
- Attrition fragmentation

Primary fragmentation is defined as the breakage of coal particles during devolatilisation of the coal, whereas secondary fragmentation is defined as coal breakage during gasification (Sasongko and Atubington, 1996). Attrition fragmentation can be described as the coal breakage due to particle collision with reactor walls and other particles (Rhodes, 2008).

An increase in the internal gas pressure of a porous particle is observed when volatiles are released inside the coal particle, which will consequently increase the mechanical stress exerted on the coal particle (Stubington and Linjewile, 1989). Large temperature gradients

are also observed in coal particles due to devolatilisation conditions which cause thermal stress (Senneca *et al.*, 2011). The increase in mechanical and thermal stresses exerted on the coal particle during devolatilisation, is proposed as the reason for primary fragmentation. The studies conducted on primary fragmentation has determined that residence time, particle size, volatile matter (wt%), coal compressive strength, swelling and mineral matter, devolatilisation temperature and heating rate all influence the fragmentation of coal particles (Senneca *et al.*, 2011; Zhang *et al.*, 2002; Dacombe *et al.*, 1999). The occurrence of primary fragmentation is more apparent with increasing particle size. The particle size influence was also observed by Bunt and Waanders (2008). However, it was observed that for set gasification conditions, a thermal stable particle size exists. The observation concluded that particles smaller than the thermal stable particle size (25 mm in this study) did not fragment, whereas fragmentation was observed for particles larger than the thermal stable particle size.

The study of secondary fragmentation is important for pulverised fuel and fluidised bed combustion, and is caused by the removal of carbon bridges connecting parts of the char particle (Sasongko and Atubington, 1996; Van Dyk, 2001). The char particle shape after devolatilisation is observed to play an important role in secondary fragmentation (Liu *et al.*, 2000).

2.4.3 Char structure

The pore structure is classified in terms of the size distribution of pores. The classification of pores, according to the IUPAC Manual of Symbols and Technology, is divided into micropores (< 2nm), mescopores (2 to 50 nm) and macropores (> 50 nm). It is proposed that the pore structure changes throughout the burn-off life of the particle. The devolatilisation time for pulverised fuel combustion is in the order of 100 milliseconds and up to 4 seconds for complete combustion (Field *et al.*, 1967). The change in pore structure during devolatilisation will affect the gasification from start to finish. Therefore, numerous studies on the change in pore structure during devolatilisation and gasification, respectively, have been conducted.

A study conducted by Davini *et al.* (1996) concluded that an increase in devolatilisation temperature results in an increase in surface area, and maximum surface area is obtained after complete devolatilisation. The same observation was found by Lorenz *et al.* (2000), who further observed that an increase in micropore structure is obtained with an increase in heating rate. The increase in micropore structure is due to the rapid volatile release with an

increase in heating rate (Cai *et al.*, 1996). The increase in surface area with increasing devolatilisation temperatures is a well established phenomenon. However, there is no consensus on the influence of surface area on the steam gasification rate of chars (Molina and Mondragon, 1998).

The Random Pore Model proposed for gas-solid reactions by Bhatia and Perlmutter (1980) allows for the modelling of coal gasification with arbitrary pore size distributions in the porous reacting solid. Numerous studies done on char pore structure during gasification have since been conducted to increase the understanding of how the pore structure changes with increasing conversion. An investigation conducted by Davini *et al.* (1996) showed that the surface area increases until a maximum surface area is obtained at the highest carbon consumption rate. Once the maximum surface area is obtained, the reactivity starts to decrease along with the surface area. This observation was also found by Lorenz *et al.* (2000), Feng and Bhatia (2003) and Sadukhan *et al.* (2009) and is proposed to be due to coalescence of the pore walls.

2.4.4 Petrographics

The petrographic analysis is the study of the maceral composition of coal, and is subdivided into organic petrology, inorganic petrology and coal rank (Suárez-Ruiz and Crelling, 2008). The biological material from which the coal is derived will consequently determine the maceral composition of the coal (Bertrand *et al.*, 1993). Coal rank, on the other hand, is characterised by the degree of maturity of the maceral constituents in the coal (Suárez-Ruiz and Crelling, 2008).

Numerous studies have been conducted on the maceral reactivity of coal for gasification reactions, and investigators have published contradictory results. It has been observed that maceral reactivity is in the order of vitrinite > liptinite > inertinite (Sun *et al.*, 2004; Messenbock *et al.*, 2000) or inertinite > vitrinite > liptinite (Megraritis *et al.*, 1999; Cai *et al.*, 1998). However, it was found that the amount of volatiles released decreases in the order of liptinite > vitrinite > inertinite (Messenbock *et al.*, 2000; Megraritis *et al.*, 1999; Alonso *et al.*, 1999; Cai *et al.*, 1998).

It is proposed that the opposing results found in literature are due to the variation in maceral rank, carbon content, holding time and mineral matter for the various coals investigated. The study conducted by Megaritis *et al.* (1999) concluded that the rate of reaction for vitrinite

decreases sharply with an increase in rank. It was found that high ranked inertinite reacted significantly faster than vitrinite of the same rank. A study conducted by Cai *et al.* (1998) concluded that an increase in carbon content resulted in a decrease in char reactivity. Cai *et al.* (1998) proposed to compare maceral reactivity of similar carbon content, so as not to obtain contradictory results. The holding time of gasification was also found to be an important factor influencing maceral reactivity (Megraritis *et al.*, 1999; Messenbock *et al.*, 2000). A study conducted by Megaritis *et al.* (1999) showed that the order of maceral reactivity varies from vitrinite > liptinite > inertinite to inertinite > vitrinite > liptinite with an increase in holding time from 10 to 200 seconds. Sun *et al.* (2004) determined that the reactivity of demineralised vitrinite is higher than demineralised inertinite chars, which suggests that vitrinite has a higher intrinsic reactivity when compared to inertinite. Lastly, Alonso *et al.* (1999) determined that low volatile, vitrinite-rich bituminous coal reacts slower than inertinite-rich bituminous coal, and that high volatile, vitrinite-rich, bituminous coal reacts the fastest.

2.4.5 Chemical constituents

There are two main constituents in raw coal which influence the steam gasification reactivity, namely carbon content and mineral matter (Kabe *et al.*, 2004). Numerous studies have been conducted in order to determine the influence of carbon content on coal reactivity (Miura *et al.*, 1989), while mineral matter has received considerable attention due to the catalytic effect on the gasification reactivity.

An investigation conducted by Hattingh *et al.* (2011) on three South-African coals, containing similar elemental, structural and petrographical properties, observed significantly different reaction rates. The difference in coal reactivity cannot be explained due to the elemental, structural and petrographical properties. It was therefore proposed to study the mineral matter and determine the effect of inorganic constituents on the reactivity. It was concluded that the increase in coal reactivity was due to the difference in CaO and MgO content in the different coals. The increase in inherent catalysts can be quantified using the alkali index as proposed by Sakawa *et al.* (1982). Shenqi *et al.* (2011) studied the effect of alkali earth metals (Na and K) on the pyrolysis and gasification behaviour of a high-rank bituminous coal. It was observed that the alkali earth metals inhibited the progress of graphitisation of the carbon structure, which resulted in an increase in reactivity.

Studies conducted on raw and demineralised coal have given more insight into the increased reactivity obtained due to the inherent catalysts present in the coal (Sun *et al.*,

2004; Adanez and De Diego, 1993). Sun and co-workers (2004) showed that the catalytic effect for K and Na is more pronounced than the catalytic influence of Fe and Ca. This phenomenon was first proven by Kapteijn *et al.* (1984), who determined that the increase in reactivity due to alkali earth metals are in the order of Cs > Rb > K > Na > Li.

2.5 Coal reactivity studies

This chapter consists of the reactivity studies conducted on coal using reactivity models to interpret the data. Coal reactivity studies are conducted either by varying particle size or keeping a constant particle size. The particle size variation allows for the study of the influence of particle size on the reactivity of coal. For the purpose of this dissertation, the particle size fraction is sub-divided into powdered and large coal particles. Small coal particle sizes are defined as -1 mm with larger coal particles defined as large coal particles.

2.5.1 Small particle

A summary containing studies conducted on the steam gasification reactivity of coal, without comparing particle size, on small coal particles are shown in Table 2.1.

Table 2.1: Summary of small coal particle research without comparing particle size.

Author	Particle size	Temperature (°C)	Reactivity model evaluated
Yang and Watkinson (1994)	1.3 mm	870-930	Homogenous model
Lee and Kim (1995)	+297 -707 µm	700- 850	SCM, modified volumetric model
Kajitani *et al.* (2002)	Powders	1200-1400	RPM
Feng and Bhatia (2003)	90-180 µm	900	RPM
Everson *et al.* (2006)	Powders	800 - 950	SCM, Langmuir-Hinshelwood
Wu *et al.* (2006)	3-6 mm	900 - 1200	Homogenous, SCM
Gul-e-Rana and Ji-yu (2009)	-154 µm	700- 900	SCM
Matsuoka *et al.* (2009)	0.5-1 mm	800	Langmuir-Hinshelwood
Fermoso *et al.* (2010)	1-2 mm	900	Volumetric, grain and random pore model
Karimi *et al.* (2010)	< 120 µm	800	SCM

The reactivity models mostly used to predict the reactivity of coal are the homogenous, shrinking core and random pore model. The homogenous model assumes that the reaction occurs at a constant rate throughout the entire particle. The homogeneous model was

derived by reducing the heterogeneous gas-solid reaction into a homogenous reaction (Molina and Mondragon, 1998).

The shrinking core model consists of an unreacted core and reaction only occurs on the external surface. As the reaction proceeds, the carbon reacts and an ash film is formed on the external surface. The ash film increases while the unreacted core decreases as the reaction proceeds. The model prediction can include reaction, ash diffusion and mass transfer rate controlling steps (Levenspiel, 1999).

The random pore model takes into account the structural changes occurring during carbon conversion. This model allows for the prediction of reaction rates where the reaction rate initially increases to a maximum and then decreases as the reaction progresses, due to an increase in surface area during gasification. The random pore model can also predict experimental data in the reaction control or internal diffusion regime (Bhatia and Perlmutter, 1980).

Reactivity research is also conducted on small coal particles to optimise pulverised fuel combustion and integrated-gasification combined cycle processes (Kadyszewski, 2003). Extensive size reduction is required to produce the ultra fine coal used for pulverised fuel technologies, which results in research investigating the influence of coal particle size (small coal particles) on the reactivity of coal.

Yu *et al.* (2005), Man *et al.* (1998) and Estrele *et al.* (2002) all found that an increase in vitrinite content, a subsequent decrease in inertinite content, is observed with a decrease in particle size. This is proposed to be as a result of the brittleness of vitrinite when compared to inertinite.

It is also expected that, during particle size reduction, more minerals are liberated from the coal and will increase the reactivity due to inherent catalysts (Fung *et al.*, 1998). Zhu *et al.* (2008) conducted a study on Shangwan bituminous coal and Houlinhe lignite coal and found that the ash value increased with decreasing particle size. Particle size ranges of – 120, 120-180 µm and 180-250 µm were used for this investigation. A decrease in reactivity with an increase in particle size was observed, and was attributed to the decrease in inherent catalyst (decreasing ash content). Both coals were also demineralised and used to determine the effect of particle size on the steam gasification reactivity of coal. It was observed that the reactivity of demineralised coal was independent of particle size.

Revankar *et al.* (1987) studied catalytic steam gasification using four particle sizes (45.45, 68.5, 125 and 418 µm) of petroleum coke. The reactivity data obtained for the raw and catalysed samples was modelled using the SCM with reaction control. Experimental results indicated that an increase in particle size resulted in an increase in reactivity, for both the raw and catalysed systems. The activation energy was found to be independent of particle size for the uncatalysed particles. However, the activation energy was found to be influenced by the particle size, with the addition of a catalyst.

2.5.2 Large particle

For the purpose of this investigation, particles with a diameter exceeding 1mm are defined as large particles. Table 2.2 summarises previous research conducted on large coal particle gasification:

Table 2.2: Previous research done on steam gasification of large particles.

Study	Particle size range (mm)
Kühl *et al.* (1992)	1-3
Hüttinger and Natterman (1994)	2-3
Hanson *et al.* (2002)	0.5-2.8
Schmal *et al.* (1982)	0.8-1.4
Ye *et al.* (1998)	0.8-1.6 & 2.4-4.1
Huang and Watkinson (1996)	0.8-3.0

One Columbian (La Jagua) and one English (Daw Mill) coal were studied by Hanson *et al.* (2002) using the particle size ranges (in mm) $0.5< d_p< 1.0$, $1.0< d_p< 1.4$, $1.4< d_p< 2.0$, $2.0< d_p< 2.4$, $2.4< d_p< 2.8$. Experimental results indicated that the smaller size fractions tend to swell and agglomerate more than the large coal fractions, during devolatilisation. A stable particle size of 1.4-2.0 mm was obtained for both coals. Due to equipment constraints, TGA experiments were conducted using only CO_2 and air. The conclusion drawn from the TGA experiments were that char reactivity was independent of particle size for CO_2 gasification and combustion. The steam gasification reactivity experiments were carried out in a spouted bed reactor (at 900 °C), and it was found that the reactivity was independent of particle size.

Schmal *et al.* (1982) studied a Brazilian sub-bituminous, high ash coal using the particle range of 0.8 to 1.4 mm. The reactivity study was done to determine the steam gasification kinetics in a temperature range between 800 and 1000 ˚C using the shrinking core and homogenous model. The study found that chemical-reaction is the rate-limiting step and the kinetic data was sufficiently predicted using both the models. However, it was found that the shrinking core model more accurately predicts the kinetics at higher temperatures (>850 ˚C),

whereas the continuous model more accurately describes the kinetics at lower experimental temperatures (<850 ˚C). Furthermore, it was determined that both the models predicted the same reaction kinetics and activation energy.

Ye *et al.* (1998) used two particle size ranges for steam gasification and three particle sizes for CO_2-gasification. The two particle size ranges used for steam gasification were 0.8 – 1.6 mm and 2.4 - 4.1 mm. The steam gasification experiments were conducted at a temperature of 765 ˚C and at atmospheric pressure. The results from this study are shown in Figure 2.3.

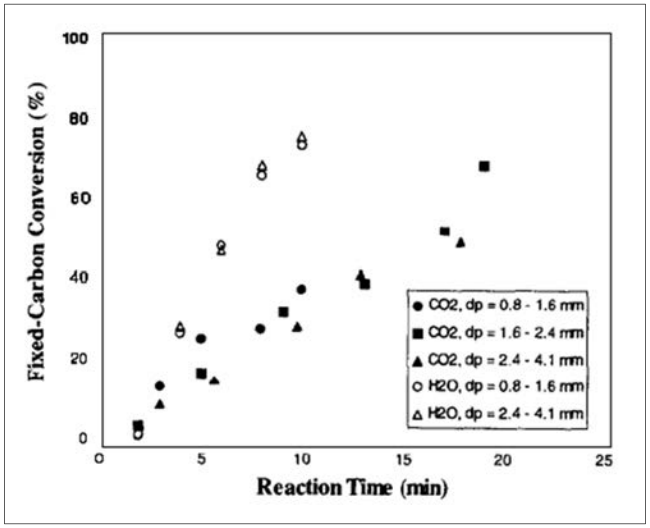

Figure 2.3: Carbon conversion versus time taken from Ye *et al.* (1998).

It was found that the gasification rate for steam and CO_2 was independent of the particle size which indicates that the experiments were conducted in the chemical reaction control regime. This hypothesis was confirmed using the homogeneous and shrinking core models.

Huang and Watkinson (1996) conducted a study on two Canadian non-caking chars and investigated the influence of particle size on the reactivity of steam gasification in a stirred bed reactor. Particle size ranges of 0.85-1.4 mm, 1.5-2.0 mm and 2.36-3.0 mm were used for the Highvale chars, while particle size ranges of 1.0-2.0 mm, 2.0-2.36 mm and 2.36-3.0 mm were selected for the Coal Valley chars. The reactivity obtained for the Coal Valley chars were found to be particle-size independent. However, an increase in the particle size resulted in a decrease in reactivity for the Highvale chars. The influence of particle size on the steam gasification reactivity is due to pore diffusion limitations. It was proposed that a more reactive char will result in increased diffusional effects at the same temperature and particle size compared to a less reactive char.

Remiarova *et al.* (2004) conducted combustion experiments using lump coal, for a temperature range between 450 and 800 °C. It was found that at low temperatures (below 530 °C) the reaction was controlled by pore diffusion and at higher temperature the reaction was controlled by chemical reaction. This observation is not expected according to conventional gas-solid reaction theory, which states that increased pore diffusional effects are observed with an increase in temperature.

2.6 Summary

Different coals have different chemical constituents (such as inherent catalyst), coal structures (such as pore structure) and petrographic compositions, which attribute to the heterogeneous characteristics of coal. Due to this heterogeneous nature, each coal source will react differently towards gasification conditions, which may result in different degrees of fragmentation and variation in char structure formations. Investigation of a single factor influencing coal reactivity becomes increasingly complex due to the variation in coal properties. The coal properties of two different coals may vary, but it is also possible that the coal properties of various particle sizes of the same coal may differ. Therefore, it has become increasingly important to study the influence of particle size on coal reactivity. Previous research conducted on the particle size influence with respect to reactivity, is summarised in Table 2.3.

Table 2.3: Influence of particle size on the reactivity of coal

	Particle size range	Influence
Zhu *et al.* (2008)	$120<d_p<250$ µm	Increase in particle size increase the reactivity
Revankar *et al.* (2008)	$45<d_p<418$ µm	Increase in particle size increase the reactivity
Hanson *et al.* (2008)	$0.5<d_p<2.8$ mm	Independent of particle size
Ye *et al.* (2008)	$0.8<d_p<4.1$ mm	Independent of particle size
Huang *et al.* (2008)	$0.85<d_p<3.0$ mm	Independent of particle size
	$1.0<d_p<3.0$ mm	Increase in particle size decrease the reactivity

Previous investigators have not observed a definite trend with regards to the influence of particle size on gasification reactivity. In studies where particle size did have an influence on reactivity, it was proposed that mineral matter and pore diffusion were the contributing factors. Different reactivity models were used to predict the reactivity of the coal, and investigators found that the reactivity of the various particle sizes could be predicted accurately with the same model.

Reactivity studies conducted on small particles and powders have given insight into the fundamentals of gasification, with specific reference to the influence of particle size. However, previous research has not focused on using large coal particles, thus creating a deficiency in the field of coal gasification. Since large particles are used on an industrial scale, it will be beneficial to conduct a study using large coal particles to obtain a better understanding of the influence and behaviour of these particles in gasification processes.

Chapter 3: Coal preparation and characterisation

This chapter comprises of the coal characterisation and the subsequent sample preparation required. The sample preparation consists of the size and density separation, where the density preparation involves the use of a mercury submersion technique. The coal characterisation analyses conducted include: particle density analysis, conventional analysis, pore structure analysis and petrographic analysis. The conventional analysis includes the proximate analysis, ultimate analysis, gross calorific value and ash composition analysis. Char pore structure is studied using gas adsorption analysis and mercury porosimetry.

The origin of the coal sample is specified in Section 3.1, while the coal size and density preparations are described in Section 3.2. The experimental methodology followed for the coal characterisation is given in Section 3.3, and the characterisation results are presented and discussed in Section 3.4. A summary of the coal preparation and characterisation is given in Section 3.5.

3.1 Coal sample origin

The coal used in this study originates from a Highveld number 4 seam coalfield and is mostly used in the petrochemical industry. Studies conducted by Oberholzer (2009) and Pinheiro (1999) were done on coal from the same seam and colliery. Pinheiro (1999) investigated the coal characteristics, whereas, Oberholzer (2009) investigated both the coal characteristics and steam gasification reactivity of 5 mm coal particles.*

3.2 Sample preparation

3.2.1 Size preparation

A run-of-mine coal sample (approximately 350 kg) was collected by SGS Laboratories (Pty) Ltd. A fraction of the run-of-mine coal was sampled and used for the conventional characterisation, with the remainder of the bulk sample sieved to obtain the particle size fractions shown in Table 3.1.

*due to classification of this study (Oberholzer, 2009)), only the coal characterisation results are referred to and not the reactivity results.

Table 3.1: Particle size fractions obtained from size separation.

Particle size fraction
+40mm
+25 mm to -40 mm
+14 mm to -25 mm
+5 mm to -14 mm
- 5 mm

The –5 and +40 mm particle size fractions were discarded and the other particle size ranges were used for selection of single coal particles. Single particles were handpicked on a dimensional basis, which includes the length, width and height. The particles were also evaluated on the shape, and preferably spherical particles were selected. The particle is placed on 5mm grid paper for dimensional analysis and the overlapping edges are trimmed off using to reduce the size and increase sphericity, using pliers. Figure 3.1 shows the resulting particle shape obtained from the size reduction of a 20 mm coal particle.

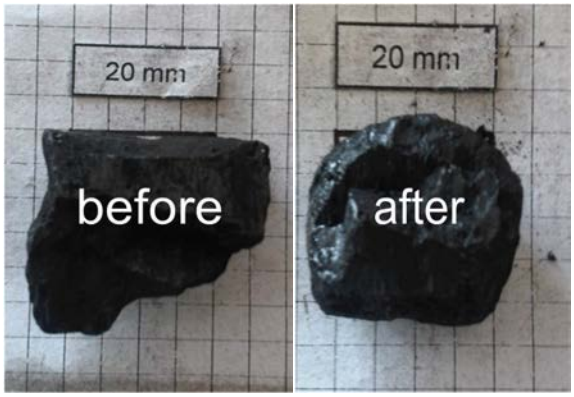

Figure 3.1: Particle shape transformation for a 20 mm particle.

The particle has dimensions of approximately 23(W)x22(L)x19(H) mm and is classified as a 20 mm coal particle. The 20 and 30 mm particles were size and shape selected using handpicking. However, the 5 and 10 mm particles were first sieved into particle size ranges (+4.6 – 5.5 mm and +9.6 -11.2 mm) and afterwards selected based on shape.

3.2.2 Density preparation

The particle density of coal particles can be used to increase the homogeneity of the sample in terms of ash content and maceral composition (Van Niekerk and Mathews, 2010; Maroto-Valer *et al.*, 1998; Wang *et al.*, 2006; Choi and Dyrkacz, 1989; Aktas *et al.*, 1998). The particle density of the handpicked coal particles was determined using mercury submersion analysis (as described in Section 3.3.1). A density cut for each particle size is used to increase the homogeneity of the coal samples used for reactivity experimentation and characterisation analyses.

3.2.3 Reactivity and coal characterisation sample

Table 3.2 summarises the particle sizes, density cut and sample preparation used for the coal characterisation and reactivity experimentation.

Table 3.2: Summary of sample preparation.

	Particle size mm	Density cut kg/m^3	Preparation	Analysis particle size
Conventional analysis*	-	-	Raw coal	-3 mm
Pore structure analysis	5, 10, 20 and 30	1400-1500	Char (at 900 °C)	Mercury porosimetry: -5 mm
				CO_2 gas adsorption: -212 µm
Petrographic analysis	5 and 30	1400-1500	Raw coal	-3 mm
Reactivity experiments	5, 10, 20 and 30	1400-1500	Raw coal	-

* on bulk run-of-mine coal sample

The conventional analysis results of a similar Highveld seam 4 coal has been reported as being independent of particle size (Van der Merwe, 2010), therefore the influence of particle size on the conventional analysis was not investigated. The pore structure analysis was done on chars, which were prepared at 900 ˚C for one hour to ensure complete devolatilisation. A Fritsch Pulverisette 6-ball mill was used to pulverise the char sample for the CO_2 gas adsorption analysis. Bags developed by Nampak were used to store the coal samples; the bags are lined with aluminium foil to reduce gases diffusing into the bag. The sample is loaded into the bag and the bag is purged with nitrogen before sealing.

3.3 Experimental methodology

3.3.1 Mercury submersion

The mercury submersion experimental methodology is discussed in two sections: the experimental equipment and procedure.

Experimental equipment

Mercury submersion analysis is used for the determination of particle density on either single or multiple coal particles. For this, a laboratory mass balance (Sartorius ED 42025, maximum weight: 4.2 kg, accuracy: 0.01 g) and double distilled mercury (ACE (Pty) Ltd, purity > 99.5%) were used. The experimental setup for the mercury submersion analysis is shown schematically in Figure 3.2:

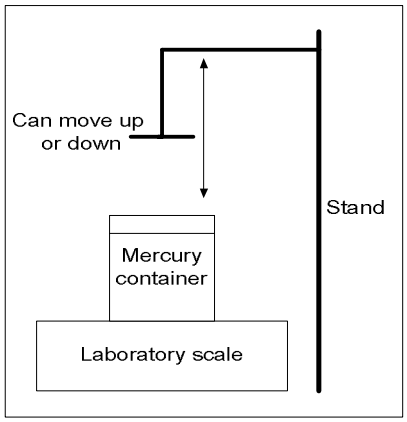

Figure 3.2: Schematic representation of mercury submersion equipment.

The setup is located inside a ventilation chamber to remove mercury vapour. The container is filled with mercury and placed onto the laboratory scale. The stand is used to submerge the coal particle into the mercury and can be moved up and down. The mercury submersion analysis is designed to determine the volume of particles having a diameter smaller than 40 mm. There are different plungers used for the various coal particle sizes. A basket plunger is used for the 5 and 10 mm particles, whereas a flat plate plunger is used for the 20 and 30 mm particles.

Experimental procedure

Single large coal particles were used for the 20 and 30 mm particle size density analysis, while multiple particles (between 10 and 20 particles) were used for the 5 and 10 mm particle sizes to ensure adequate mass. The three weight measurements required to determine the particle density of a coal sample are illustrated in Figure 3.3.

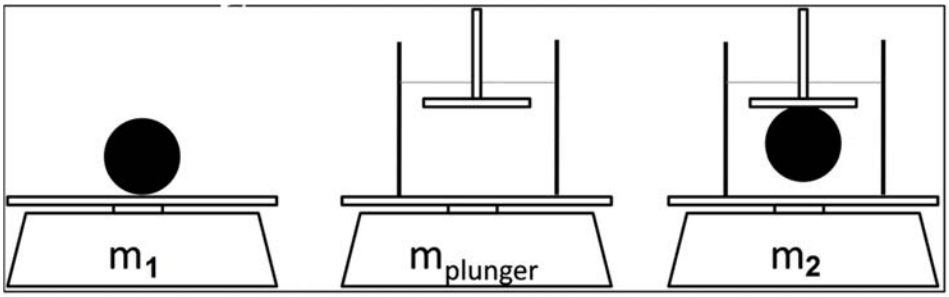

Figure 3.3: Three measurements required for particle density calculation.

The weight of the particle (m_1), weight of the submerged plunger ($m_{plunger}$) and weight of the submerged particle and plunger (m_2) are required to determine the particle density of the coal sample. The particle density (ρ_P) is calculated using Equation 3.1.

$$\rho_P = \left(\frac{m_1}{m_2 - m_{plunger}} \right) x \rho_{mercury} \qquad \text{Eq 3.1}$$

The experiment is repeated three times to determine repeatability and error of the particle density results. The largest error (95% confidence interval) obtained for the mercury submersion analysis is ± 3 kg/m^3 which is negligible when compared to the particle density (in the order of 1200 – 2200 kg/m^3). An equivalent spherical radius (r_p) is calculated using Equation 3.2.

$$r_p = \sqrt[3]{\frac{3m_1}{4\pi\rho_p}} \qquad \text{Eq 3.2}$$

The bulk sample selected on dimension and particle density was used for the reactivity experiments, pore structure analysis and petrographic analysis.

3.3.2 Conventional analysis

The proximate, ultimate and calorific value analysis was outsourced to Advanced Coal Technology Laboratories (Pty) Ltd. The ash composition analysis was outsourced to UIS Analytical Services. The standards used for the conventional analysis are shown in Table 3.3.

Table 3.3: Standards used for the conventional analysis.

Procedure	Standard used
Proximate analysis	
Sample preparation	SANS 18283: 2007 / ISO 18283: 2006
Moisture content	SANS 5925: 2007
Ash content	SABS ISO 1171: 1997
Volatile matter content	SABS ISO 562: 1998
Ultimate analysis	
Ultimate analysis	ISO 12902
Total sulphur	ISO 19579
Ash composition	
XRF	ASTM D4326
Calorific value	
Calorific value	SABS ISO 1928

3.3.3 Petrographic analysis

The petrographic analysis was outsourced to Petrographics SA. Petrographic blocks were prepared and polished in accordance with the ISO Standard 7404-2 (1985). The Vitrinite random reflectance was done on 100 readings according to ISO Standard 7404-5 (1994), whereas ISO standard 7404-3 (1994) was followed to analyse the group macerals (500 point-count technique). The total maceral reflectance scan was done on 250 random reflection readings and the coal microlithotype, carbominerite and minerite analysis was done according to ISO Standard 7404-4 (1988). The reactive inertinite macerals were identified according to the method developed by Smith *et al.* (1983) for South African high inertinite coal. The petrographical analysis is conducted to determine the associated distribution of maceral composition as a function of particle size due to natural breakage (from milling and transportation).

3.3.4 Gas adsorption analysis

The gas adsorption analysis was done at the North-West University. A Micrometrics ASAP 2010 Analyser was used to perform the CO_2 gas adsorption experiments. The char samples were degassed in the Analyser at 25 ˚C and a pressure < 4µm Hg for a period of 48 hours. After degassing, the char sample was analysed at a temperature of 0 °C using ice water as coolant. The Micrometrics ASAP 2010 Analyser software was used to determine the surface area using the BET and Langmuir gas adsorption models (Pohlmann *et al.*, 2010; Feng and Bhatia, 2003; Gürda and Yalçin, 2001; Marsh, 1987).

3.3.5 Mercury porosimetry analysis

The mercury porosimetry analysis on the char was done at the North-West University using a Micrometrics AutoPore IV 9500 VI.05 Analyzer. The penetrometer used was also supplied by Micrometrics and has a stem volume of 0.392 cm^3. The sample was loaded into the penetrometer and degassed at a pressure of 50 µmHg for 5 minutes. The bulk density was determined using low pressure analysis (3.59 kPa) and the skeletal density and total pore area was determined by high pressure analysis using a pressure range of 0.69 kPa to 413.7 MPa.

3.4 Results and discussion

3.4.1 Particle density analysis

The particle density results obtained for the 5, 10, 20 and 30 mm particles are shown in Figure 3.4.

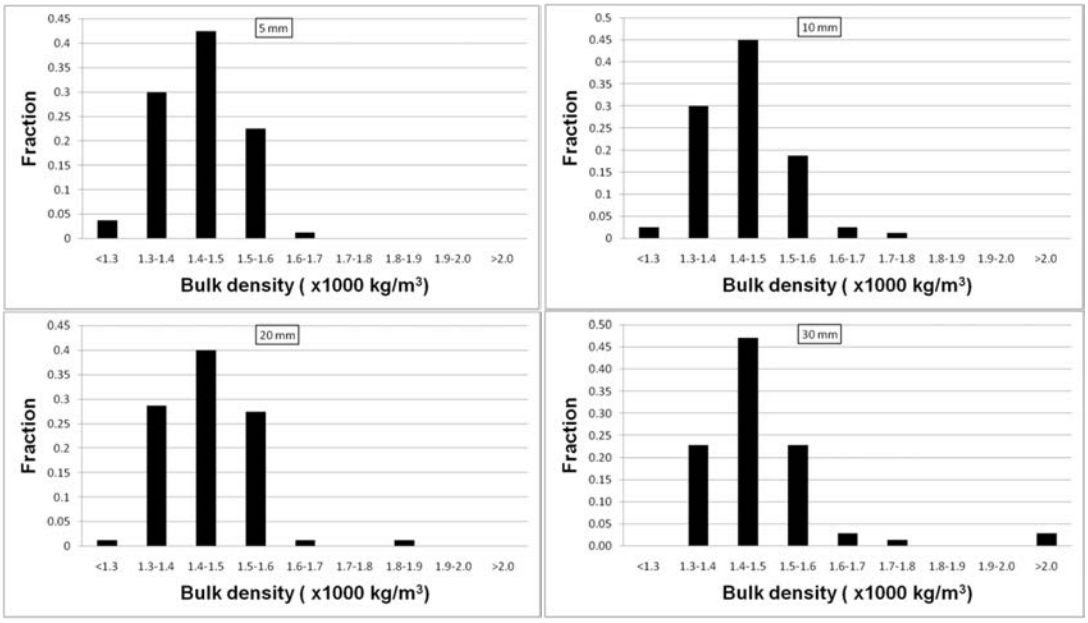

Figure 3.4: Particle density results for the 5, 10, 20 and 30 mm particles.

The particle density obtained falls between 1200 to 2200 kg/m^3 for all the particle sizes and a similar trend is also observed for all the particle sizes. The majority of the coal particles have a particle density between 1400 and 1500 kg/m^3, with the average particle density obtained for the 5, 10, 20 and 30 mm particles being 1435, 1440, 1457 and 1460 kg/m^3,

respectively. Similar values are reported by Rushdi and Gupta (2005) for Australian bituminous coals. The particle density range compares well to literature published by Finkelman *et al.* (1998), who observed a density range of $1200<\rho<1900$ kg/m^3 for low ash bituminous coal. A similar range ($1500<\rho<1900$ kg/m^3) was also observed by Saghafi *et al.* (2008) for Highveld coal. Everson *et al.* (2006) found densities as high as 2560 kg/m^3 for Highveld coal discards (very high ash content shale). A density cut between 1400 and 1500 kg/m^3 was used to screen the coal particles to increase the homogeneity of the coal samples used.

3.4.2 Proximate analysis

The results obtained for the proximate analysis are shown in Table 3.4, together with the results obtained by Pinheiro (1999) and Oberholzer (2009).

Table 3.4: Proximate analysis comparison (air dry basis).

Procedure	This study (wt%)	Oberholzer (2009) (wt%)	Pinheiro (1999) (wt%)
Moisture content	7.0	6.5	5.6
Ash content	18.4	20.5	28.3
Volatile matter content	23.4	22.3	22.0
Fixed carbon content	51.2	50.7	44.1
Fuel ratio	2.2	2.3	2.0

The results obtained for the proximate analysis are in accordance with results obtained by Oberholzer (2009). However, the ash and fixed carbon content differs when compared to Pinheiro (1999). The difference in the composition of the coal is possibly due to the different areas of the coal field mined over the past 11 years.

The results also compare well to previously published literature on various Highveld coals (Hattingh *et al.*, 2011; Saghafi *et al.*, 2008; Campbell *et al.*, 2010). The ash content for this coal is low when compared to the high ash values (25-40 wt%) reported for Highveld coal by Everson *et al.* (2006), Van Niekerk *et al.* (2008), Mishra *et al.* (2010) and Van Dyk *et al.* (2009). The fixed carbon content falls within the range (41 – 60 %wt) reported by Hattingh *et al.* (2011), Saghafi *et al.* (2008) and Campbell *et al.* (2010).

3.4.3 Ultimate analysis

The ultimate analysis is done on the raw coal sample and the results obtained are compared with Oberholzer (2009) and Pinheiro (1999), as shown in Table 3.5.

Table 3.5: Ultimate analysis results and comparison (dry ash free basis).

Procedure	This study (wt%)	Oberholzer (2009) (wt%)	Pinheiro (1999) (wt%)
Carbon content	72.8	70.9	78.9
Hydrogen content	4.5	5.0	4.2
Nitrogen content	1.8	1.7	2.0
Sulphur content	0.7	0.47	1.1
Oxygen content	20.1	21.8	13.8

The ultimate analysis results correlate well with the work done by Oberholzer (2009). However, a deviation is observed when the results are compared to that of Pinheiro (1999) i.e. the carbon and sulphur content is significantly higher, whereas, the oxygen content is lower. The higher ash content found by Pinheiro (1999) may contribute to the increase in carbon and sulphur content. The organic and inorganic composition of the coal contains both carbon and sulphur. During the ultimate analysis, mineral carbonates and sulphates decompose to release carbon dioxide and sulphur dioxide, increasing the measured carbon and sulphur contents (Speight, 2005).

The hydrogen, nitrogen and sulphur content is similar when compared to the ultimate analysis results reported on various Highveld coals by Van Niekerk *et al.* (2008), Everson *et al.* (2006), Wagner and Hlatshwayo (2005) and Hattingh *et al* (2011). However, the carbon content is lower, resulting in higher oxygen content, when compared to reported results. The carbon and oxygen content does, however, compare to the values reported by Hattingh *et al.* (2011).

3.4.4 Gross calorific value

The results obtained for the gross calorific value is compared to literature, as shown in Table 3.6

Table 3.6: Calorific value (MJ/kg) result and comparison (air dry basis).

Procedure	This study	Oberholzer (2009)	Pinheiro (1999)
Calorific value	22.6	22.3	19.7

The calorific value falls into the range (15 – 34.4 MJ/kg) reported for other Highveld coals (Hattingh *et al.*, 2011; Wagner and Hlatshwayo, 2005; Kruszewska, 2003), and also correlates well with what Oberholzer (2009) found. However, the calorific value obtained by Pinheiro (1999) is lower, which can be attributed to the relatively high ash content and low volatile matter content of the coal used by Pinheiro (1998) (Speight, 2005).

3.4.5 Ash composition

The results obtained from the XRF analysis are presented in Table 3.7.

Table 3.7: Results and comparison of ash composition.

Procedure	This study (%)	Oberholzer (2009) (%)	Pinheiro (1999) (%)
SiO_2	44.87	42.90	54.6
Al_2O_3	23.99	25.30	24.4
Fe_2O_3	2.92	1.29	4.35
P_2O_5	1.73	1.67	0.53
TiO_2	1.46	1.60	1.54
CaO	14.62	14.90	6.27
MgO	3.35	4.20	2.28
K_2O	0.38	0.32	0.87
Na_2O	0.84	0.89	0.47
SO_3	3.25	4.42	3.57
Other	2.59	2.51	1.12
Alkali index	5.9	5.8	3.3

The mineral matter present in the coal consists mostly of SiO_2 and Al_2O_3, with CaO the third most predominant inorganic species. The high concentrations of SiO_2 and Al_2O_3 compare to the values reported for Highveld coal (Matjie *et al.*, 2011; Mishra *et al.*, 2010; Van Dyk *et al.*, 2009; Hattingh *et al.*, 2011).

The CaO values reported for other Highveld coals range from 4.27 to 8.5 wt%, which is significantly lower than the value obtained for this coal (Matjie *et al.*, 2011; Mishra *et al.*, 2010; Van Dyk *et al.*, 2009). However, the value of 15.28 % reported by Hattingh *et al.* (2011) is comparable to the CaO value obtained in this study.

The XRF results obtained are comparable to Oberholzer (2009) and Pinheiro (1999). The fraction of SiO_2 and Fe_2O_3 is lower than found by Pinheiro (1999) and an increase is seen for the P_2O_5, CaO and Na_2O fractions. The alkali index as defined by Sakawa *et al.* (1982) is used to normalise the catalytic active and non-active species present in the coal. The alkali index for this sample is higher when compared to literature, due to an increased CaO

concentration. The alkali index calculated for this study correlates well with results presented by Oberholzer (2009), and a similar catalytic activity is expected due to inherent catalysis of the inorganic species.

3.4.6 Petrographic analysis

Petrographic analysis is used to determine the vitrinite random reflectance, group macerals, reactive inertinite macerals, total maceral reflectance, microlithotype, carbominerite and minerite analyses. The reflectance results obtained are shown in Table 3.8.

Table 3.8: Reflectance results and comparison.

	5 mm (vol%)	30 mm (vol%)	Oberholzer (2009) (vol%)	Pinheiro (1999) (vol%)
Vitrinite random reflectance	0.62	0.67	0.57	0.63
Total maceral reflectance	1.12	1.01	1.11	-

The vitrinite random reflectance obtained for both the samples are in the range reported for Highveld coal (0.57 – 0.8 vol%) (Van Dyk *et al.*, 2009; Campbell *et al.*, 2010; Hattingh *et al.*, 2011; Wagner and Hlatshwayo, 2005). The results obtained for the vitrinite random reflectance demonstrate that the different coal size fractions are of the same maturity, and using ISO standard 11760(2005), it is determined that both samples are characterised as bituminous medium Rank C and is a typical classification for Highveld coal (Hattingh *et al.*, 2011; Kruszewska, 2003). The same rank classification is noted by Oberholzer (2009) and Pinheiro (1999). The results obtained for the monomaceral analysis is shown in Table 3.9.

Table 3.9: Monomacerals analysis results and comparison (mineral matter free basis).

	5 mm (vol%)	30 mm (vol%)	Oberholzer (2009) (vol%)	Pinheiro (1999) (vol%)
Vitrinite	25	42	24	25
Liptinite	3	3	4	5
Inertinite	71	55	72	70

Both the coal size fractions are classified as an inertinite rich coal, as is expected for Highveld coal (Van Niekerk, 2008). The low liptinite content observed is also typical for Highveld coal (Van Niekerk, 2008; Wagner and Hlatshwayo, 2005; Hattingh *et al.*, 2011; Everson *et al.*, 2006). An increase in the vitrinite content is observed with an increase in particle size, however, this observation cannot be validated since only two particle sizes where used. In order to validate this trend, all particle sizes and repeatability tests should be conducted to ensure adequate validation due to the heterogeneous nature of coal. This

trend is opposite to what is observed by Yu *et al.* (2005), Man *et al.* (1998) and Estrele *et al.* (2002), as discussed in Section 2.5.1. The results obtained for the microlithotype analysis is shown in Table 3.10.

Table 3.10: Microlithotype analysis results and comparison.

	5 mm (vol%)	30 mm (vol%)	Oberholzer (2009) (vol%)
Pure vitrinite	12	18	9
Pure inertinite	37	29	40
Clarite	2	2	2
Durite	3	3	11
Vitrinertite	16	17	9
Trimacerite	10	13	8
Carbominerite	16	14	14
Minerite	4	4	7

The change in carbominerite, minerite, bi- and tri-macerals does not show significant deviation for the 2 different size fractions. The change observed for the different coal fractions of pure vitrinite and inertinite compares well to the monomacerals composition shown in Table 3.9. The results of the monomacerals and microlithotype analysis for the 5 mm coal sample compares to the literature obtained for coal from the same mine. However, the results for the 30 mm coal sample differ, which suggests that the particle size influences the monomacerals.

3.4.7 Mercury porosimetry analysis

The mercury porosimetry results for the different char particle sizes are presented in Table 3.11.

Table 3.11: Mercury porosimetry results for the different particle sizes.

	Pore area (m^2/g)	Average pore diameter (nm)	Bulk density (g/mL)	Skeletal density (g/ml)	Porosity (%)
5 mm	5.8	90	1.45	1.79	19
	7.7	79	1.42	1.81	22
	7.9	82	1.34	1.72	22
10 mm	7.9	54	1.40	1.65	15
	7.0	74	1.43	1.75	18
	6.4	60	1.54	1.80	15
20 mm	7.9	63	1.36	1.63	17
	8.3	65	1.34	1.63	18
	7.3	53	1.44	1.67	14
30 mm	10.1	40	1.44	1.69	14
	10.3	34	1.48	1.70	13
Average					
5 mm	7.2 ±2	84 ±11	1.40 ±0.11	1.77 ±0.09	21 ±3
10 mm	7.5 ±2	64 ±20	1.42 ±0.14	1.70 ±0.15	17 ±4
20 mm	7.8 ±1	60 ±12	1.38 ±0.10	1.65 ±0.05	16 ±4
30 mm	10.2 ±1	37 ±8	1.46 ±0.06	1.69 ±0.01	14 ±2

The bulk and skeletal density is independent of particle size, due to the density cut used to prepare the sample. The pore area observed (5.8 to 10.3 m^2/g) falls in the range reported (6.94 to 16.24 m^2/g) for chars by Wang *et al.* (2006). Bituminous char porosities reported in literature, for chars prepared at 900 ˚C, range from 4 to 50% (Gale *et al.*, 1995; Okolo, 2011), shows that the porosity obtained is within this range.

The pore area, average pore diameter and porosity are dependent on particle size. An increase in the particle size results in a decrease in the porosity and average pore diameter and an increase in the pore area. The phenomenon is explained combining the research conducted by Gale *et al.* (1995) and Stubington and Sasongko (1997). Gale *et al.* (1995), discovered that a decrease in heating rate results in a decrease in porosity for the Utah Blind Canyon coal. Stubington and Sasongko (1997) determined the influence of heating rate and volatile yield on the structural change of large coal particles. It was found that a decrease in surface area is observed for an increase in particle diameter. Therefore, it can be concluded that the decrease in porosity (with an increase in particle size) is possibly due to a large decrease in heating rate associated with an increase in particle size.

3.4.8 Gas adsorption analysis

Gas adsorption is used to characterise the surface area and pore structure of the coal using low-pressure adsorptions of gases. CO_2 is used to determine the micropore range. Figure 3.5 illustrates the influence of particle size on the micropore surface area obtained.

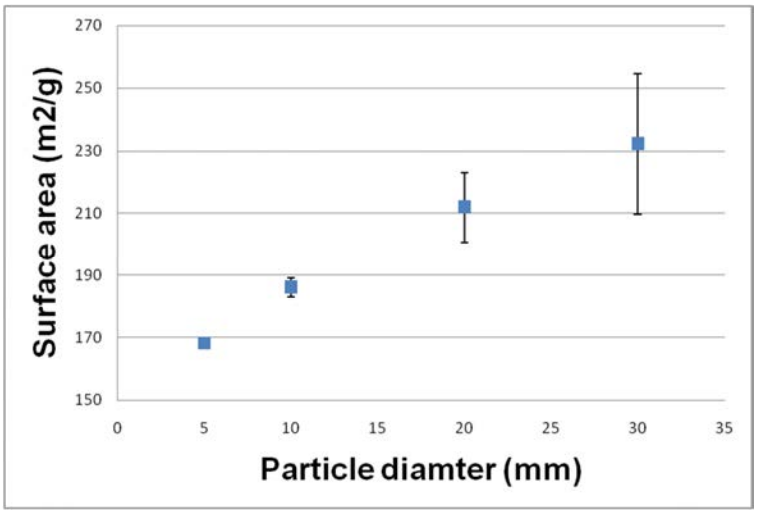

Figure 3.5: Particle influence on the char micropore surface area.

The values obtained for the BET and Langmuir micropore surface area range from 169 m^2/g to 255 m^2/g. Excellent repeatability is observed for the 5 and 10 mm gas adsorption results. However, for the 20 and 30 mm particles the micropore surface area deviates significantly and the deviation is attributed to the heterogeneous structure of the large coal particles. The surface area values obtained do fall in the range obtained by Liu *et al.* (2000) and Ruiz *et al.* (2001). Liu *et al.* (2000), studied 6 Australian bituminous coals and reported CO_2 BET up to 300 m^2/g (charred at 1100 ˚C).

From Figure 3.5 it is also noted that an increase in the particle size results in an increase in micropore surface area. The same trend was observed by Tomeczek and Mlonka (1998) and Yu *et al.* (2007). Combining the mercury porosimetry and gas adsorption analysis the following results are observed:

- Increase in particle size reduces the porosity obtained from mercury porosimetry.
- Increase in particle size reduces the pore diameter obtained from the mercury porosimetry.
- Increase in particle size increase the surface area (CO_2 gas adsorption analysis) and pore area (mercury porosimetry).

Combining these results suggests that less macro- and mesopores develop and more micropores develop during devolatilisation with an increase in particle size.

3.5 Summary

The majority of the coal particles have a particle density between 1400 and 1500 kg/m^3 while the average bulk density obtained for the 5, 10, 20 and 30 mm particles is 1435, 1440, 1457 and 1460 kg/m^3, respectively. A density cut between 1400 and 1500 kg/m^3 is used to increase the homogeneity of the coal sample used. All the coal characterisation analysis results are typical of South African Highveld seam 4 coal, when compared to literature. The results obtained for the coal and char characterisation are summarised in Table 3.12.

The petrographic analysis shows that the Highveld coal is inertinite-rich and that the coal maturity is independent of particle size. However, a higher vitrinite content is found in the larger coal particles.

The results obtained for the char pore structure analysis shows an increase in micropore structure with an increase in particle size. The slower heating rate of large coal particles results in the above-mentioned phenomena.

Table 3.12: Coal and char characterisation results.

Proximate analysis (as received)			
Sample preparation	**Density cut (kg/m^3)**	**Analysis**	**Result (wt%)**
Representative sample of the run-of-mine coal	-	Moisture content	7.0
		Ash content	18.4
		Volatile matter content	23.4
		Fixed carbon content	51.2
Ultimate analysis (dry ash free)			
Sample preparation	**Density cut (kg/m^3)**	**Analysis**	**Result (wt %)**
Representative sample of the run-of-mine coal	-	Carbon content	72.8
		Hydrogen content	4.5
		Nitrogen content	1.8
		Sulphur content	0.7
		Oxygen content	20.1
Calorific value (as received)			
Sample preparation	**Density cut (kg/m^3)**	**Analysis**	**Result (MJ/kg)**
Representative sample of the run-of-mine coal	-	CV value	22.6
Ash composition (as received)			
Sample preparation	**Density cut (kg/m^3)**	**Analysis**	**Result**
Representative sample of the run-of-mine coal	-	Alkali index	5.9

Mercury porosimetry						
Sample preparation	**Density cut (kg/m^3)**	**Analysis**	**Result**			
			5	**10**	**20**	**30**
Representative sample of the 5, 10, 20 and 30 mm. Charred at 900 C for 1hr. Crushed to -5mm using a plastic hammer.	1400 -1500	Pore area (m^2/g)	7.2 ±2	7.5 ±2	7.8 ±1	10.2 ±1
		Average pore diameter (nm)	84 ±11	64 ±20	60 ±12	37 ±8
		Porosity	21 ±3	17 ±4	16 ±4	14 ±2

CO_2 gas adsorption						
Sample preparation	**Density cut (kg/m^3)**	**Analysis**	**Result**			
			5	**10**	**20**	**30**
Representative sample of the 5, 10, 20 and 30 mm. Charred at 900 C for 1hr. Pulverised to -212 µm.	1400 -1500	BET micropore surface area (m^2/g)	168 ±1	186 ±3	212 ±11	232 ±23

Petrographic analysis (as received)				
Sample preparation	**Density cut (kg/m^3)**	**Analysis**	**Result**	
			5	**30**
A 150 g representative sample of the 5, 10, 20 and 30 mm particles was crushed to -3 mm using a plastic hammer	1400 -1500	Vitrinite random reflectance (vol%)	0.62	0.67
		Total maceral reflectance (vol%)	1.12	1.01
		Vitrinite (vol%)	25	42
		Liptinite (vol%)	3	3
		Inertinite (vol%)	71	55
		Pure vitrinite (vol%)	12	18
		Pure inertinite (vol%)	37	29
		Clarite (vol%)	2	2
		Durite (vol%)	3	3
		Vitrinertite (vol%)	16	17
		Trimacerite (vol%)	10	13
		Carbominerite (vol%)	16	14
		Minerite (vol%)	4	4

Chapter 4: Reactivity experimentation

The reactivity experimentation chapter consists of all the aspects required to produce the steam gasification reactivity results. The experimental methodology (Section 5.1) contains the experimental equipment, setup and procedures. Section 5.2 discusses the data acquisition procedures followed to determine the influence of particle size on the reactivity of coal. The qualitative influence of particle fragmentation, temperature and particle size on the reactivity of coal is discussed in Section 5.3. The validity of reactivity models applied on powder experiments are tested on the reactivity data obtained for large coal particles in Section 5.4. The quantitative influence of temperature and particle size on the steam gasification reactivity, using the initial reactivity obtained from reactivity models, is discussed in Section 5.5. The summary of Chapter 5 follows in Section 5.6.

4.1 Experimental methodology

4.1.1 Experimental equipment and setup

An in-house constructed large particle TGA was used for the reactivity experiments and was designed for using particle sizes up to 40 mm. The experimental setup is shown schematically in Figure 4.1:

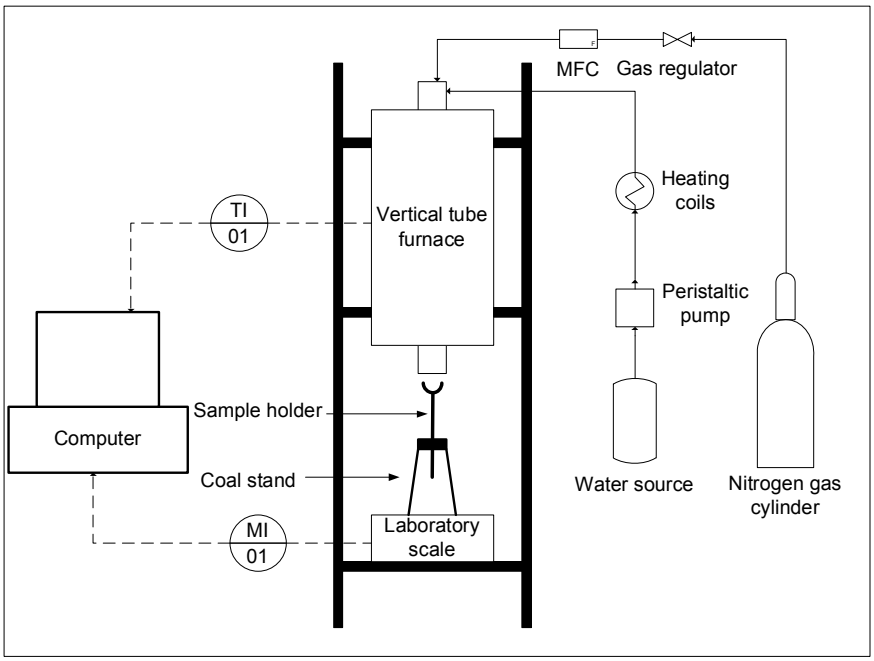

Figure 4.1: Schematic representation of reactivity experimental setup.

A vertical pipe furnace (supplied by Lenton Ltd.) with an inner pipe diameter of 50 mm was used. The furnace can be heated up with variable heating rates (up to 25 ˚C/min) and can reach a maximum temperature of 1500 ˚C. A 1 mm, K-type thermocouple was used to determine the temperature of the reaction zone inside the furnace, located in the gasification zone. The TGA is equipped with a steam generation unit consisting of a water source, heating mantle, stainless steel coils and a peristaltic pump. The water source is filled with deionised water (15 L storage capacity) and connected to the peristaltic pump (323 S/D Watson-Marlow Bredel high-performance variable speed pump). The steam is generated by pumping the water through the stainless steel coils (1/4 inch pipe) located inside the heating mantle. The heating mantle temperature was controlled at 300 ˚C. The nitrogen gas flow is controlled with a Brooks model 0254 mass flow controller and both the nitrogen and steam are introduced into the reactor at the top.

The sample mass is continually measured using a Radwag PS 750/C/2 precision balance. The coal sample is placed in a sample holder comprising of an aluminium tripod and quartz coal stand. The quartz coal stand was designed to increase the gas flow around the particle. The equipment and materials used are listed in Table 4.1.

Table 4.1: Experimental equipment and materials used for reactivity experimentation.

Equipment required	**Model**	**Range**
Furnace	Elite Thermal systems Ltd. TSV 15/50/180	Ambient – 1500 ˚C
Mass flow controller	Brooks Instruments	0 – 5 L/min
Peristaltic pump	Watson Marlow Bredel Pumps 323 U	0 – 0.115 L/min
Heating coils	Hi-Tech elements heating mantle	Ambient - 450 ˚C
Laboratory scale	Radwag PS 750/c/2	0-750 g
Materials used	**Grade**	**Purity**
Nitrogen gas	Ultra high purity grade	>99.999%
Water	Deionised	-

4.1.2 Experimental procedure

The reactor temperature was set to a required gasification temperature and the set nitrogen flow was injected into the reactor. Once thermal stable conditions were reached, the empty coal stand was inserted into the reactor and the mass balance was tared. Single coal (for the 20 and 30 mm) or multiple (for the 5 and 10 mm) particles were loaded into the basket and placed on the mass balance. The computer software was initialised and the furnace lowered over the coal sample. The mass and temperature were logged every 2 seconds for the duration of the experiment. Once mass loss had stabilised the particle was left in the heating zone for another 10 minutes to ensure complete devolatilisation. After the extra 10

minutes the peristaltic pump was started and steam was introduced into the reactor. The operating conditions used are shown in Table 4.2.

Table 4.2: Reactor operating conditions.

Condition	Value
Reaction temperature	775, 800, 850 and 900 °C
Reactor pressure	Atmospheric (87 kPa)
Steam concentration	80 mol %
Nitrogen flow	130 NL/hr
Particle size	5, 10, 20 and 30 mm

If a run was stopped due to power failure and adequate conversion (>70%) was obtained, the coal sample was ashed in the reactor. The nitrogen and steam flow to the reactor were closed and the particle was left in the reactor to combust until mass loss had stabilised. The stabilised reading was used as the ash mass for the specific reactivity experiment.

4.2 Data acquisition

The reactor temperature, sample mass and time were logged onto a csv file and imported into Microsoft Office Excel or Matlab®. Due to the array size limitations of Microsoft Excel, the data was first imported into Matlab® for processing. The raw data obtained for the 20 mm gasification experiments at 900 ˚C are shown in Figure 4.2.

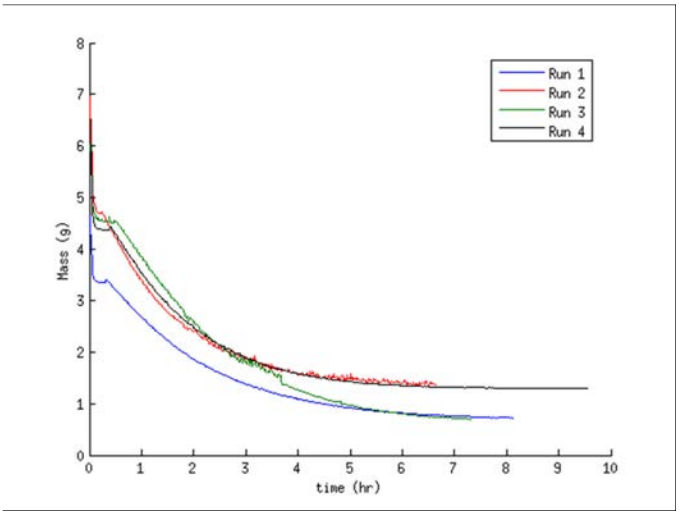

Figure 4.2: Mass loss curve of the 20 mm coal particles gasified at 900 ˚C.

Since not all the coal samples have the same mass, the raw data is normalised using Equation 4.1.

$$n_i = \frac{m_i}{m_0} \qquad \text{Eq 4.1}$$

The normalised data is sampled every minute to reduce the amount of data points to be processed. The normalised data obtained for the 20 mm gasification experiments at 900 °C is shown in Figure 4.3.

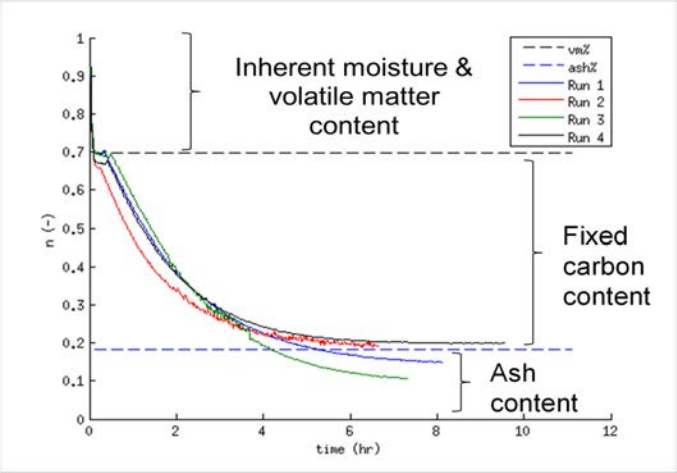

Figure 4.3: Normalised data versus time for the 20 mm steam gasification runs at 900 °C.

From Figure 4.3 it is seen that the normalised data can be sub-divided into the devolatilisation and carbon conversion reactions. The devolatilisation period occurs during the first 30 minutes of the experiment and is much faster than the carbon conversion period. Carbon conversion occurs due to the introduction of steam and is in the order of 12 hours (depending on gasification temperature). The volatile matter content (including inherent moisture, vm%) and ash content (ash%) according to the proximate analysis is shown on the graph to gauge complete devolatilisation and gasification. The observed volatile matter and ash content for all the reactivity experiments are 29 ±5 wt% and 17 ±6 wt% which compare well to the proximate analysis values (30.4 and 18.4 wt% respectively). The normalised data is used to determine the carbon conversion for each reactivity experiment using Equation 4.2.

$$X_i = \frac{n_g - n_i}{n_g - n_{ash}} \qquad \text{Eq 4.2}$$

The carbon conversion array is exported to Microsoft Office Excel and sampled using the Data Analysis tool pack to produce between 20 and 40 data points per run. The conversion versus time graph for the 20 mm particles gasified at 900 °C is shown in Figure 4.4.

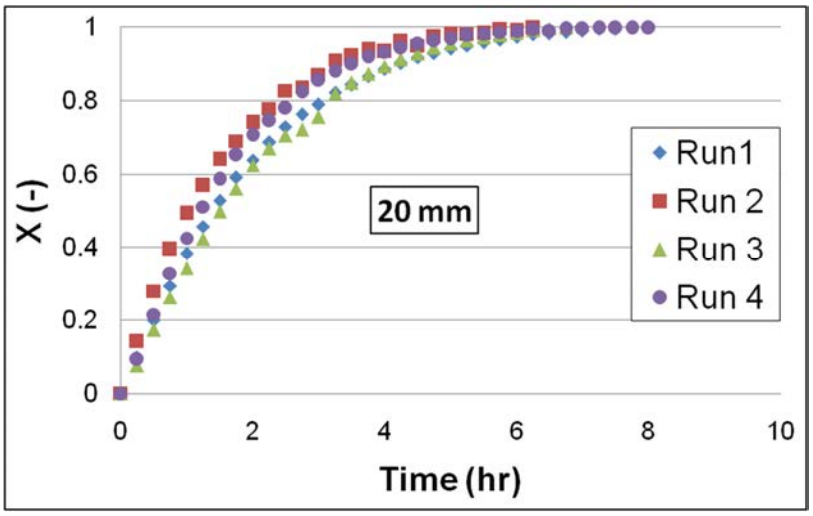

Figure 4.4: Conversion versus time graph of the 20 mm steam gasification reactions at 900 °C.

The average carbon conversion is obtained for the multiple runs and an experimental error is obtained using either average standard deviation (for 3 or more runs) or Equation 4.3 (for 2 runs).

$$\text{error} = \frac{\sum_{i=1}^{N} \frac{\left|X_{1,i} - X_{2,i}\right|}{\left(\frac{\left|X_{1,i} - X_{2,i}\right|}{2}\right)}}{N} \qquad \text{Eq 4.3}$$

The average carbon conversion and the error obtained for the 4 runs are shown in Figure 4.5.

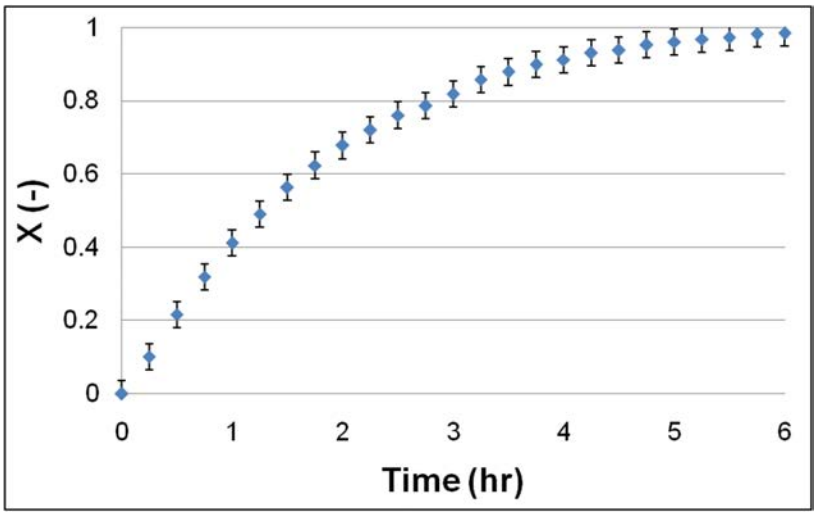

Figure 4.5: Average carbon conversion versus time graph for the 20 mm gasification at 900 °C.

The error obtained for all the gasification temperatures and particle sizes, range from 2 to 5 %. From here on, all carbon conversion results discussed in this section will be based on the average values. The data acquisition is repeated for all the particle sizes and gasification temperatures.

4.3 Conversion experiments

The influence observed for the particle fragmentation (Section 4.3.1), gasification temperature (Section 4.3.2) and particle size (Section 4.3.3) is qualitatively evaluated from the conversion experimental results.

4.3.1 Particle fragmentation

The ash produced after gasification was studied to determine the degree of fragmentation occurring during the gasification process. The results obtained from gasification at 900 °C are shown because devolatilisation at 900 °C is the severest case of fragmentation conditions undergone (highest temperature). Figure 4.6 shows the raw coal particles and the ash produced for the gasification of 5 mm coal particles at 900 °C.

Figure 4.6: Ash fragmentation visual inspection photo of 5 mm coal particles.

The photos in Figure 4.6 show no visible un-burnt carbon (dark spots) remaining after the reactivity experiments are completed. The particles also tend to reduce in size during gasification; this is due to the random distribution of ash as well as the low ash content in the particle. The particles which have undergone fragmentation are marked with yellow circles. The small fraction of 5 mm coal particles which fragmented, results in a small degree of

fragmentation for the 5 mm coal particles. The same observation is made for the all of the 5 and 10 mm reactivity experiments, irrespective of gasification temperature. At lower temperatures the amount and severity of visible cracks reduce even further. The ash fragmentation visual inspection photo of a 20 mm coal particle, gasified at 900 ˚C is shown in Figure 4.7.

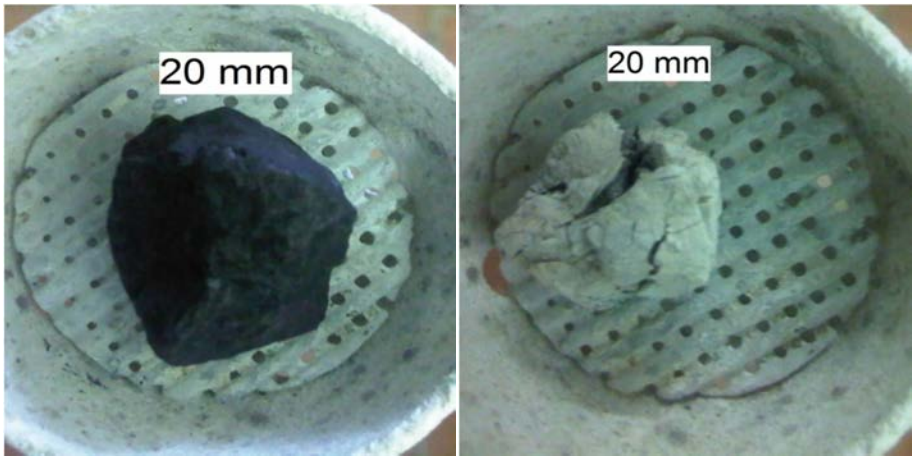

Figure 4.7: Ash fragmentation visual inspection photo of 20 mm coal particles.

An inspection of the 20 mm coal particle after gasification shows severe cracks. The cracks are larger than those observed for the 5 and 10 mm coal particles, however, the cracks did not fragment the particle. Although severe cracks are observed for the ashed particle, it stayed intact even after removal from the coal stand. The particle is still mechanically stable which also results in a small degree of particle fragmentation observed for the 20 mm coal particles. Figure 4.8 illustrates the ash fragmentation visual inspection of a 30 mm coal particle gasified at 900 ˚C.

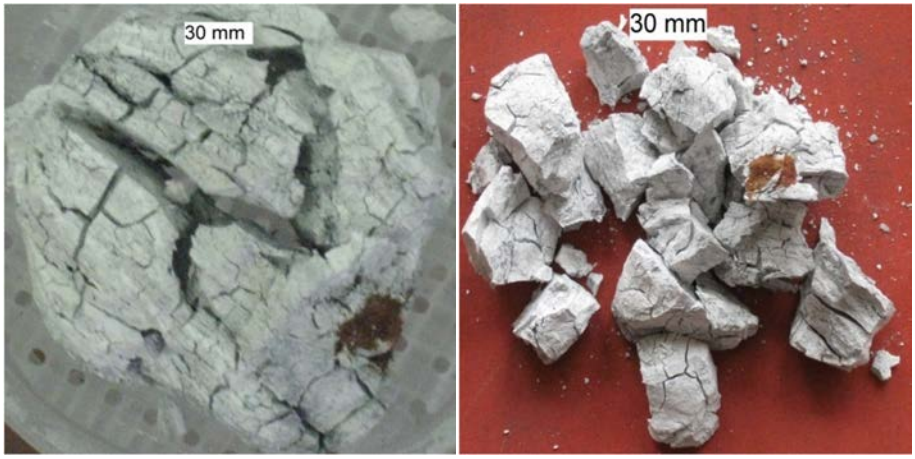

Figure 4.8: Ash fragmentation inspection photos of a 30 mm coal particle gasified at 900 ˚C.

The 30 mm particle also shows cracks on the edges of the particle (as seen for the 20 mm particle), however, very large cracks have caused fragmentation of the particle. The ash does not stay intact and is very brittle, naturally breaking into smaller particles on removal from the coal stand.

The particle fragmentation observed in this section includes primary and secondary fragmentation. Particle fragmentation will always occur for large coal particles, however, the observed fragmentation increases dramatically for the 30 mm particles. The 5, 10 and 20 mm particles are observed to be thermally stable and do not show a large degree of fragmentation.

4.3.2 Temperature dependence

The temperature dependence of the coal reactivity is determined by comparing the time versus conversion graphs for a set particle size at the different gasification temperatures. The time versus conversion graphs for the 5, 10, 20 and 30 mm particle sizes are shown in Figure 4.9.

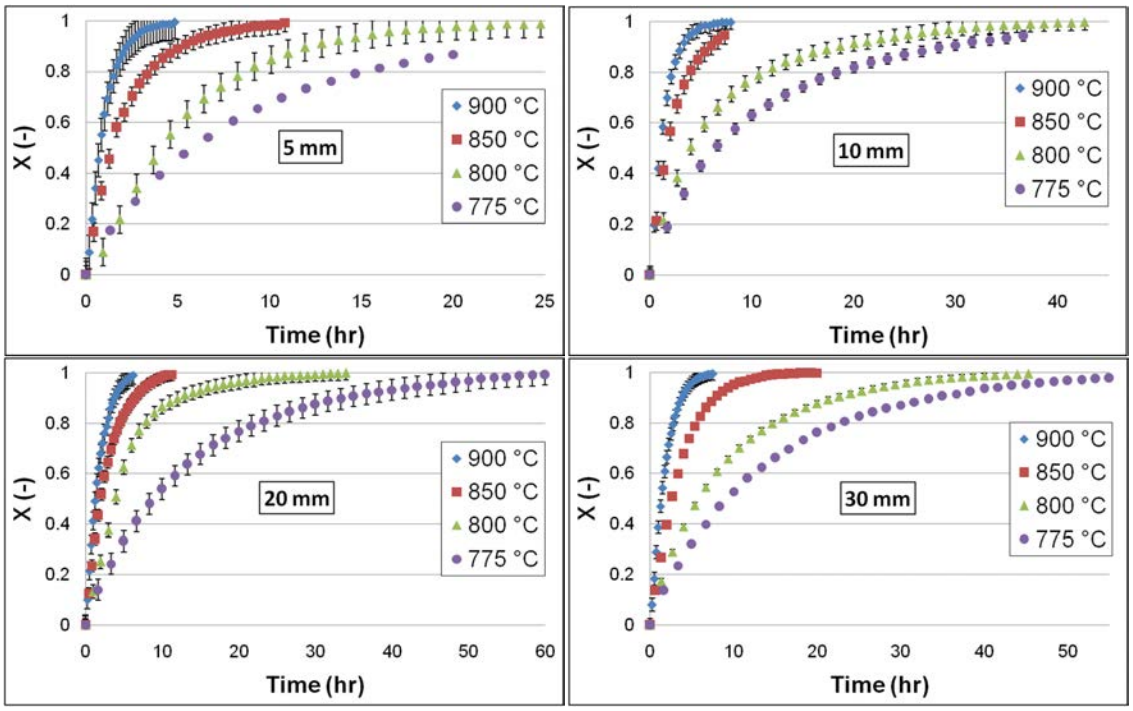

Figure 4.9: Conversion versus time graphs for the different particle sizes.

From Figure 4.9 it is observed that an increase in temperature decreases the time for full conversion for all 4 particle sizes. The temperature dependence of steam gasification

observed is what is expected when compared to literature *i.e.* Wu *et al.* (2006), Ye *et al.* (1998), Pinto *et al.* (2003), Xu *et al.* (2011) and Chu *et al.* (2006). The decrease in time for full conversion with an increase in temperature is interpreted as an increase in coal reactivity

4.3.3 Particle size dependence

To determine the influence of particle size on the reactivity of coal, the reactivity experimentation results for the different particle sizes are compared at a set temperature. The carbon conversion versus time graphs for the 775, 800, 850 and 900 ˚C gasification temperatures are shown in Figure 4.10.

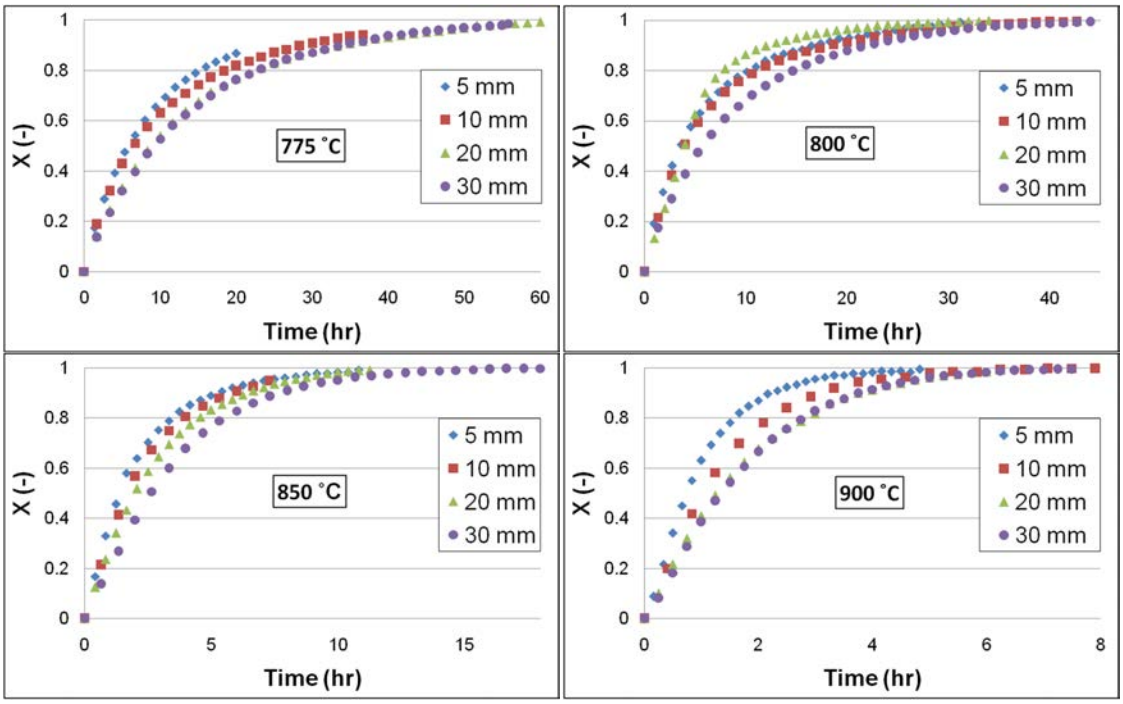

Figure 4.10: Carbon conversion versus time for 775, 800, 850 and 900 ˚C gasification temperatures.

A clear trend is observed for all the gasification temperatures. An increase in the particle size increases the time for full conversion. It is also observed that the 20 and 30 mm particle follow the same trend for most gasification temperatures. The only exception is at 800 ˚C, where the 20 mm coal particles showed the fastest conversion*.

* this phenomenon could not be explained and the trend is observed after 4 gasification experimental repeats with a very small experimental error of ±5%.

4.4 Model validation

The validation of powdered reactivity models on large coal particle experimental data is discussed in this section. The temperature and particle dependence of the dX/dt versus conversion graphs are studied in Section 4.4.1, followed by the model fitting procedure in Section 4.4.2. The models tested are divided into fundamental and empirical models. The homogenous, random pore and shrinking core models are classified as fundamental models and the Wen model is classified as a semi-empirical model. The validity of the fundamental and empirical models is discussed in Section 4.4.3 and 4.4.4, respectively.

4.4.1 Rate of carbon conversion

The rate of carbon conversion (gasification rate) was used by Wu *et al.* (2011), Kajitani *et al.* (2006), Wu *et al.* (2006) and Kajitani *et al.* (2002) to aid in the validation of reactivity models. The shape of the rate of carbon conversion is studied and compared to the shape obtained from the reactivity models. The rate of carbon conversion (r_c) is calculated using Equation 4.4 (Wu *et al.*, 2011).

$$r_{c,i} = \frac{dX_i}{dt_i} = \frac{X_i - X_{i-1}}{t_i - t_{i-1}} \qquad \text{Eq 4.4}$$

$$\text{normalised } \frac{dX_i}{dt_i} = \frac{dX_i}{dt_i} \Big/ \frac{dX_0}{dt_0} \qquad \text{Eq 4.5}$$

In order to compare the shape of multiple runs, the normalised dX/dt is used and calculated using Equation 4.5. The normalised dX/dt versus conversion curves for the different particle sizes at 900 ˚C, are shown in Figure 4.11.

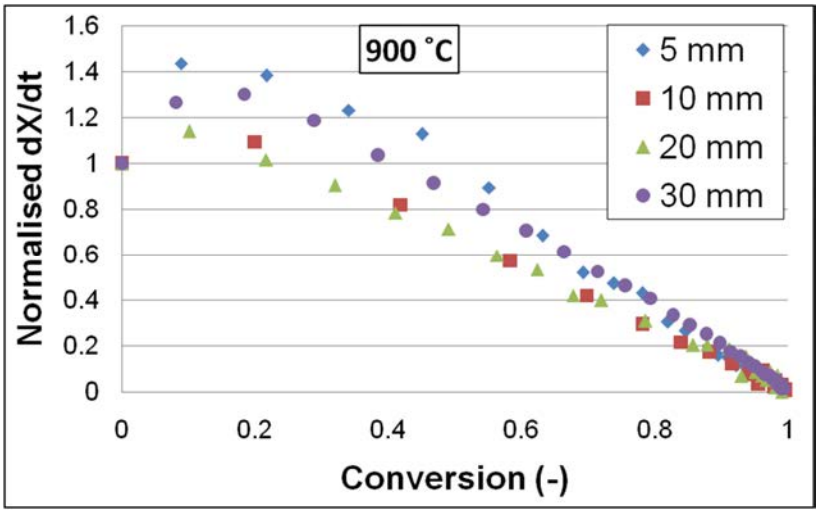

Figure 4.11: Influence of particle size on the shape of dX/dt versus conversion curves.

From Figure 4.11, similar shapes are observed for all particle sizes at 900 ˚C. The initial reactivity increases until a maximum is observed and then decreases until full conversion is obtained. The normalised dX/dt versus conversion curves for the 30 mm coal particles at 775, 800, 850 and 900 °C are shown in Figure 4.12.

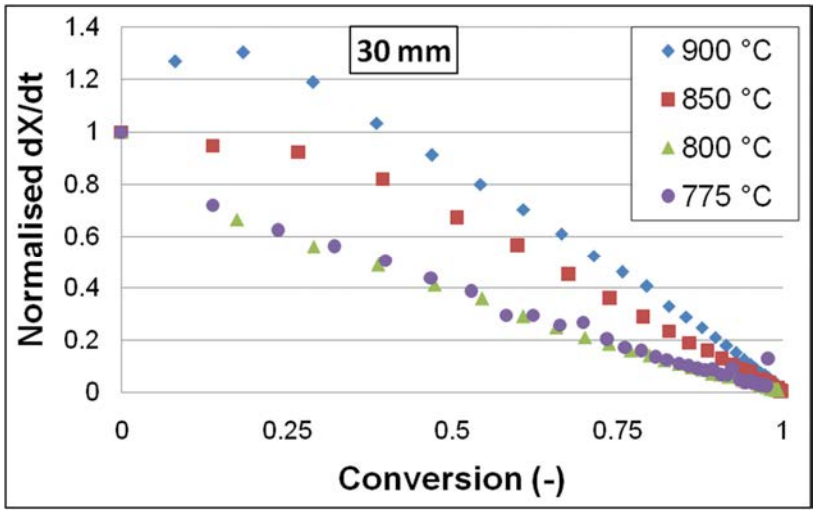

Figure 4.12: Influence of temperature on the shape of dX/dt versus conversion curves.

From Figure 4.12, it is observed that the dX/dt shape is dependent on the gasification temperature. At the highest temperature (900 ˚C) the reactivity increases to a maximum and then decreases. A maximum in carbon conversion rate was also reported by Wu *et al.* (2011), Kajitani *et al.* (2006), Wu *et al.* (2006) and Kajitani *et al.* (2002). According to Katjitani *et al.* (2002), this maximum can be predicted by the chemical controlled random pore model and not by the chemical reaction controlled shrinking core model. Wu *et al.*

(2006) also determined that the chemical reaction controlled shrinking core and homogenous model cannot predict the moderate peak, however, a combination of reaction and diffusion controlled shrinking core model can accurately predict the maximum observed in Figure 4.12. At the lower temperatures, the initial reactivity is the maximum and only a steady decrease is observed. This shape is observed for the chemical reaction controlled shrinking core model and homogenous model (Kajitani *et al.*, 2002; Wu *et al.*, 2006). It is also observed that the shape of the 775 and 800 °C curves (for the 5, 10 and 30 mm) is independent of gasification temperature (see Appendix A.5, Figure A.5). The temperature dependence of conversion rates suggests different mechanisms playing a role at different temperatures.

4.4.2 Model fitting procedure

The models are fitted to each individual reactivity run, and not to the average conversion. The particle diameter and bulk density (obtained as discussed in Section 4.2.2) of each run is used as constants, where needed. The fitting parameters are obtained using the sum of the least squared error. The reactivity models are fitted up to 90% conversion.

4.4.3 Fundamental models

In this section the fundamental models used on powdered reactivity experiments are tested to determine the validity of use on large coal particle research. The model evaluation is based on model fit as well as fitting parameter evaluation. The model fit, based on carbon conversion, predicts the carbon loss during gasification, while the fitting parameters are used to determine the steam gasification kinetics. The model fit, as well as the values of the fitting parameters are evaluated to determine the validity of a specific model.

Homogenous model

The homogenous model was used by Yang and Watkinson (1994), Lee and Kim (1995) and Fermoso *et al.* (2010), to predict carbon conversion reactivity results (without studying the influence of particle size). The homogenous model was also used to determine the influence of particle size on the reactivity of coal by Schmal *et al.* (1982) and Ye *et al.* (1998). The homogenous model equations are shown in Appendix B.1.1, as Equation B.1 and B.2 (Schmal *et al.*, 1982). The homogenous model is a particle shape and size independent model and therefore the resulting fitting parameter should be independent of particle size

(Ye *et al.*, 1998). Ye *et al.* (1998) further proposed that the homogenous model fit as well as the particle dependence of the fitting parameter should be investigated before concluding the validity of the homogenous model.

The homogenous model fits the carbon conversion for nearly all the particle sizes and gasification temperatures (see Appendix B.1.1, Figure B.1 to B.4). The values obtained from the homogenous model fits are shown in Appendix B.1.1, Table B.1. The reactivity constant of the 5, 10, 20 and 30 mm reactivity experiments increases from 0.11 to 1.11 s^{-1}, 0.08 to 0.78 s^{-1}, 0.07 to 0.7 s^{-1} and 0.06 to 0.66 s^{-1}, respectively which shows that an increase in the gasification temperature results in an increase in the reactivity constant for all particle sizes. This observation compares to the trends reported in literature (Lee and Kim, 1995; Ye *et al.*, 1998; Schmal *et al.*, 1982). Comparing the reactivity constant of the different particle size (at constant temperature) it is observed that a decrease in particle size results in an increase in reactivity. Although the homogenous model accurately predicts the carbon conversion, the particle dependence of the reactivity constant suggests that the homogenous model should not be used to calculate the steam gasification kinetics.

Shrinking core model

The shrinking core model (see Appendix B.1.2, Equation B.3 to B.5) has been used by Lee and Kim (1995), Gul-e-Rana and Ji-yu (2009), Karimi *et al*. (2010) to predict carbon conversion, while Revankar *et al.* (1987), Ye *et al.* (1998) and Huang and Watkinson (1996) determined the effect of particle size on the reactivity of coal using this model. All of the above-mentioned authors only studied the chemical reaction controlled regime, while Everson *et al.* (2005) and Wu *et al.* (2006) incorporated internal diffusion.

In order to determine the rate controlling step(s), the carbon conversion curves are normalised with respects to time. This allows carbon conversion shape comparison irrespective of time for full conversion. The normalisation is based upon time for 90% conversion (t_{90}), shown in Equation 4.6.

$$\text{normalised time} = \frac{t_i}{t_{90}} \qquad \text{Eq 4.6}$$

The normalisation of time also results in the 3 controlling step shapes being independent of the fitting parameter (as shown in Appendix B.1.2, Equation B.6 to B.8). The conversion versus normalised time for the experimental as well as the rate controlling steps of the shrinking core model, are compared in Appendix B.1.2, Figure B.5. From Figure B.5, it is

observed that the normalised conversion curves fall between the chemical reaction and ash diffusion control regime, which suggests that a combination of the chemical reaction and ash diffusion controlled regime determines the conversion rate. It is also observed that the carbon conversion curves at 900 °C (all particle sizes) follow similar trends to the chemical reaction control regime and as the temperature decrease the shape curves more towards the ash diffusion controlled shape. The equation used to fit the carbon conversion graphs is shown in Appendix B.1.2, Equation B.9.

The combined shrinking core model fits nearly all of the experimental data obtained (see Appendix B.1.2, Figure B.6 to B.9). The results obtained from fitting all the reactivity data with the combined shrinking core model are shown in Table B.2. The increase in gasification temperature results in an increase in the reactivity constant. This temperature dependence of the reactivity constant is also reported by Everson *et al.* (2005) and Wu *et al.* (2006) for the combined shrinking core model. The same trend is obtained for the temperature dependence of the effective ash diffusion coefficient (D_e), where an increase in gasification temperature increases D_e. The temperature dependence obtained for the D_e contradicts the results reported by Everson *et al.* (2005).
A decrease in the D_e value results in an increased ash diffusion effect (Van der Merwe, 2011). Combining this with the temperature dependence of the D_e results in an increased ash diffusion effect with a decrease in temperature, and contradicts the elementary gas-solid reaction principles proposed by Walker *et al.* (1959). Since the fitting parameter values oppose gas-solid reaction theory, it is proposed that the shrinking core model cannot be used to predict the steam gasification kinetics.

Random pore model

The chemical reaction controlled random pore model has been used to predict the reactivity of coal by Kajitani *et al.* (2002), Feng and Bhatia (2003) and Fermoso *et al.* (2010). The reaction rate and normalised time equations of the chemical reaction controlled random pore model are shown in Appendix B.1.3, Equation B.10 and B.11 (Bhatia and Perlmutter, 1980; Everson et al., 2011).

The chemical controlled random pore model is a particle size and gasification temperature independent model and is only dependent on the coal/char pore structure. The normalisation of time results in exclusion of the constant parameter (r_s, S_0 and ε_0) and thus the normalised time random pore model is only dependent on the structural parameter. The normalised time random pore model's (with structural parameter $\psi \rightarrow 0$, $\psi=1$ and $\psi=6$)

prediction of carbon conversion is compared to the experimental carbon conversion and shown in Appendix B.1.3, Figure B.10. From Figure B.10 a general trend is observed for all particle sizes used. The normalised time graph for the experimental data at 775 and 800 °C follows the exact same trend (for all particle sizes). The graphs are also more curved when compared to the 850 and 900 °C experimental data graphs. A narrow band, between the ψ=0 and ψ=6 graphs, is also observed in which the chemical reaction controlled random pore model will be able to predict the carbon conversion. However, most of the experimental data lies above the curve where ψ=0, which consequently results in a negative value for the structural parameter. A negative value for ψ will result in negative values for either L_0, S_0 or ε_0, since the structural parameter is a function of L_0, S_0 and ε_0 (see Appendix B.1.3, Equation B.12). Since these parameters all represent a physical measurement (pore length, surface area and porosity), negative values for these parameters will have no physical meaning.

According to Everson *et al.* (2011), the temperature dependence observed for the experimental results can be explained by increased pore diffusion effects. The random pore model is modified to include the Thiele modulus and accounts for pore diffusion. The fitting methodology assumes that at the lowest temperature the Thiele modulus is very small and little pore diffusion effects are observed. This assumption is only valid if enough evidence is provided that the lowest temperature is in the chemical reaction control regime. As mentioned above, the fitted structural parameter at the lowest temperature was negative, which is incorrect from a fundamental perspective. This indicates that the random pore model (chemical reaction controlled or including pore diffusion) cannot predict the entire range of experimental data.

The chemical controlled random pore model can only predict the carbon conversion at gasification temperatures of 850 and 900 ˚C, for the 20 and 30 mm coal particles. These fits are shown in Figure B.11 and B.12. The structural parameters obtained for the different particle sizes at 850 and 900 ˚C vary from 0.1 to 0.4 and 0.1 to 1.1, respectively (see Appendix B.1.4, Table B.3). A large variation is observed for the structural parameter obtained and it is also dependent on particle size and temperature. The particle size and temperature dependence of the structural parameter, combined with the inability of the random pore model to predict reactivity for the 5 and 10 mm coal particles, prove the invalidity of the random pore model to predict the steam gasification kinetics.

From the results obtained for the fundamental model validation, it can be concluded that the fundamental models accurately fit the carbon loss of most of the gasification reactivity experiments. However, critical evaluation of the fitting parameters, and the underlying

fundamental assumptions of the various models, result in meaningless chemical or physical properties.

4.4.4 Semi-empirical model

Because of the inability of the fundamental models to accurately predict the steam gasification kinetics, a semi-empirical model was chosen to predict the steam gasification kinetics. The Wen model was chosen as the semi-empirical model. The Wen model was introduced in 1968 by C.Y. Wen as an empirical model to predict a wide variety of rate of carbon conversion shapes. The model could also predict exact trends observed for the fundamental models (homogenous, shrinking core and random pore model). The equation proposed by Wen (1968) is shown in Equation 4.7.

$$\frac{dX}{dt} = k(1-X)^m \qquad \text{Eq. 4.7}$$

Since the order of solid reaction (m) is not set, the Wen model is a very robust model. When m = 2/3, the Wen model predicts similar trends to the reaction control shrinking core model, and when m=1 the Wen model predicts the homogenous model trend (Wen, 1968).

The Wen model accurately predicts the reactivity of coal for all particle sizes and gasification temperatures and results in a more accurate prediction when compared to the homogenous model due to the second fitting parameter (m, carbon reaction order), the fits are shown in Appendix B.1.4, Figure B.13 to B.16. The results for the fitting parameters obtained are shown in Table 4.3.

Table 4.3: Fitting parameters obtained using the Wen model.

	775 ˚C		800 ˚C		850 ˚C		900 ˚C	
	k	**m**	**k**	**m**	**k**	**m**	**k**	**m**
	0.13	1.25	0.23	1.30	0.48	1.12	0.90	0.95
5 mm	0.12	1.16	0.20	1.43	0.60	1.20	0.96	0.85
	0.14	1.27						
	0.12	1.33	0.21	1.36	0.51	1.04	0.62	0.87
10 mm	0.11	1.29	0.19	1.39	0.42	1.04	0.74	0.94
					0.36	1.04		
	0.076	1.18	0.18	1.04	0.31	0.87	0.48	0.88
20 mm	0.088	1.13	0.16	1.04	0.30	0.88	0.64	0.90
			0.21	1.16	0.36	1.01	0.40	0.69
			0.19	0.85			0.54	0.81
	0.072	1.13	0.13	1.14	0.25	0.82	0.44	0.81
30 mm	0.087	1.23	0.11	1.11	0.26	0.90	0.43	0.65
	0.076	1.01	0.13	1.23			0.54	0.77

A general trend is observed for the fitting parameter k, *i.e.* an increase in the temperature results in an increase in k. The fitting parameter m is defined as the order of reaction for the solid particles. The fitting parameter increases from <1 at 900 ˚C to >1 at 775 ˚C gasification temperature, which is not as common. The temperature dependence of m also predicts that different reaction models (with the corresponding m) will describe the reactivity of coal better at different temperatures. The Wen model is deemed to accurately predict the carbon loss as well as the steam gasification kinetics and can be used to quantitatively study the influence of temperature and particle size.

4.5 Temperature influence

The temperature influence can be quantitatively studied using the Arrhenius plot and the calculated activation energy. The Arrhenius plot for all coal particle sizes obtained from the Wen model is shown in Figure 4.13.

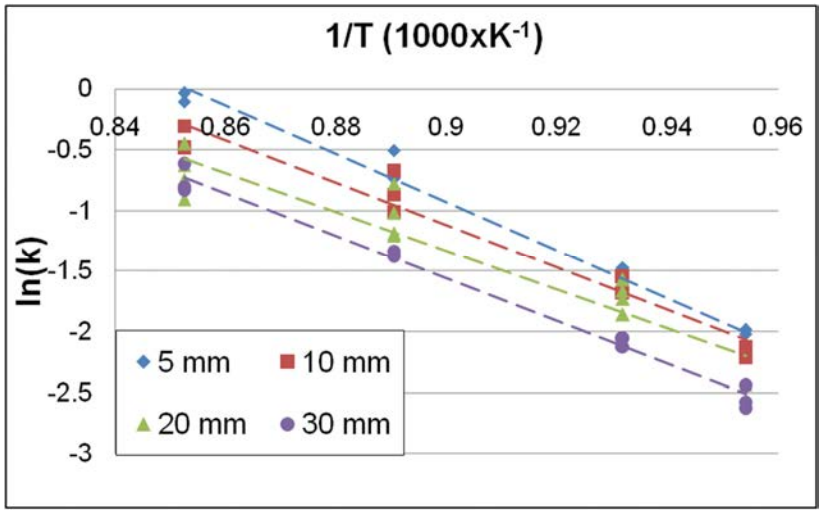

Figure 4.13: Arrhenius plot for the 5, 10, 20 and 30 mm coal particles.

The activation energy calculated for all the particle sizes are shown in Table 4.4.

Table 4.4: Activation energies calculated using the initial reactivity

	Activation energy (kJ/mol)
5 mm	165 ±11
10 mm	145 ±10
20 mm	141 ±10
30 mm	143 +9

The range of the activation energy (141 -165 kJ/mol) falls within the values reported in literature (Schmal *et al.*, 1983; Linares-Solano *et al.*, 1979; Kasoako *et al.*, 1985; Everson *et al.*, 2006; Ye *et al.*, 1998). Typical values reported on the steam gasification of South African Highveld coal by Everson *et al.* (2006) and Ye *et al.* (1998) are 143 and 131 kJ/mol, respectively. The activation energy obtained (141–165 kJ/mol) is in the range reported for Highveld coal (131-143 kJ/mol) and is even slightly higher which suggests that internal pore diffusion resistance is negligible and that the conversion is in the chemical reaction controlled regime.

The activation energy of the 5 mm coal particles is slightly higher than what is observed for the 10, 20 and 30 mm coal particles. The vitrinite content of the 5 and 30 mm coal particles is 25 and 42 vol%, respectively. It is proposed that the coal reactivity of the 5 mm particles is more dependent on temperature fluctuations partially due to the difference in petrographic composition.

4.6 Particle size influence

The observed particle influence is a combination of reactivity model mechanism as well as the particle's physical and chemical properties. The influence of the reactivity model mechanism is defined as the relation between reactivity and particle size (*i.e.* linear for the shrinking core model), whereas the particle's physical and chemical properties are also dependent on particle size as discussed in Section 3.4.6 and 3.4.7. To quantitatively determine the influence of particle size on the reactivity of coal, the increased reactivity observed for the decrease in particle size is studied. In order to do this the reactivity constant obtained from the Wen model is normalised using Equation 4.8.

$$\text{Average normalised } k_{i,T} = \frac{\overline{k_{i,T}}}{\overline{k_{30,T}}} \qquad \text{Eq. 4.8}$$

The average reactivity constant of the 5, 10 and 20 mm coal particles is normalised using the average reactivity constant of the 30 mm coal particles (at a set temperature). The results obtained for the average normalised reactivity constants are shown in Table 4.5.

Table 4.5: Average normalised reactivity constant obtained from the Wen model.

	775 ˚C Normalised k	800 ˚C Normalised k	850 ˚C Normalised k	900 ˚C Normalised k
5 mm	1.66 ±0.16	1.74 ±0.17	2.12 ±0.21	1.98 ±0.10
10 mm	1.47 ±0.12	1.62 ±0.13	1.69 ±0.22	1.45 ±0.14
20 mm	1.05 ±0.12	1.50 ±0.19	1.27 ±0.12	1.10 ±0.13
30 mm	1.00 ±0.11	1.00 ±0.09	1.00 ±0.05	1.00 ±0.08

From the normalised reactivity, it is observed that there is no significant influence in particle size when comparing the 20 and the 30 mm reactivity (except for the 800 °C). The large amount of fragmentation observed for the 30 mm coal particles may be responsible for particle size independent reactivity. The increase observed at 800 °C for the 20 mm coal particle was discussed in Section 4.3.3. A definite increase in the normalised reactivity is observed with a decrease in particle size for the 5 and 10 20 mm reactivity.

For all the gasification temperatures an increase of around 2 is observed when the particle size decreased from 30 to 5 mm. This result does show that an increase in particle size decreases the reactivity. Megraritis *et al.* (1999) and Cai *et al.* (1998) determined that the reactivity of inertinite is faster when compared to vitrinite and Sun *et al.* (2004) determined that the inherent catalyst increased the reactivity of inertinite more when compared to the vitrinite reactivity. The high inherent content of calcium (see Section 3.4.5, Table 3.7) may influence the reactivity of the monomacerals, which may explain the increased reactivity observed for the 5 mm coal particles.

As discussed in Section 4.5.1, the particle dependence of the steam gasification reactivity is not only dependent on reactivity model mechanism but might also be due to the combination of several different factors, such as fragmentation, petrographic composition and char pore structure which all vary with coal particle size.

4.7 Summary

Chapter 4 consists of the qualitative and quantitative study on the influence of particle fragmentation, gasification temperature and particle size. A large degree of particle fragmentation was observed for the 30 mm coal particle, which was not observed for the 20 mm (and smaller) coal particles. The qualitative analysis shows that an increase in temperature and decrease in particles size, increased the coal reactivity.

In order to quantitatively study the influence of temperature and particle size on the steam gasification of coal, steam gasification was obtained from reactivity models used for powdered experiment predictions. The temperature dependence of the dX/dt versus conversion graphs shows that different conversion mechanisms may apply at different gasification temperatures. The homogenous and shrinking core model fit the reactivity of coal, however, the fitting parameters of both models were considered not to be applicable. The chemical reaction controlled random pore model can only predict the reactivity data of

the 20 and 30 mm coal particles at gasification temperatures of 850 and 900 °C. The fundamental models used to predict powdered coal reactivity, accurately fit the carbon loss data but cannot be used to predict the steam gasification kinetics. A semi-empirical model (Wen model) was used to obtain the steam gasification kinetics. The temperature dependence of m (solid order of reaction) confirms the hypothesis that different conversion mechanisms may apply at different gasification temperatures.

The activation energy calculated from the Wen model range from 143 to 165 kJ/mol. The influence of particle size for the 20 and 30 mm reactivity is negligible which may be due to the large degree of particle fragmentation observed for the 30 mm coal particles. A non-linear decrease is observed in the reactivity with a decrease in particle size from 30 to 5 mm. The particle dependence of the steam gasification reactivity is not only dependent on reactivity model mechanism but includes a combination of several different factors, such as fragmentation, petrographic composition and char pore structure, which varies with coal particle size.

Chapter 5: Conclusions and recommendations

5.1 Conclusions

A general coal characterisation (including conventional characterisation, petrographic composition and char pore structure) was conducted on the coal. The reactivity data of the different particle sizes were obtained and model prediction of the different powdered reactivity models were tested. The following conclusions regarding the characterisation and coal reactivity can be drawn:

5.1.1 Coal characterisation

The conventional coal characterisation, petrographic analysis and char structure analysis all showed results typical for Highveld seam 4 coal/chars. To increase the homogeneity of coal sample a density cut was used, the average particle density of the different particle sizes falls in the range of 1400-1500 kg/m^3, which was used as the density cut. The size, shape and density selected particles were used for the petrographic analysis, char pore structure analysis and reactivity experiments

The particle size did not influence the coal rank (or coal maturity) and microlithotype composition. However, the particle size influenced the monomaceral composition. The vitrinite content increased from 25 to 42 vol% for the 5 and 30 mm particles, respectively. The particle size was also determined to influence the char pore structure using CO_2 gas adsorption and mercury porosimetry analysis. An increase in particle size resulted in decrease in porosity, smaller average pore diameter and an increase in surface area (BET surface area for CO_2 gas adsorption and pore area for mercury porosimetry).

5.1.2 Reactivity experiments

From the reactivity experimentation the following qualitative conclusions were made:

- Particle fragmentation was dependent on particle size.
- The reaction rate was dependent on gasification temperature.
- The reaction rate was dependent on coal particle size.

It was found that the 30 mm coal particles experienced a large degree of fragmentation during devolatilisation and gasification which was not observed for the other particle sizes. An increase in gasification temperature resulted in an increase in the reaction rate. It was also found that increasing the particle size decreased the reaction rate.

5.1.3 Experimental data modelling

Three fundamental models, the homogenous, shrinking core and random pore model, and one semi-empirical model (Wen model) were used to predict the reactivity of large coal particles. The fundamental models were able to predict the experimental carbon conversion, but after critically evaluating the fitting parameters it was determined that fundamental models could not be used to determine the steam gasification kinetics. A semi-empirical model (Wen model) was therefore used to obtain the various reaction kinetics constants.

The initial reactivity obtained from the Wen model was used to qualitatively determine the influence of gasification temperature and particle size on the steam gasification kinetics. The activation energy calculated for the 5, 10, 20 and 30 mm coal particles are 165, 145, 150 and 143 kJ/mol, respectively. The activation energy was calculated using the initial reactivity, gasification temperatures and Arrhenius plots. The high activation energy obtained for the 5 mm coal particle is proposed to be due to the difference in petrographic composition.

The initial reactivity obtained from the Wen model was normalised using the 30 mm initial reactivity, in order to study the influence of particle size on the steam gasification kinetics. A six fold increase in the particle size results in a twofold decrease in reactivity; the increase is also found to be non-linear. When comparing the normalised initial reactivity of the 20 and 30 mm coal particles, no significant difference is observed. The large degree of particle fragmentation observed for the 30 mm coal particle is proposed to cause this phenomenon. The observed influence of particle size on the steam gasification kinetics can be attributed to both the reaction model mechanism, and chemical and physical properties particle of the sample, such as fragmentation, petrographic composition and char pore structure, which all varies with coal particle size.

5.2 Recommendations for future investigations

The following recommendations are proposed to assist future studies in the field of steam gasification of large coal particles:

- Study the reactivity of powdered coal to aid in the explanation of observed results for large coal particles, since gasification with powdered coal is less associated with fragmentation and diffusion effects.
- Study the influence of devolatilisation temperature on the char pore structure in more detail.
- Create a batch char (at a set temperature and heating rate) for the reactivity experiments to reduce influence of particle size on char pore structure.
- Study the change in char pore structure during the gasification process to aid in the determination of models or modification of fundamental models.
- Study the effect of steam partial pressure on the steam gasification of large coal particles.
- Do petrographic analysis on the intermediate particle sizes in order to improve correlation of steam gasification kinetics with petrographic composition.
- Study the influence of particle size on the steam gasification mechanism, in order to determine the influence of particle size on the hydrogen inhibition and multi-gas gasification Langmuir-Hinshelwood constants. Test the validity of the Langmuir-Hinselwood including hydrogen and multigas gasification effects on the reactivity data

Bibliography

ADANEZ, J. and L. F. DE DIEGO. 1993. Reactivity of lignite chars with CO_2: Influence of the mineral matter. *International Chemical Engineering*. **33**(4), pp.656-662.

AKTAS, Z., F. KARACAN, and A. OLCAY. 1998. Centrifugal float-sink separation of fine Turkish coals in dense media. *Fuel Precessing Technology*. **55**, pp.235-250.

ALONSO, M., A. G. BORREGO, D. ALVAREZ, and R. MENENDEZ. 1999. Pyrolysis behaviour of pulverised coals at different temperatures. *Fuel*. **78**, pp.1501-1513.

BARRANCO, R., M. CLOKE, and E. LESTER. 2003. Prediction of the burnout performance of some South American coals using a drop-tube furnace. *Fuel*. **82**, pp.1893-1899.

BAYARSAIKHAN, B., N. SONOYAMA, S. HOSOKAI, T. SHIMADA, J. -I. HAYASHI, C. -Z. LI and T. CHIBA. 2006. Inhibition of steam gasification of char by volatiles in a fluidized bed under continuous feeding of a brown coal. *Fuel*. **85**, p.340–349.

BERTRAND, P., M. L. BORDENAVE, E. BROSSE, J. ESPITALIR, J. P. HOUZAY, B. PRADIER, M. VAN DER BROUCKE and F. WALGENWITZ. 1993. Other methods and tools for source rock appraisal. *In*: M. L. BORDENAVE, (ed). *Applied Petroleum Geochemistry*, Paris : France: Editions Technip, p.524.

BHATIA, S. K. and D. D. PERLMUTTER. 1980. A random pore model for fluid-solid reactions: 1. Isothermal, kinetic control. *AIChE Journal*. **26**(3), pp.379-385.

BUNT, J. R. and F. B. WAANDERS. 2008. An understanding of lump coal physical property behaviour (density and particle size effects) impacting on a commercial-scale Sasol-Lurgi FBDB gasifier. *Fuel*. **87**, pp.2856-2865.

CAI, H. Y., A. J. GUELL, I. N. CHATZAKIS, J. Y. LIM, D. R. DUGWELL and R. KANDIYOTI. 1996. Combustion reactivity and morphological change in coal chars: Effect of pyrolysis temperature, heating rate and pressure. *Fuel*. **75**, pp.15-24.

CAI, H. -Y., A. MEGARITIS, R. MESSENBOCK, M. DIX, D. R. DUGWELL and R. KANDIYOTI. 1998. Pyrolysis of coal maceral concentrates under pf-combustion conditions (1): change in volatile release and char combustibility as a function of rank. *Fuel*. **77**, pp.1273-1282.

CAMPBELL, Q. P., J. R. BUNT, and F. DE WAAL. 2010. Investigation of lump coal agglomeration in a non-pressurized reactor. *Journal of Analytical and Applied Pyrolysis*. **89**(2), pp.271-277.

CARD, J. B. A. and A. R. JONES. 1995. A drop tube furnace study of coal combustion and unburned carbon content using optical techniques. *Combustion and flame*. **101**, pp.539-547.

CETIN, E., B. MOGHTADERI, R. GUPTA, and T. F. WALL. 2004. Influence of pyrolysis conditions on the structure and gasification reactivity of biomass chars. *Fuel*. **83**, pp.2139-2150.

CHEN, S. G., R. T. YANG, F. KAPTEIJN, and J. A. MOULIJN. 1993. A New Surface Oxygen Complex on Carbon: Toward a Unified Mechanism for Carbon Gasification Reactions. *Ind. Eng. Chem. Res.* **32**, pp.2835-2840.

CHOI, C. and G. DYRKACZ. 1989. Base-Catalyzed Separation of Coal Macerals. *Energy & Fuels*. **3**, pp.579-585.

CHU, X., W. LI, B. LI, and H. CHEN. 2006. Gasification property of direct coal liquefaction residue with steam. *Process safety and environmental protection*. **84**(B6), pp.440-445.

COUSINS, A., N. PATERSON, D. R. DUGWELL, and R. KANDIYOTI. 2006. An Investigation of the Reactivity of Chars Formed in Fluidized Bed Gasifiers: The Effect of Reaction Conditions and Particle Size on Coal Char Reactivity. *Energy & Fuels*. **20**, pp.2489-2497.

DACOMBE, P., M. POURKASHANIAN, A. WILLIAMS, and L. YAP. 1999. Combustion-induced fragmentation behavior of isolated coal particles. *Fuel*. **78**, pp.1847-1857.

DAVINI, P., P. GHETTI, L. BONFANTI, and G. DE MICHELE. 1996. Investigation of the combustion of particles of coal. *Fuel*. **75**(9), pp.1083-1088.

DE LA PUENTE, G., M. J. IGLESIAS, E. FUENTE, and J. J. PISS. 1998. Changes in the structure of coals of different rank due to oxidation-effects on pyrolysis behaviour. *Journal of Analytical and Applied Pyrolysis*. **47**, pp.33-42.

DEMIRBAS, A. 2009. *Biohydrogen: for future engine fuel demands*. London: Springer. pp.275.

DENBIGH, K. G. and J. C. TURNER. 1971. *Chemical reactor theory: An introduction*. 2nd ed. London: Cambridge University Press. pp.224

DENBIGH, K. G. 1966. *Chemical reactor theory*. London: Cambridge University Press. pp.184

DEVI, T. G. and M. P. KANNAN. 2000. Gasification of Biomass Chars in Air - Effect of Heat Treatment Temperature. *Energy & Fuels*. **14**, pp.127-130.

DOMAZETIS, G., M. RAOARUN, B. D. JAMES, and J. LIESEGANG. 2008. Molecular modelling and experimental studies on steam gasification of low-rank coals catalysed by iron species. *Applied Catalysis A: General*. **340**, p.105–118.

DU, S. -W., W. -H. CHEN, and J. A. LUCAS. 2010. Pulverized coal burnout in blast furnace simulated by a drop tube furnace. *Energy*. **32**, pp.576-581.

EVERSON, R., H. NEOMAGUS, and R. KAITANO. 2005. The modeling of the combustion of high-ash coal–char particles suitable for pressurised fluidized bed combustion: shrinking reacted core model. *Fuel*. **84**, pp.1136-1143.

EVERSON, R. C., H. W. J. P. NEOMAGUS, and R. KAITANO. 2011. The random pore model with intraparticle diffusion for the description of combustion of char particles derived from mineral- and inertinite rich coal. *Fuel*. **90**(7), pp.2347-2352.

EVERSON, R. C., H. W. J. P. NEOMAGUS, R. KAITANO, R. FALCON, C. VAN ALPHEN and V. M. DU CANN. 2008. Properties of high ash char particles derived from inertinite-rich coal: 1. Chemical, structural and petrographic characteristics. *Fuel*. **87**, pp.3082-3090.

EVERSON, R. C., H. W. NEOMAGUS, H. KASAINI, and D. NJAPHA. 2006. Reaction kinetics of pulverized coal-chars derived from inertinite-rich coal discards: Gasification with carbon dioxide and steam. *Fuel*. **85**, p.1076–1082.

ESTRELE, J.S.,Y. KOLATSCHEK, and G.O. O'BRIEN. 2002. Relationship between in situ coal stratigraphy and particle size and composition after breakage in bituminous coals. *International Journal of Coal Geology*. **49**, pp.95-214.

FENG, B. and S. K. BHATIA. 2003. Variation of the pore structure of coal chars during gasification. *Carbon*. **41**, pp.507-523.

FENG, B., S. K. BHATIA, and J. C. BARRY. 2003. Variation of the crystalline structure of coal char during gasification. *Energy & Fuels*. **17**, pp.744-754.

FERMOSO, J., M. V. GIL, C. PEVIDA, J. J. PIS AND F. RUBIERA. 2010. Kinetic models comparison for non-isothermal steam gasification of coal-biomass blend chars. *Chemical Engineering Journal*. **161**, pp.276-284.

FIELD, M. A., D. W. GILL, B. B. MORGAN, and P. G. W. HAWKSLEY. 1967. *Combustion of pulverised coal*. London: Leatherhead: The British Coal Utilisation Research. pp. 413

FINKELMAN, R. B., N. H. BOSTICK, F. T. DULONG, F. E. SENFTLE and A. N. THORPE. 1998. Influence of an igneous intrusion on the inorganic geochemistry of a bituminous coal from Pitkin County, Colorado. *International Journal of Coal Geology*. **36**, pp.223-241.

FUNG, D., C. FAIRBRIDGE, and R. ANDERSON. 1998. Gasification reactivity of Canadian anthracite and semi-anthracite chars. *Fuel*. **67**, p.753.

FUSHIMI, C., T. WADA, and A. TSUTSUMI. 2011. Inhibition of steam gasification of biomass. *Biomass and bioenergy*. **35**, pp.179-185.

FU, W. B. and Q. H. WANG. 2001. A general relationship between the kinetic parameters for the gasification of coal chars with CO_2 and coal type. *Fuel processing technology*. **72**, pp.63-77.

GALE, T. K., C. H. BARTHOLOMEW, and T. H. FLETCHER. 1995. Decreases in the Swelling and Porosity of Bituminous Coals during Devolatilization at High Heating Rates. *Combustion and Flame*. **100**, pp.94-100.

GINTER, D. M., G. A. SOMORJAI, and H. HEINEMANN. 1993. Factors affecting the reactivity of chars and cokes during low-temperature (640℃) steam gasification. *Energy & Fuels*. **7**, p.393.

GUL-E-RANA, J. and Z. JI-YU. 2009. Catalytic gasification of Pakistani Lakhra and Thar lignite chars in steam gasification. *Journal of Fuel chemistry and technology*. **37**(1), pp.11-19.

GÜRDA, G. and M. N. YALÇIN. 2001. Pore volume and surface area of the Carboniferous coals from the Zonguldak basin (NW Turkey) and their variations. *International journal of coal geology*. **48**, pp.133-144.

HANSON, S., J. W. PATRICK, and A. WALKER. 2002. The effect of coal particle size on the pyrolysis and steam gasification. *Fuel*. **81**, pp.531-537.

HATTINGH, B. B., R. C. EVERSON, H. W. J. P. NEOMAGUS, and J. R. BUNT. 2011. Assessing the catalytic effect of coal ash constituents on the CO_2 gasification rate of high ash, South African coal. *Fuel Processing Technology*. **92**, pp.2048-2054.

HIGMAN, C. and M. VAN DER BURGT. 2008. *Gasification*. 2nd ed. Gulf Professional Publishing. pp.435

HOLIKOVA, K., R. ŽAJDLIK, J. MARKOS, and L. JELEMENSKY. 2005. Comparison of Single Coal Char Particle Combustion at Different Conditions. *Chemical Papers*. **59**, p.413-420.

HUANG, J. and A. P. WATKINSON. 1996. Coal gasification in a stirred bed reactor. *Fuel*. **75**, pp.1617-1624.

HUANG, Z., J. ZHANG, Y. ZHAO, H. ZHANG and Y. GUANXI. 2010. Kinetic studies of char gasification by steam and CO_2 in the presence of H_2 and CO. *Fuel Processing Technology*. **91**, p.843–847.

HÜTTINGER, K. J. and C. NATTERMAN. 1994. Correlation between coal reactivity and inorganic matter content for pressure gasification with steam and carbon dioxide. *Fuel*. **73**, pp.1682-1684.

JONES, R. B., C. B. MCCOURT, C. MORLEY, and K. KING. 1985. Maceral and rank influence on the morphology of coal char. *Fuel*. **64**, pp.1460-1467.

KABE, T., A. ISHIHARA, E. W. QIAN, I. P. SUTRISAN and Y. KABE. 2004. *Coal and coal-related compounds: Structures, reactivity and catalytic reactions*. Tokyo, Japan: Elsevier.

KADYSZEWSKI, J. 2003. Monitoring Carbon Adsorption in the Terrestrial Ecosphere. *In*: *National Academy of Engineering, 2003*. Washington: Washington DC: National Academies Press, p.131.

KAJITANI, S., S. HARA, and H. MATSUDA. 2002. Gasification rate analysis of coal char with a pressurized drop tube furnace. *Fuel*. **81**(5), pp.539-546.

KAJITANI, S., N. SUZUKI, M. ASHIZAWA, and S. HARA. 2006. CO_2 gasification rate analysis of coal char in entrained flow coal gasifier. *Fuel*. **85**, pp.163-169.

KAPTEIJN, F., G. ABBEL, and J. A. MOULIJN. 1984. CO_2 gasification of carbon catalysed by alkali metals: Reactivity and mechanism. *Fuel*. **63**(8), pp.1036-1042.

KAPTEIJN, F., R. MEIJER, and J. A. MOULIJN. 1992. Transient Kinetic Techniques for Detailed Insight in Gas-Solid Reactions. *Energy & Fuels*. **6**, pp.494-497.

KARIMI, A., N. SEMAGINA, and M. R. GRAY. 2011. Kinetics of catalytic steam gasification of bitumen coke. *Fuel*. **90**, pp.1285-1291.

KASOAKO, S., Y. SAKATA, and C. TONG. 1985. Kinetic evaluation of the reactivity of various coals for gasification with carbon dioxide in comparison with steam. *International Chemical Engineering*. **25**(1), pp.160-175.

KLOSE, W. and M. WOLKI. 2005. On the intrinsic reaction rate of biomass char gasification with carbon dioxide and steam. *Fuel*. **84** , p.885–892.

KOLASINSKI, K. W. 2008. *Surface science: foundations of catalysis and nanoscience*. 2nd ed. Hoboken, NJ: John Wiley & Sons Inc. pp.486

KRUSZEWSKA, K. J. 2003. Fluorescing macerals in South African coals. *International Journal of Coal Geology*. **54**, pp.79-94.

KÜHL, H., M. M. KASHANI-MOTLAGH, H. J. MÜHLEN, and K. H. VAN HEEK. 1992. Controlled gasification of different carbon materials and development of pore structure. *Fuel*. **71**, pp.879-882.

KWON, T., S. D. KIM, and D. P. C. FUNG. 1987. Reaction kinetics of char-CO_2 gasification. *Fuel*. **67**, pp.530-535.

LAPIDUS, L. and N. R. AMUNDSON. 1977. *Chemical reactor theory: A review*. Englewood Cliffs:N.J.: Prentice-Hall, Inc. pp. 856

LEE, J. W. and S. D. KIM. 1995. Catalytic activity of alkali and transition metal salt mixture for steam-char gasification. *Fuel*. **74**(9), pp.1387-1393.

LEVENSPIEL, O. 1999. *Chemical reaction engineering*. 3rd ed. Hoboken, NJ: Wiley & Sons, Inc. pp.668

LINARES-SOLANO, A., O. P. MAHAJAN, and P. L. WALKER. 1979. Reactivity of heat-treated coals in steam. *Fuel*. **58**, pp.327-332.

LIU, K., Z. CUI, and T. H. FLETCHER. 2010. Coal gasification. *In*: K. LIU, C. SONG, and V. SUBRAMANI, (eds). *Hydrogen and Syngas Production and Purification Technologies*, Hoboken : New Jersey: John Wiley & Sons, Inc., p.533.

LIU, G.-S., A. G. TATE, G. W. BRYANT, and T. F. WALL. 2000. Mathematical modeling of coal char reactivity with CO_2 at high pressures and temperatures. *Fuel*. **79**, pp.1145-1154.

LIU, G., H. WU, R. P. GUPTA, J. A. LUCAS, A. G. TATE and T. F. WALL. 2000. Modeling the fragmentation of non-uniform porous char particles during pulverized coal combustion. *Fuel*. **79**, pp.627-633.

LORENZ, H., E. CARREA, M. TAMURA, and J. HAAS. 2000. The role of char surface structure development in pulverised fuel combustion. *Fuel*. **79**, pp.1161-1172.

LU, G. Q. and D. D. DO. 1992. A kinetic study of coal reject-derived char activation with CO_2, H_2O and air. *Carbon*. **30**(1), pp.21-29.

LUSSIER, M., Z. ZHANG, and D. J. MILLER. 1998. Characterizing rate inhibition in steam/hydrogen gasification via analysis of adsorbed hydrogen. *Carbon*. **36**, p.1361–1369.

MAN, C.K., J. JACOBS and J.R. GIBBINS. 1998. Selective maceral enrichment during grinding and effect of particle size on coal devolatilisation yields. *Fuel Processing Technology*. **56**, pp.215-227.

MAROTO-VALER, M., D. TAULBEE, J. ANDRESEN, J. C. HOWER and C. E. SNAPE. 1998. Quantitative ^{13}C NMR study of structural variations within the vitrinite and inertinite maceral groups for a semifusinite-rich bituminous coal. *Fuel*. **77**(8), pp.805-813.

MARSH, H. 1987. Adsorption methods to study microporosity in coals and carbon-a critique. *Carbon*. **25**, pp.49-58.

MASEL, R. I. 1996. *Principles of adsorption and reaction on solid surfaces*. Hoboken, NJ: John Wiley and Sons. pp.804.

MATJIE, R. H., D. FRENCH, C. R. WARD, P. C. PISTORIUS and Z. LI. 2011. Behaviour of coal mineral matter in sintering and slagging of ash during the gasification process. *Fuel Processing Technology*. **92**(8), pp.1426-1433.

MATSUOKA, K., D. KAJIWARA, K. KURAMOTO, A. SHARMA and Y. SUZUKI. 2009. Factors affecting steam gasification rate of low rank coal char in a pressurized fluidized bed. *Fuel Processing Technology*. **90**, p.895–900.

MEGARITIS, A., Y. ZHUO, R. MESSENBOCK, D. R. DUGWELL and R. KANDIYOTI. 1998. Pyrolysis and Gasification in a Bench-Scale High-Pressure Fluidised-Bed Reactor. *Energy & Fuel*. **12**, pp.144-151.

MEGRARITIS, A., R. C. MESSENBOCK, I. N. CHATZAKIS, D. R. DUGWELL and R. KANDIYOTI. 1999. High-pressure pyrolysis and CO_2-gasification of coal maceral concentrates: conversions and char combustion reactivities. *Fuel*. **78**, pp.871-882.

MERMOUDA, F., S. SALVADORB, L. VAN DE STEENE, and F. GOLFIER. 2006. Influence of the pyrolysis heating rate on the steam gasification rate of large wood char particles. *Fuel*. **85**, pp.1473-1482.

MESSENBOCK, R. C., N. P. PATERSON, D. R. DUGWELL, and R. KANDIYOTI. 2000. Factors governing reactivity in low temperature coal gasification. Part 1. An attempt to correlate results from a suite of coals with experiments on maceral concentrates. *Fuel*. **79**, pp.109-121.

MILLER, B. G. 2005. *Coal energy systems*. San Diego : California: Elsevier Ltd. pp.526.

MILLER, B. G. and A. DAVID. 2008. *Combustion engineering issues for solid fuel systems*. London : Elsevier Inc. pp.496.

MIMS, C. A. and J. K. PABST. 1983. Role of surface salt complexes in alkali-catalysed carbon gasification. *Fuel*. **62**, pp.176-179.

MISHRA, S. B., S. P. LANGWENYA, B. B. MAMBA, and M. BALAKRISHNAN. 2010. Study on surface morphology and physicochemical properties of raw and activated South African coal and coal fly ash. *Physics and Chemistry of the Earth, Parts A/B/C*. **35**, pp.811-814.

MIURA, K., K. HASHIMOTO, and P. L. SILVERTON. 1989. Factors affecting the reactivity of coal chars during gasification, and indices representing reactivity. *Fuel*. **68**, pp.1461-1475.

MOLINA, A. and F. MONDRAGON. 1998. Reactivity of coal gasification with steam and CO_2. *Fuel*. **77**, p.1831–1839.

MÜHLEN, H.-J., K. H. VAN HEEK, and H. JÜNTGEN. 1985. Kinetic studies of steam gasification of char in the presence of H_2, CO_2 and CO. *Fuel*. **64**, pp.944-949.

OBERHOLZER, A. 2009. *Characterisation and steam gasification of large, low grade coal particles using a specially designed thermo gravimetric analyser*. Potchefstroom: NWU. (Dissertation - M.Eng). *Classified*

OKOLO, G. N. 2011. *The effects of chemical and physical properties of chars derived from inertinite-rich, high ash coals on gasification reaction kinetics*. Potchefstroom: NWU. (Dissertation - M.Eng)

PENG, F. F., I. C. LEE, and R. Y. K. YANG. 1995. Reactivities of in situ and ex situ coal chars during gasification in steam at 1000 - 1400℃. *Fuel Processing Technology*. **41**, p.233.

PINTO, F., C. FRANCO, R. N. ANDRE, C. TAVARES, M. DIAS, I. GULYURTLU and I. CABRITY. 2003. Effect of experimental conditions on co-gasification of coal, biomass and plastics wastes with air mixtures in a fluidized bed system. *Fuel*. **82**, pp.1967-1976.

PINHEIRO, H.J. 1999. A techno-economic and historical review of the South African coal industry in the 19th and 20th centuries AND analyses of coal product samples of South African collieries 1998-1999. (In Bulletin 113. SABS: Pretoria. 97p.)

POHLMANN, J. G., E. OSORIO, A. C. F. VILELA, and A. G. BORREGO. 2010. Reactivity to CO_2 of chars prepared in O_2/N_2 and O_2/CO_2 mixtures for pulverized coal injection (PCI) in blast furnace in relation to char petrographic characteristics. *International Journal of Coal Geology*. **84**, pp.293-300.

REVANKAR, V. V. S., A. N. GOKARN, and L. K. DORIASWAMY. 1987. Studies in Catalytic Steam Gasification of Petroleum Coke with Special Reference to the Effect of Particle Size. *Industrial Engineering Chemistry*. **26**, pp.1018-1025.

REZAIYAN, J. and N. P. CHEREMISINOFF. 2005. *Gasification Technologies: A primer for engineers and Scientists*. Boca Raton: Taylor & Francis Group. pp.336

RHODES, M. 2008. *Introduction to particle technology*. 2nd ed. Hoboken, NJ: John Whiley & Sons, Ltd. pp.450

SAGHAFI, A., K. L. PINETOWN, P. G. GROBLER, and J. H. P. VAN HEERDEN. 2008. CO_2 storage potential of South African coals and gas entrapment enhancement due to igneous intrusions. *International Journal of Coal Geology*. **73**, pp.74-87.

SAKAWA, M., Y. SAKURAI, and Y. HARA. 1982. Influence of coal characteristics on CO_2 gasification. *Fuel*. **61**, pp.717-720.

SASONGKO, D. and J. F. STUBINGTON. 1996. Significant factors affecting devolatilization of fragmenting, non-swelling coals in fluidized bed combustion. *Chemical Engineering Science*. **51**(16), pp.3909-3918.

SCARONI, A. W., P. L. WALKER, and R. H. ESSENHIGH. 1981. Kinetics of lignite pyrolysis in an entrained-flow, isothermal furnace. *Fuel*. **60**, pp.71-76.

SCHMAL, M., J. M. MONTEIRO, and J. L. CASTELLAN. 1982. Kinetics of coal gasification. *Ind. Eng. Chem. Process*. **21**, pp.256-266.

SCHMAL, M., J. L. MONTEIRO, and H. TOSCANI. 1983. Gasification of High Ash Content Coals with Steam in a Semibatch Fluidized Bed Reactor. *Industrial and Engineering Chemistry Process Design*. **22**, pp.563-570.

SCHOBERT, H. 1991. *The Chemistry of Hydrocarbon Fuels*. Butterworth-Heinemann Publishers. pp.352

SEAMES, W. S. 2003. An initial study of the fine fragmentation fly ash particle mode generated during pulverized coal combustion. *Fuel Processing Technology*. **81**(2), pp.109-125.

SEKINE, Y., K. ISHIKAWA, E. KIKUCHI, M. MATSUKATA and A. AKIMOTO. 2006. Reactivity and structural change of coal char during steam gasification. *Fuel*. **85**(2), pp.122-126.

SENNECA, O., M. URCIUOLO, R. CHIRONE, and D. CUMBO. 2011. An experimental study of fragmentation of coals during fast pyrolysis at high temperature and pressure. *Fuel*. **90**, pp.2931-2938.

SHENQI, X., Z. ZHIJIE, Y. GUANGSUO, and W. FUCHEN. 2011. Effects of alkaline metal on coal gasification at pyrolysis and gasification phases. *Fuel*. **90**, pp.1723-1730.

SHETH, A., Y. D. YEBOAH, A. GODAVARTY, Y. XU and A. AKIMOTO. 2003. Catalytic gasification of coal using eutectic salts: reaction kinetics with binary and ternary eutectic catalysts. *Fuel*. **82**, pp.305-317.

SMITH, W. H., H. J. ROUX, and J. G. H. STEYN. 1983. The classification of coal macerals and their relation to certain chemical and physical parameters of coal. *Special publication of the Geological Society of South Africa*. **7**, pp.111-115.

SOLOMON, P. R. and T. H. FLETCHER. 1994. Influence of coal pyrolysis on combustion. *In*: *Proceedings of the 25th international combustion symposium, 1994*., pp.463-474.

SPEIGHT, J. G. 2005. *Chemical Analysis: A series of monographs on analytical chemistry and its application*. New Jersey: John Wiley & Sons, Inc. pp.223.

SPLIETHOFF, H. 2010. *Power generation from solid fuels*. London: Springer-Verlag. pp.672

SRIVASTAVA, R. D., H. G. MCILVRIED, J. C. WINSLOW, C. P. MARONDE and R. P. NOCETI. 2007. Coal Technology for Power, Liquid and Chemicals. *In*: J. A. KENT, (ed). *Kent and Riegel's handbook of Industrial Chemistry and Biotechnology*, NY:NY: Springer Science+Business Media, LLC., p.931.

STUBINGTON, J. F., G. HUANG, and A. W. SCARONI. 1991. Devolatilization times of mm-size coal particles. *Fuel*. **70**(9), pp.1105-1108.

STUBINGTON, J. F. and T. M. LINJEWILE. 1989. The effects of fragmentation on devolatilization of large coal particles. *Fuel*. **68**, pp.155-160.

STUBINGTON, J. F. and D. SASONGKO. 1998. On the heating rate and volatile yield for coal particles injected into fluidised bed combustors. *Fuel*. **77**, pp.1021-1025.

SUÁREZ-RUIZ, I. and J. C. CRELLING. 2008. *Applied Coal Petrology The Role of Petrology in Coal Utilization*. San Diego, California: Elsevier, Ltd. pp.388.

SUNGGYU, L., J. G. SPEIGHT, and S. K. LOYALKA. 2007. *Handbook of alternative fuel technologies*. CRC Press. pp.552.

SUN, Q., W. LI, H. CHEN, and B. LI. 2004. The CO_2-gasification and kinetics of Shenmu maceral chars with and without catalyst. *Fuel*. **83**, pp.1787-1793.

TAMHANKAR, S. S., J. T. SEARS, and C.-Y. WEN. 1984. Coal pyrolysis at high temperatures and pressures. *Fuel*. **63**, pp.1230-1235.

TOMECZEK, J. and J. MLONKA. 1998. The parameters of a random pore network with spherical vesicles for coal structure modelling. *Fuel*. **77**(15), pp.1841-1844.

TYLER, R. J. and H. N. SCHAFER. 1980. Flash pyrolysis of coals: influence of cations on the devolatilization behaviour of brown coals. *Fuel*. **59**, pp.487-494.

VAN DER MERWE, G. W. 2011. *The influence of particle size and density on the combustion of highveld coal*. Potchefstroom: NWU. (Dissertation - M.Eng).

VAN DER MERWE, G. L. 2010. *The influence of particle size and devolatilisation conditions on the CO_2 gasification of Highveld coal*. Potchefstroom: NWU. (Dissertation - M.Eng).

VAN DYK, J. C. 2001. Development of an alternative laboratory method to determine thermal fragmentation of coal sources during pyrolysis in the gasification process. *Fuel*. **80**, pp.245-249.

VAN DYK, J. C., S. A. BENSON, M. L. LAUMB, and B. WAANDERS. 2009. Coal and coal ash characteristics to understand mineral transformations and slag formation. *Fuel*. **88**(6), pp.1057-1063.

VAN HEEK, K. H. and H. -J. MÜHLEN. 1900. Chemical kinetics of carbon and char gasification. *In*: J. LAHAYE and P. EHRBURGER, (eds). *Fundamental issues in control of carbon gasification reactivity*, Dordrecht: Kluwer Academic Publishers, p.622.

VAN NIEKERK, D. 2008. *Structural elucidation, molecular representation and solvent interactions of vitrinite-rich and inertinite-rich South African coals*. Pennsylvania: Pennsylvania Sate University. (Dissertation - PhD)

VAN NIEKERK, D. and J. MATHEWS. 2010. Molecular representations of Permian-aged vitrinite-rich and inertinite-rich South African coals. *Fuel*. **89**, pp.73-82.

VAN NIEKERK, D., R. J. PUGMIRE, M. S. SOLUM, P. C. PAINTER and J. P. MATHEWS. 2008. Structural characterization of vitrinite-rich and inertinite-rich Permian-aged South African bituminous coals. *International Journal of Coal Geology*. **74**(4), pp.290-300.

WAGNER, N. J. and B. HLATSHWAYO. 2005. The occurrence of potentially hazardous trace elements in five Highveld coals, South Africa. *International Journal of Coal Geology*. **63**, pp.228-246.

WALKER, P. L., F. RUSINKO, and L. G. AUSTIN. 1959. Gas reactions of carbon. *In*: D. D. ELEY, P. W. SELWOOD, and P. B. WEISZ, (eds). *Advances in catalysis and related subjects*, New York: Academic Press Inc., p.383.

WANG, J., M. JIANG, Y. YAO, Y. ZHANG and J. CAO. 2009. Steam gasification of coal char catalyzed by K_2CO_3 for enhanced production of hydrogen without formation of methane. *Fuel*. **88**, pp.1572-1579.

WANG, W., Y. QIN, C. WEI, Z. LI, Y. GUO and Y. ZHU. 2006. Partitioning of elements and macerals during preparation of Antaibao coal. *International Journal of Coal Geology*. **68**, pp.223-232.

WCI. 2010. *World Coal Institute*. [online]. [Accessed 01 06 2010]. Available form World Wide Web: <http://www.worldcoal.org>

WEN, C. Y. 1968. Non catalytic heterogeneous solid fluid reactions. *Industrial engineering chemistry*. **60**, pp.34-54.

WU, S., J. GU, L. LI, Y. WU and J. GAO. 2006. The reactivity and kinetics of Yanzhou coal chars from elevated pyrolysis temperatures during gasification in steam at 900 -1200 ˚C. *Process Safety and Environmental Protection*. **84**, pp.420-428.

WU, S., J. GU, X. ZHANG, Y. WU and J. GAO. 2008. Variation of carbon crystalline structures and CO_2 gasification reactivity of Shenfu coal chars at elevated temperatures. *Energy & Fuels*. **22**, pp.199-206.

WU, Y., J. WANG, S. WU, S. HUANG and J. GAO. 2011. Potassium-catalyzed steam gasification of petroleum coke for H_2 production: Reactivity, selectivity and gas release. *Fuel processing technology*. **92**, pp.523-530.

XIUMIN, J., Z. CHUGUANG, Y. CHE, L. DECHANG, Q. JIANRONG AND L. JUBIN. 2002. Physical structure and combustion properties of super fine pulverized coal particles. *Fuel*. **81**, pp.793-797.

XU, Q., S. PANG, and T. LEVI. 2011. Reaction kinetics and producer gas compositions of steam gasification of coal and biomass blend chars, part 1: Experimental investigation. *Chemical engineering science*. **66**(10), pp.2141-2148.

YAN, L., R. P. GUPTA, and T. F. WALL. 2002. A mathematical model of ash formation during pulverized coal combustion. *Fuel*. **81**(3), pp.337-344.

YANG, Y. and A. P. WATKINSON. 1994. Gasification reactivity of some Western Canadian coals. *Fuel*. **73**, pp.1786-1791.

YE, D. P., J. B. AGNEW, and D. K. ZHANG. 1998. Gasification of a South Australian low-rank coal with carbon dioxide and steam: Kinetics and reactivity studies. *Fuel*. **77**, pp.1209-1219.

YEASMIN, H., J. F. MATHEWS, and S. OUYANG. 1999. Rapid devolatilisation of Yallourn brown coal at high pressure and temperature. *Fuel*. **78**, pp.11-24.

YU, J., J. A. LUCAS, and T. F. WALL. 2007. Formation of the structure of chars during devolatilization of pulverized coal and its thermoproperties: A review. *Progress in Energy and Combustion Science*. **33**, pp.135-170.

YU, D., M. XU, J. SUI, X. LIU, Y. YU, and Q. CAO. 2005. Effect of coal particle size on the proximate composition and combustion properties. *Thermochimica Acta*. **439**, pp.103-109.

YU, Y., M. XU, H. YAO, D. YU, Y. QIAO, J. SUI, X. LIU and Q. CAO. 2007. Char characteristics and particulate matter formation during Chinese bituminous coal combustion. *Proceedings of the Combustion Institute*. **32**, pp.1947-1954.

ZHANG, H., K. CEN, J. YAN, and M. NI. 2002. The fragmentation of coal particle during coal combustion in a fluidized bed. *Fuel*. **81**, pp.1835-1840.

ZHANG, L., J. HUANG, Y. FANG, and Y. WANG. 2006. Gasification reactivity and kinetics of typical anthracite chars with steam and CO_2. *Energy & Fuels*. **20**(3), p.1201.

ZHUO, Y., R. MESSENBOCK, A. -G. COLLOT, N. PATERSON, D. R. DUGWELL and R. KANDIYOTI. 2000. Conversion of coal particles in pyrolysis and gasification: comparison of conversions in a pilot-scale gasifier and bench-scale test equipment. *Fuel*. **79**(7), pp.793-802.

ZHU, W., W. SONG, and W. LIN. 2008. Effect of the Coal Particle Size on Pyrolysis and Char Reactivity for Two Types of Coal and Demineralized Coal. *Energy & Fuels*. **22**(4), pp.2482-2487.

Appendix A: Reactivity experiments

The conversion, average conversion and error obtained for all the particle sizes at the different gasification temperatures are shown in the next few figures.

A.1 5 mm

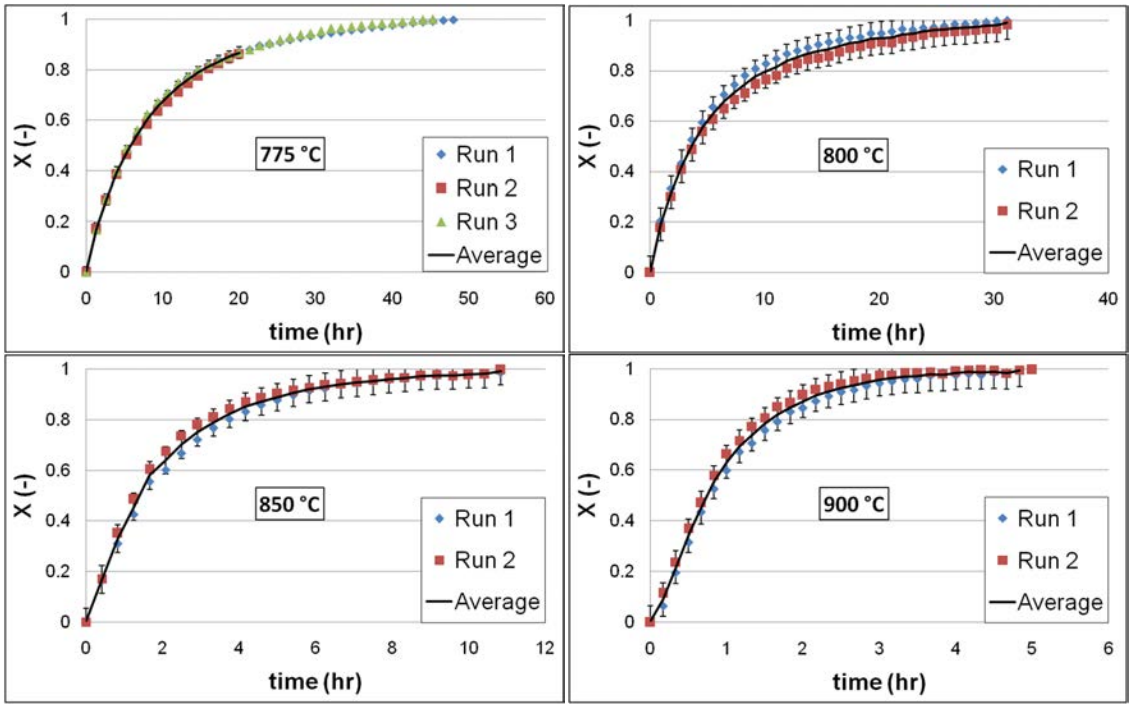

Figure A.1: The conversion, average conversion and error obtained for the 5 mm runs.

A.2 10 mm

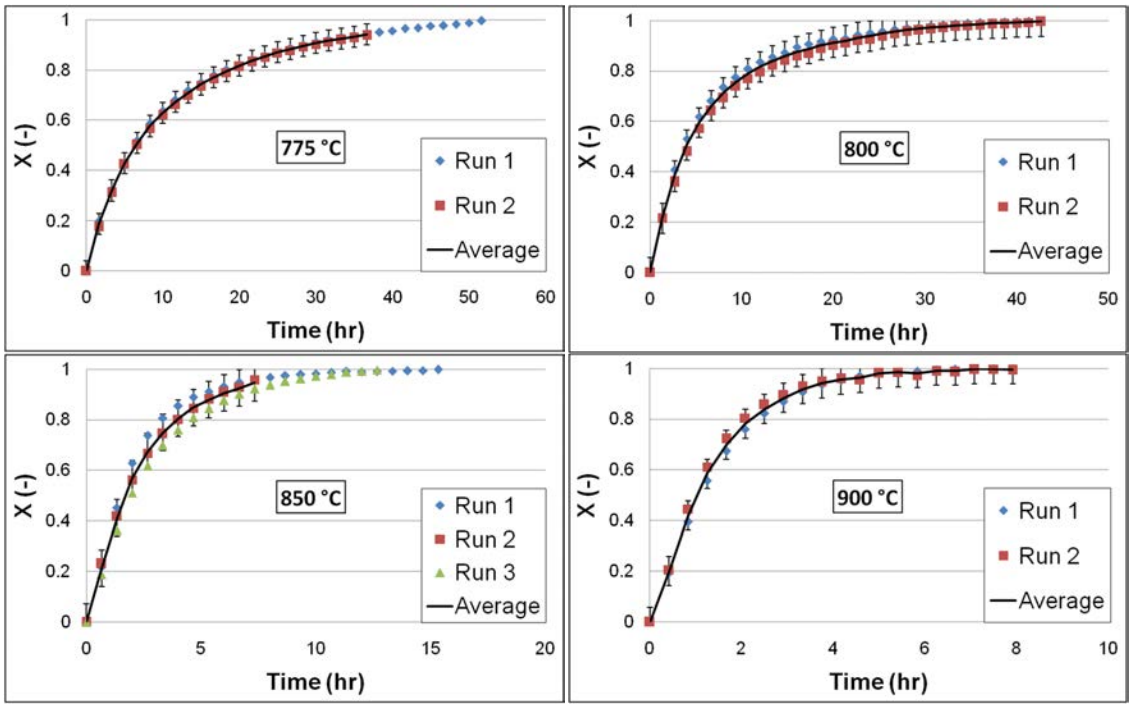

Figure A.2: The conversion, average conversion and error obtained for the 10 mm runs.

A.3 20 mm

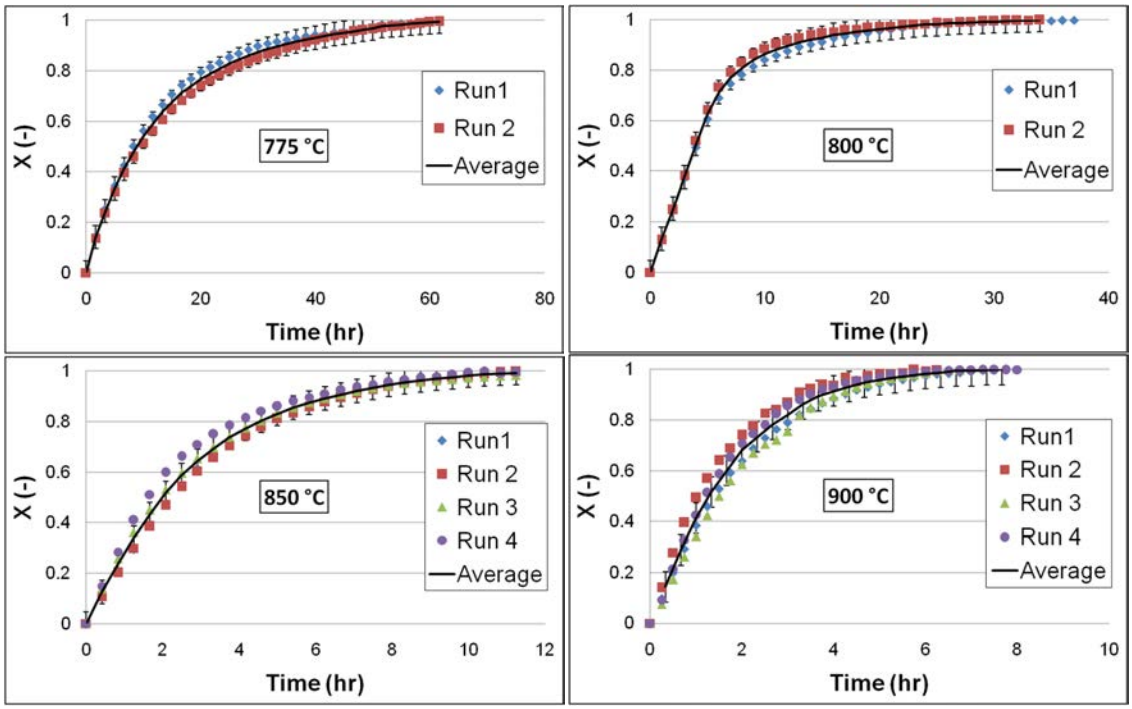

Figure A.3: The conversion, average conversion and error obtained for the 20 mm runs.

A.4 30 mm

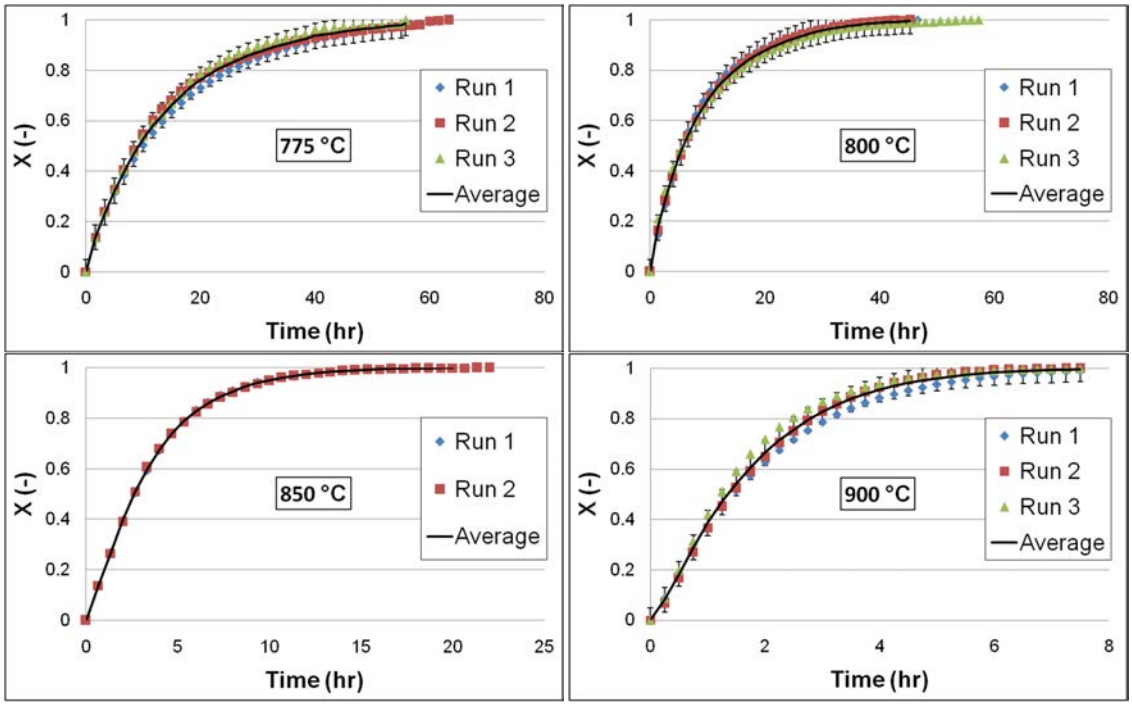

Figure A.4: The conversion, average conversion and error obtained for the 30 mm runs.

A.5 dX/dt curves

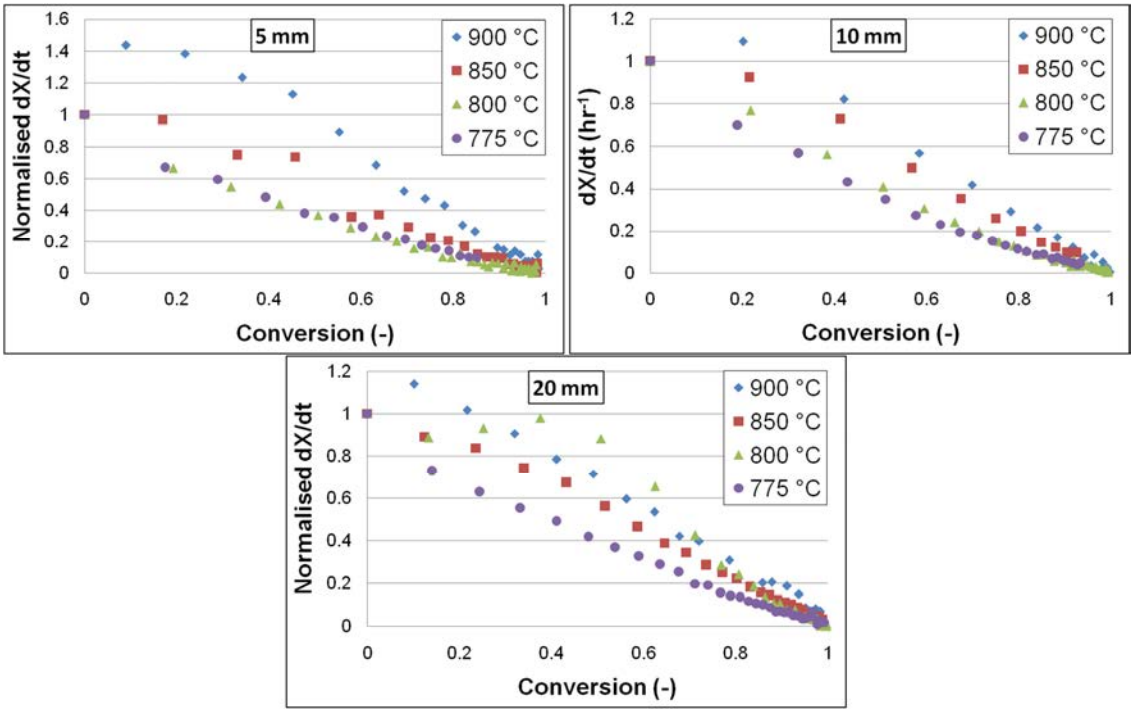

Figure A.5: Normalised reaction rate.

Appendix B: Modelling background and results

B.1 Reactivity models

B.1.1 Homogeneous model

The homogenous model equation used to predict the reactivity of coal is shown in Equation B.1 and Equation B.2 (integral form) (Schmal *et al.*, 1982).

$$\frac{dX}{dt} = k_0 (1 - X) \qquad \text{Eq B.1}$$

$$t = \frac{-1}{k_0} \ln(1 - X) \qquad \text{Eq B.2}$$

The fitting parameters obtained for the homogenous model is shown in Table B.1.

Table B.1: Fitting parameters obtained for the Homogenous model.

	775 ˚C	800 ˚C	850 ˚C	900 ˚C
5 mm	0.10	0.17	0.43	0.95
	0.10	0.14	0.50	1.11
	0.11			
10 mm	0.09	0.15	0.48	0.69
	0.08	0.13	0.40	0.78
			0.35	
20 mm	0.07	0.17	0.34	0.53
	0.08	0.15	0.33	0.70
		0.18	0.36	0.52
		0.22		0.63
30 mm	0.06	0.11	0.29	0.52
	0.07	0.11	0.29	0.58
	0.08	0.10		0.66

Homogenous model prediction of the 5 mm particles experimental results:

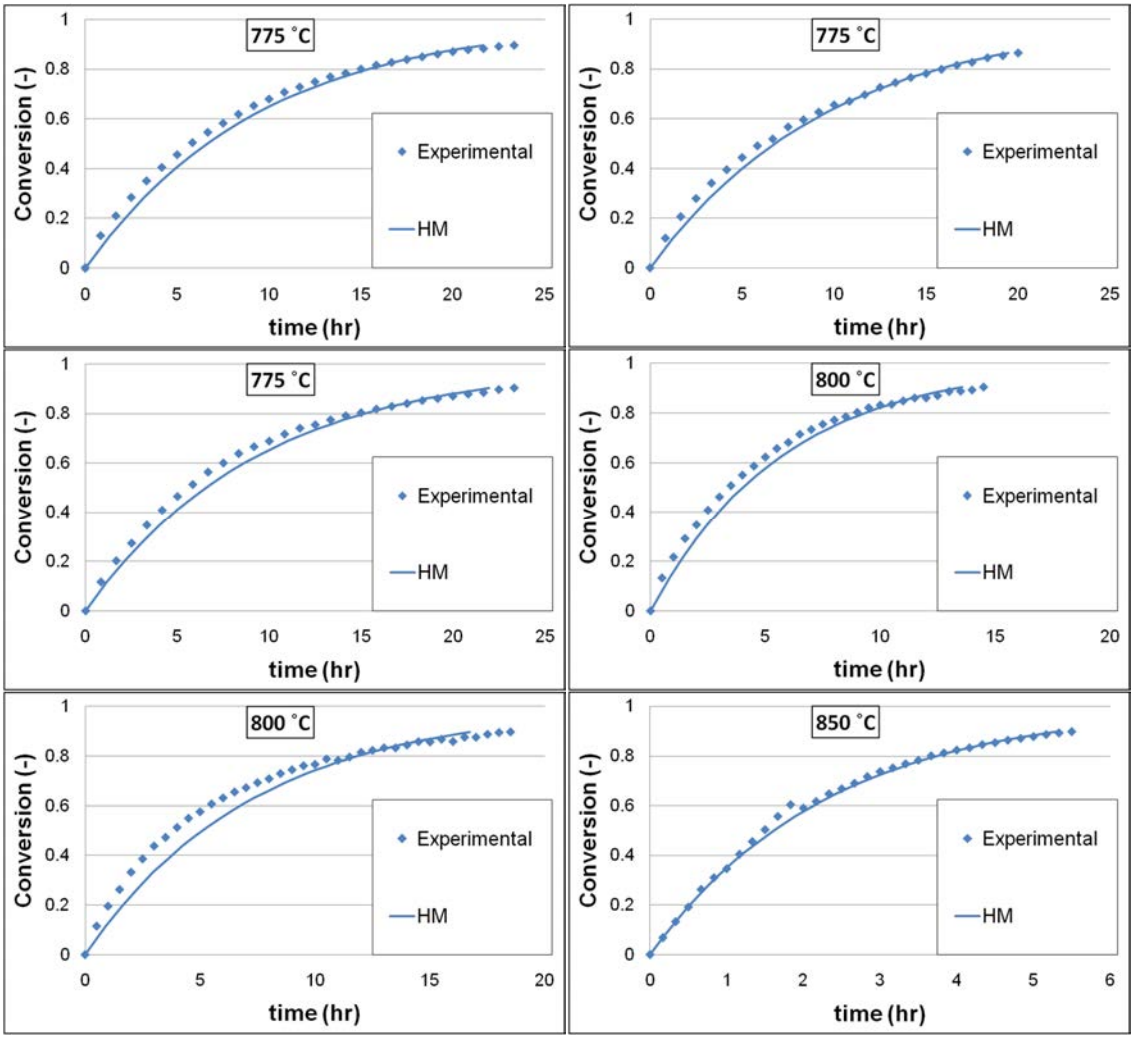

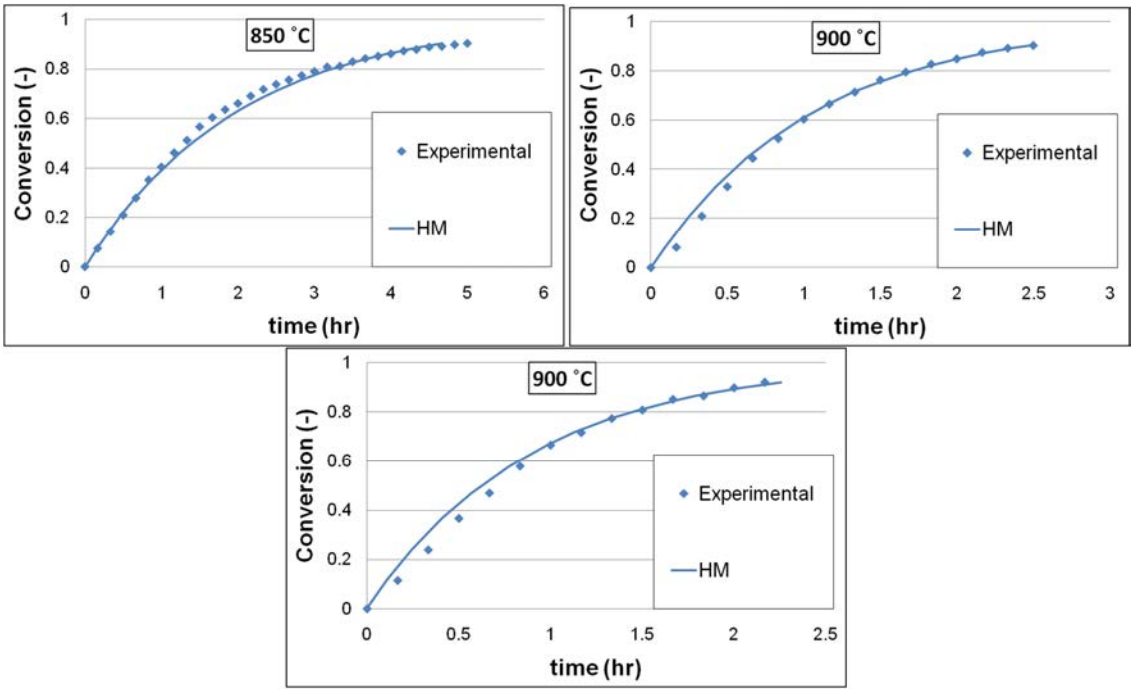

Figure B.1: Homogenous prediction of experimental results for the 5 mm particles.

Homogenous model prediction of the 10 mm particles experimental results:

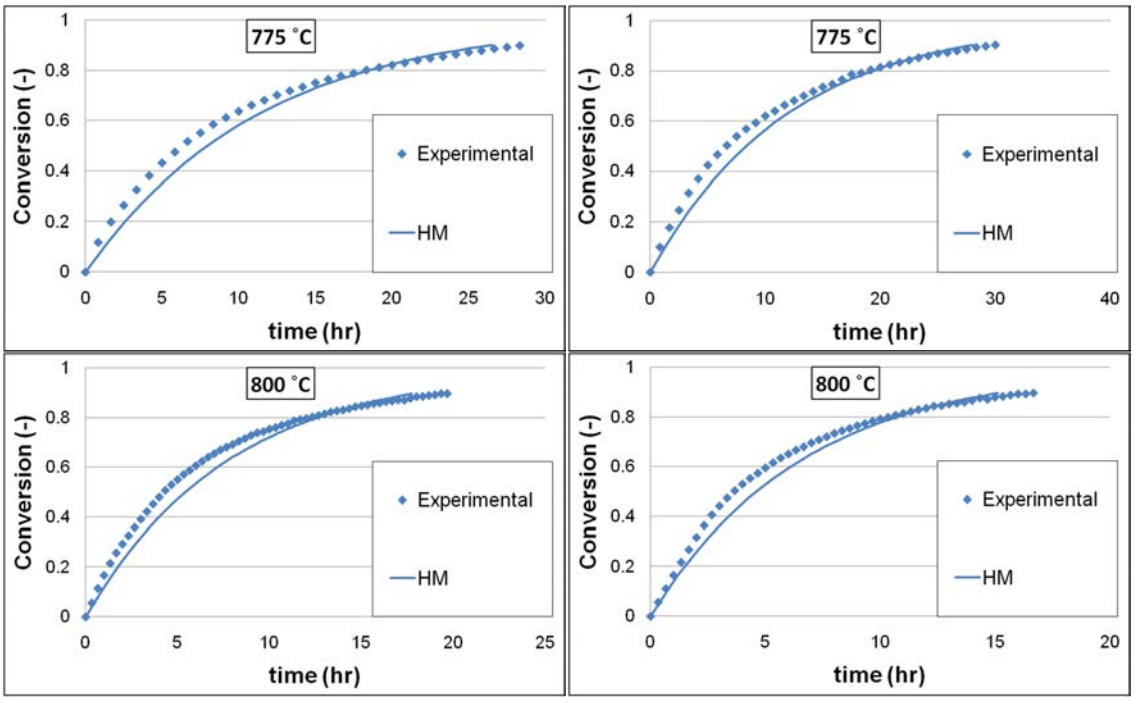

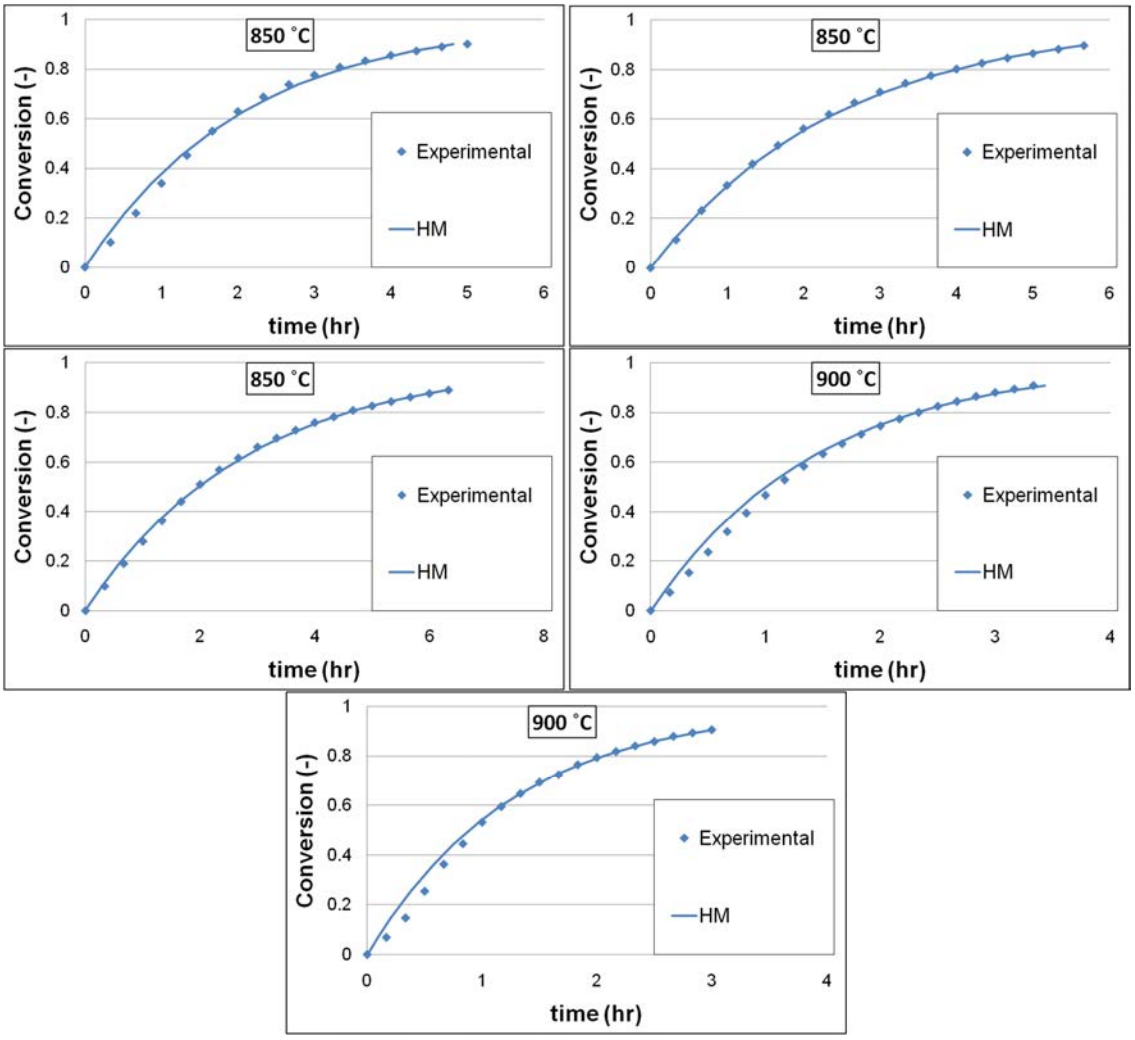

Figure B.2: Homogenous prediction of experimental results for the 10 mm particles.

Homogenous model prediction of the 20 mm particles experimental results:

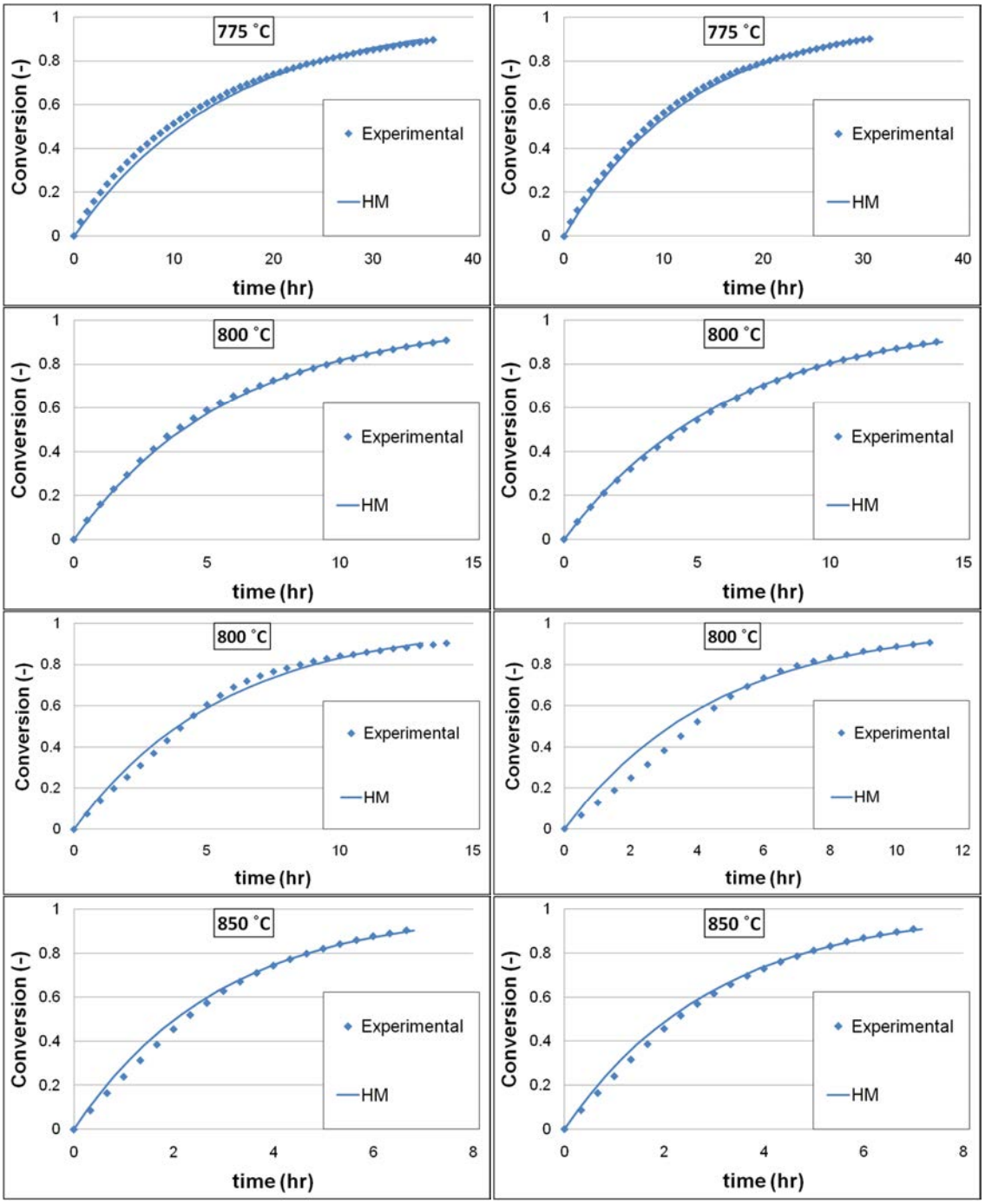

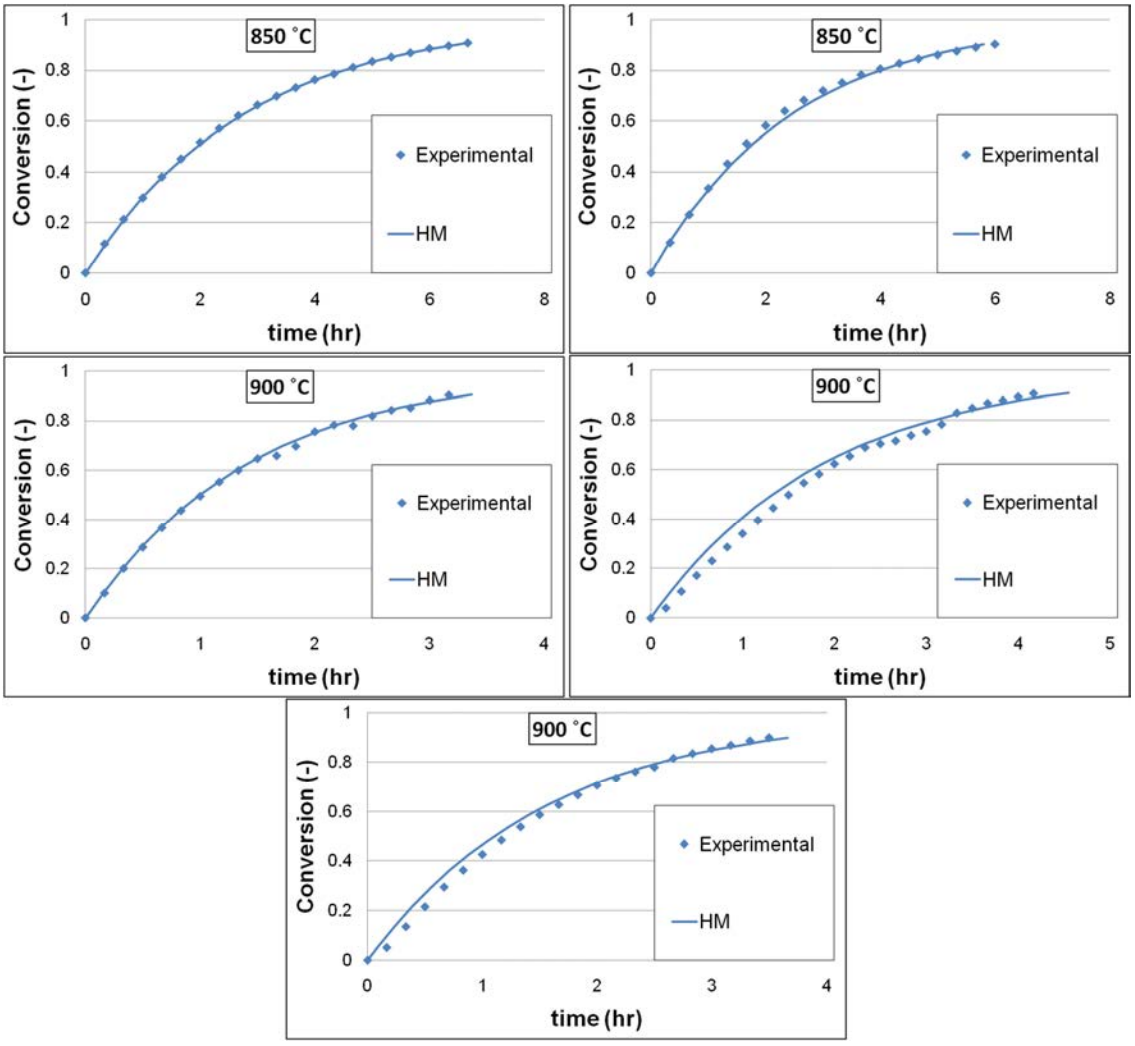

Figure B.3: Homogenous prediction of experimental results for the 20 mm particles.

Homogenous model prediction of the 30 mm particles experimental results:

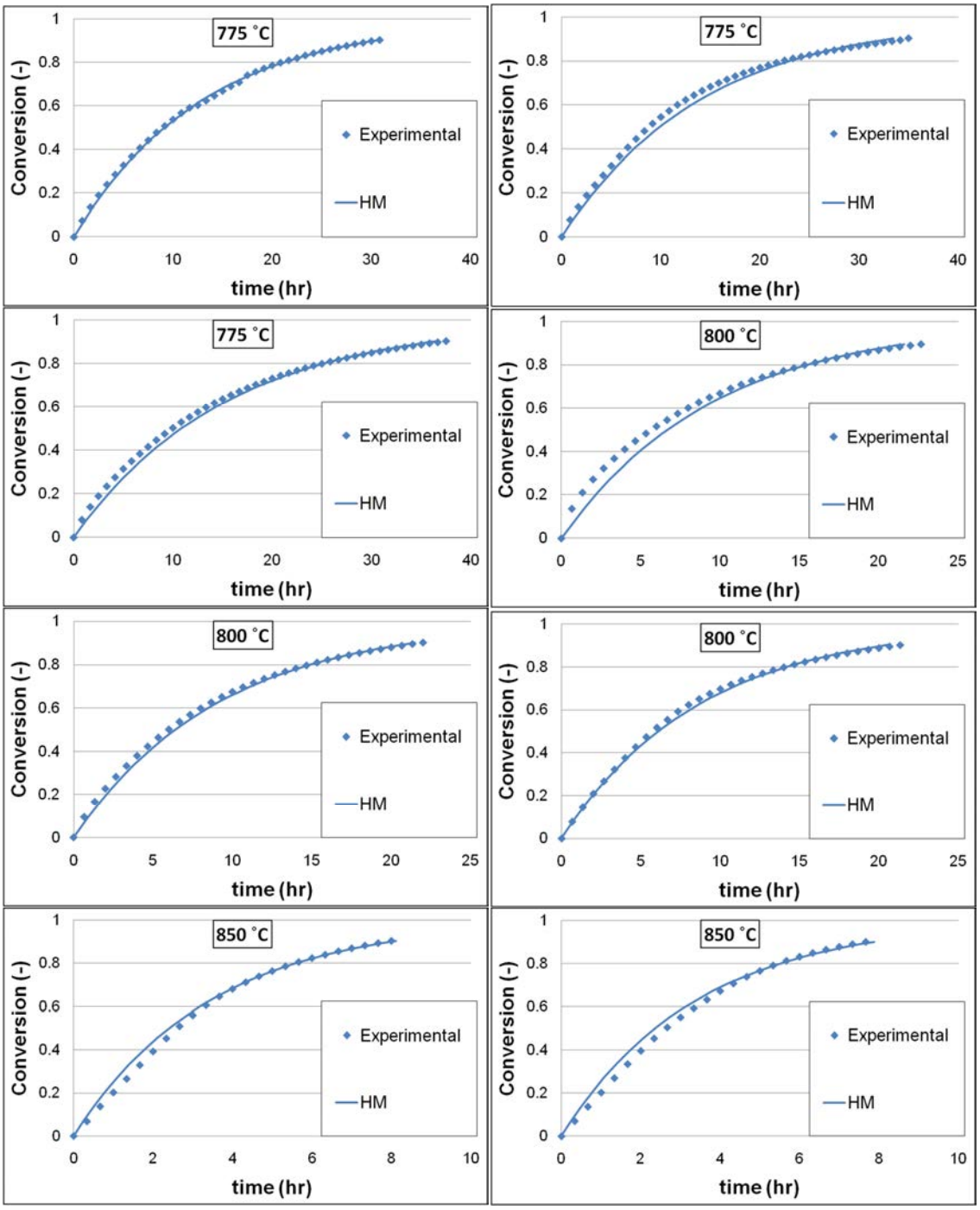
775 °C
Conversion (-)
time (hr)
Experimental
HM
775 °C
Conversion (-)
time (hr)
Experimental
HM
775 °C
Conversion (-)
time (hr)
Experimental
HM
800 °C
Conversion (-)
time (hr)
Experimental
HM
800 °C
Conversion (-)
time (hr)
Experimental
HM
800 °C
Conversion (-)
time (hr)
Experimental
HM
850 °C
Conversion (-)
time (hr)
Experimental
HM
850 °C
Conversion (-)
time (hr)
Experimental
HM

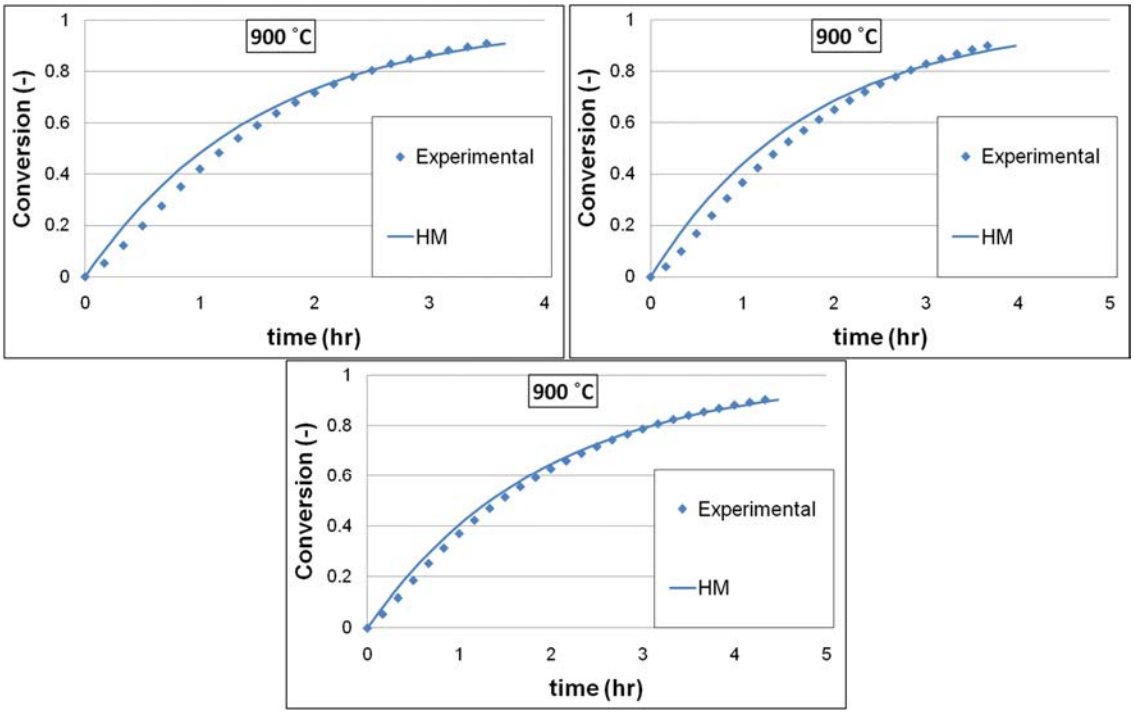

Figure B.4: Homogenous prediction of experimental results for the 30 mm particles.

B.1.2 Shrinking core model

The three rate controlling step equations (chemical reaction, ash diffusion and external mass transfer) for the shrinking core model are given in Equation B.3 to B.5, respectively (Levenspiel, 1999).

$$t = \frac{\rho_b R}{b k C_{Ag}} \left(1 - (1 - X)^{1/3}\right) \qquad \text{Eq B.3}$$

$$t = \frac{\rho_b R^2}{6 b D_e C_{Ag}} \left(1 - (1 - X)^{2/3} + 2(1 - X)\right) \qquad \text{Eq B.4}$$

$$t = \frac{\rho_b R^2}{3 b k_g C_{Ag}} X \qquad \text{Eq B.5}$$

The normalisation of rate controlling step equations (chemical reaction, ash diffusion and external mass transfer) for the shrinking core model are given in Equation B.6 to B.8, respectively (Levenspiel, 1999).

$$\frac{t}{t_{90}} = \frac{1 - (1 - X)^{\frac{1}{3}}}{1 - (1 - 0.9)^{\frac{1}{3}}} \qquad \text{Eq B.6}$$

$$\frac{t}{t_{90}} = \frac{1 - 3(1 - X)^{\frac{2}{3}} + 2(1 - X)}{1 - 3(1 - 0.9)^{\frac{2}{3}} + 2(1 - 0.9)} \qquad \text{Eq B.7}$$

$$\frac{t}{t_{90}} = \frac{X}{0.9} \qquad \text{Eq B.8}$$

The conversion versus normalised time for the experimental as well as the rate controlling steps of the shrinking core model is compared in Figure B.5.

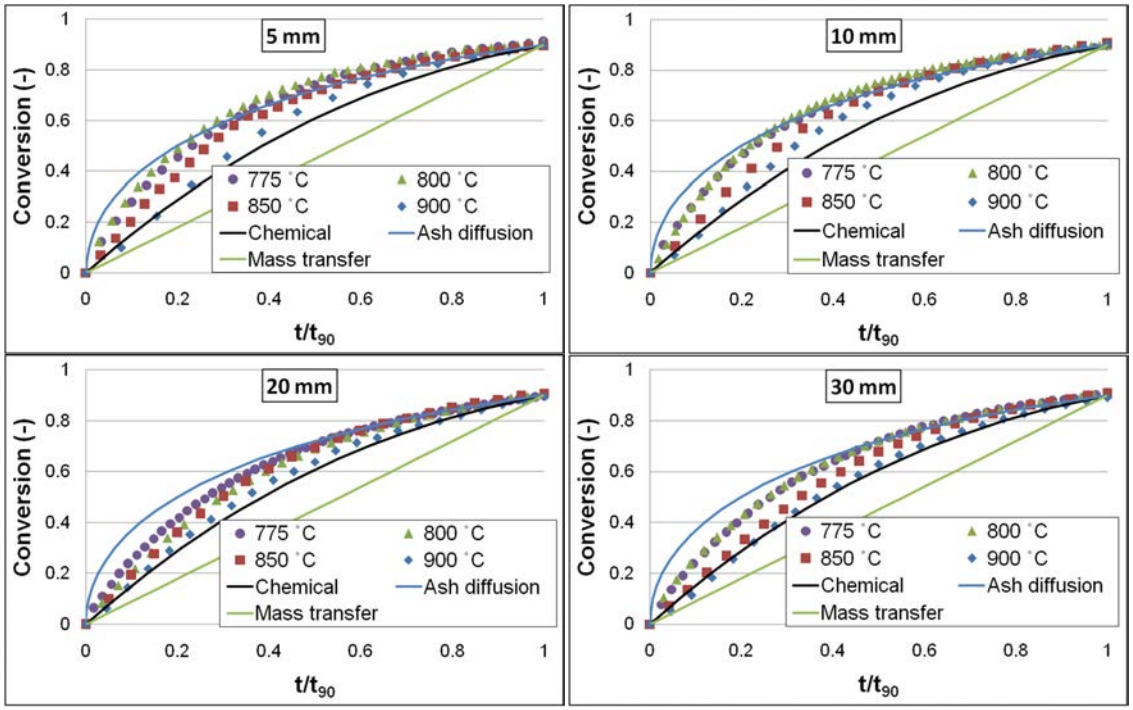

Figure B.5: Conversion versus normalised time comparison of the SCM with reactivity experiments.

The equation used to fit the carbon conversion graphs are shown in Equation B.9.

$$t = \frac{\rho_b R}{bkC_{Ag}}\left(1-(1-X)^{1/3}\right) + \frac{\rho_b R^2}{6bD_eC_{Ag}}\left(1-(1-X)^{2/3}+2(1-X)\right) \qquad \text{Eq B.9}$$

The results obtained from fitting all the reactivity data with the combined shrinking core model is shown in Table B.2.

Table B.2: Fitting parameter obtained from the combined shrinking core model fitting.

	775 °C		800 °C		850 °C		900 °C	
	k (10^{-3})	D_e (10^{-6})	k (10^{-3})	D_e (10^{-6})	k (10^{-3})	D_e (10^{-6})	k (10^{-3})	D_e (10^{-6})
	0.21	0.19	0.30	0.37	1.62	0.35	1.78	1.66
5 mm	0.17	0.29	0.23	0.23	1.96	0.39	1.90	2.57
	0.19	0.31						
	0.95	0.24	0.84	0.69	5.03	1.4	4.77	2.35
10 mm	0.92	0.22	0.51	0.79	3.04	1.3	3.03	5.38
					3.03	5.4		
	1.17	0.79	1.83	2.8	2.53	11	4.41	15
20 mm	1.03	1.1	1.57	2.6	2.75	12	6.20	19
			2.13	2.7	3.98	7.5	2.86	130
			1.36	13			4.51	30
	1.08	2.4	2.42	2.6	2.84	25	6.25	42
30 mm	1.09	1.5	2.48	3.1	3.15	18	5.40	66
	1.25	1.6	2.27	2.2			5.17	770

Combined chemical reaction and ash diffusion controlled shrinking core model prediction of the 5 mm particles experimental results:

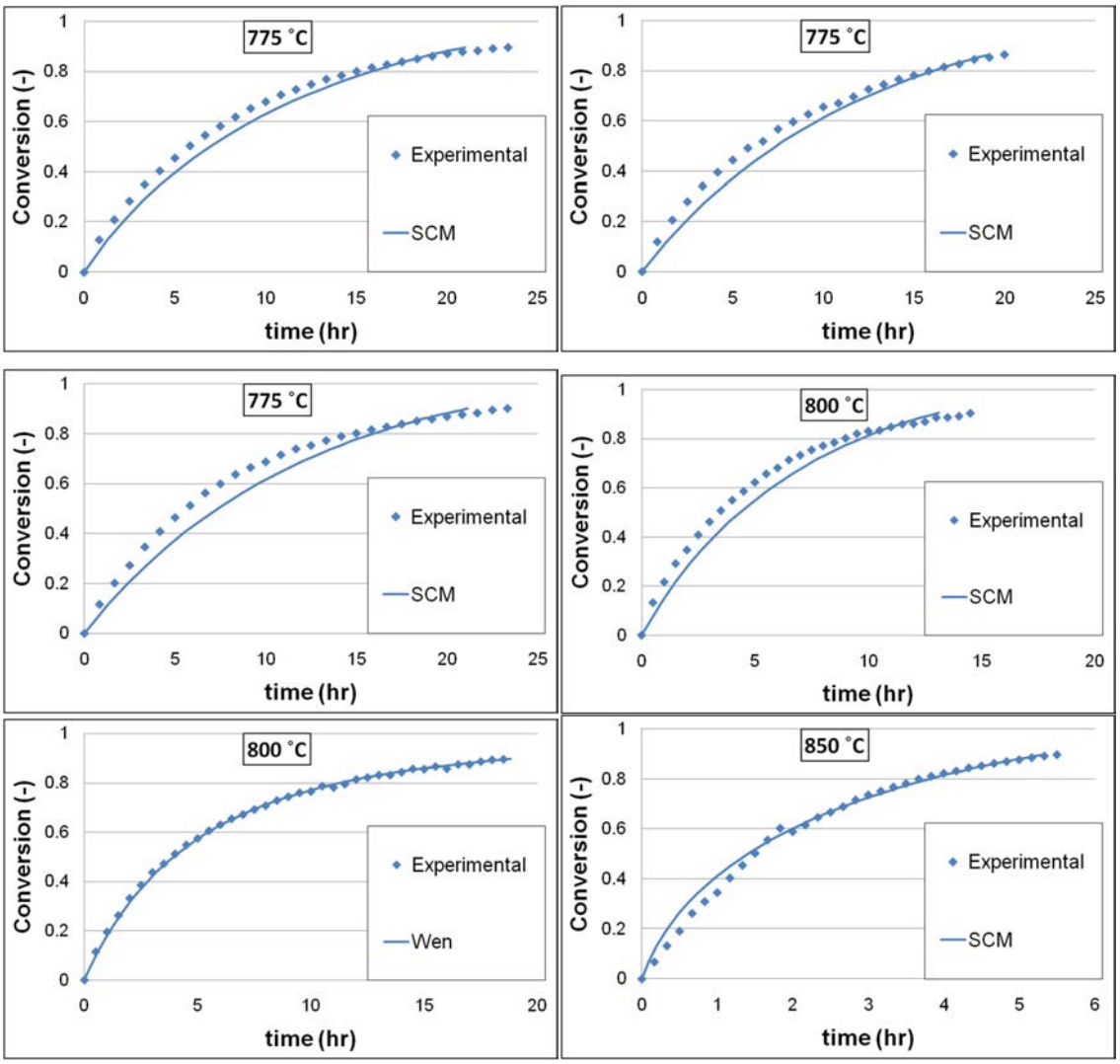

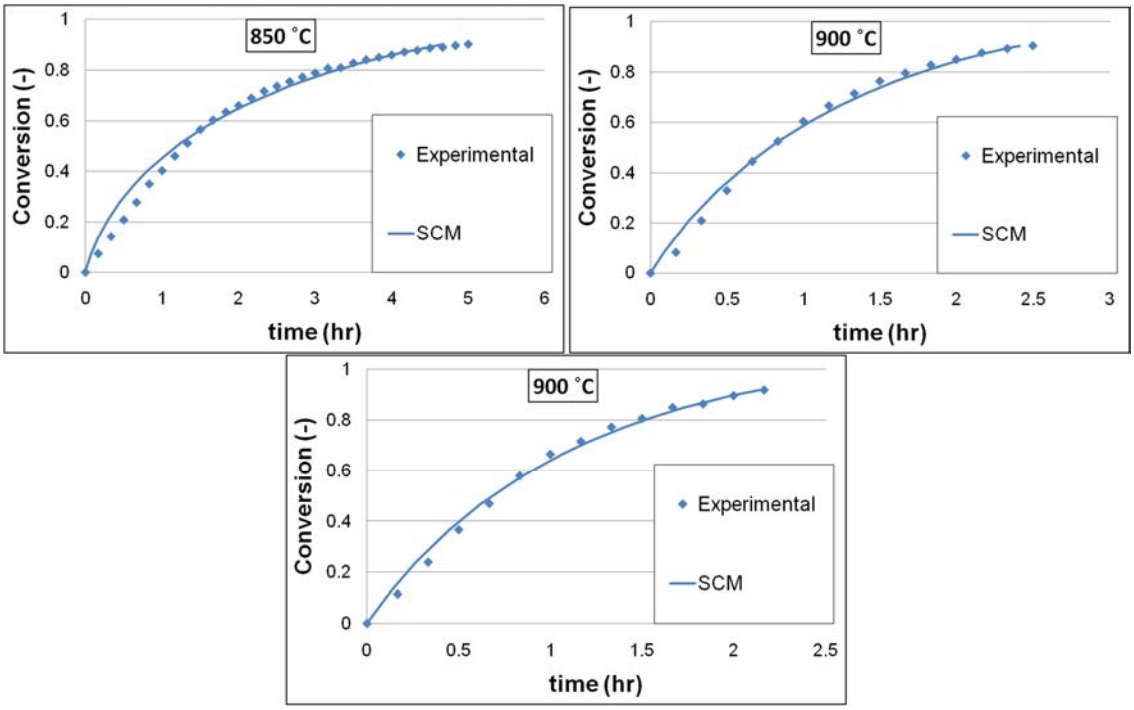

Figure B.6: Shrinking core model prediction of experimental results for the 5 mm particles.

Combined chemical reaction and ash diffusion controlled shrinking core model prediction of the 10 mm particles experimental results:

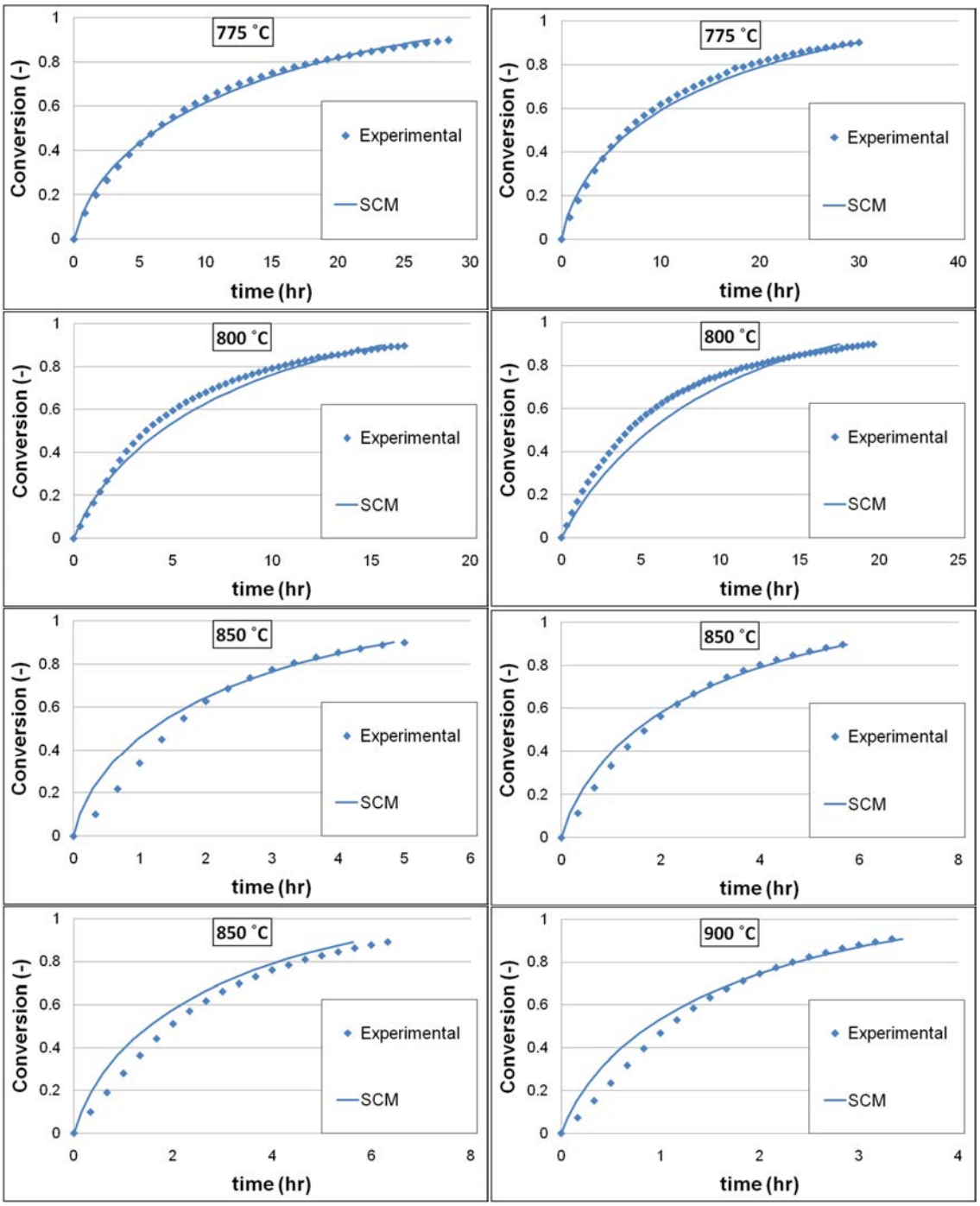

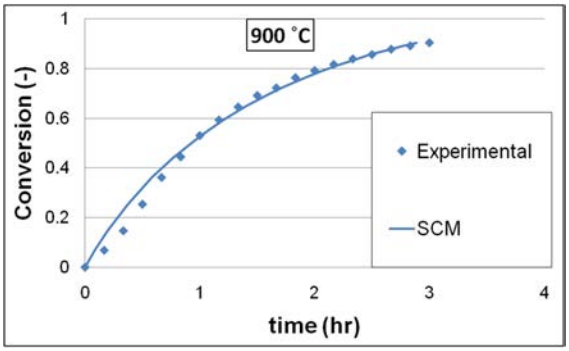

Figure B.7: Shrinking core model prediction of experimental results for the 10 mm particles.

Combined chemical reaction and ash diffusion controlled shrinking core model prediction of the 20 mm particles experimental results:

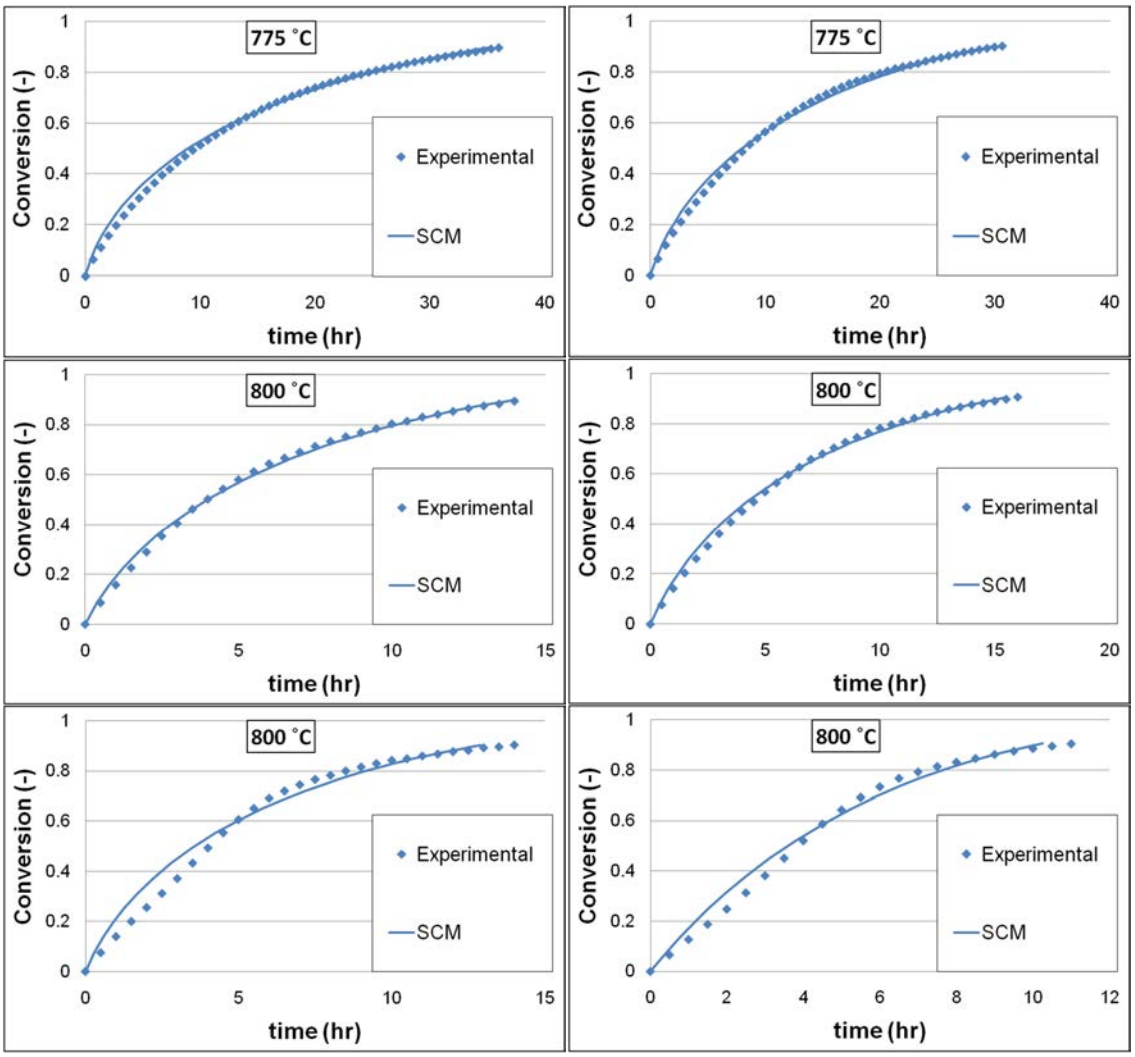

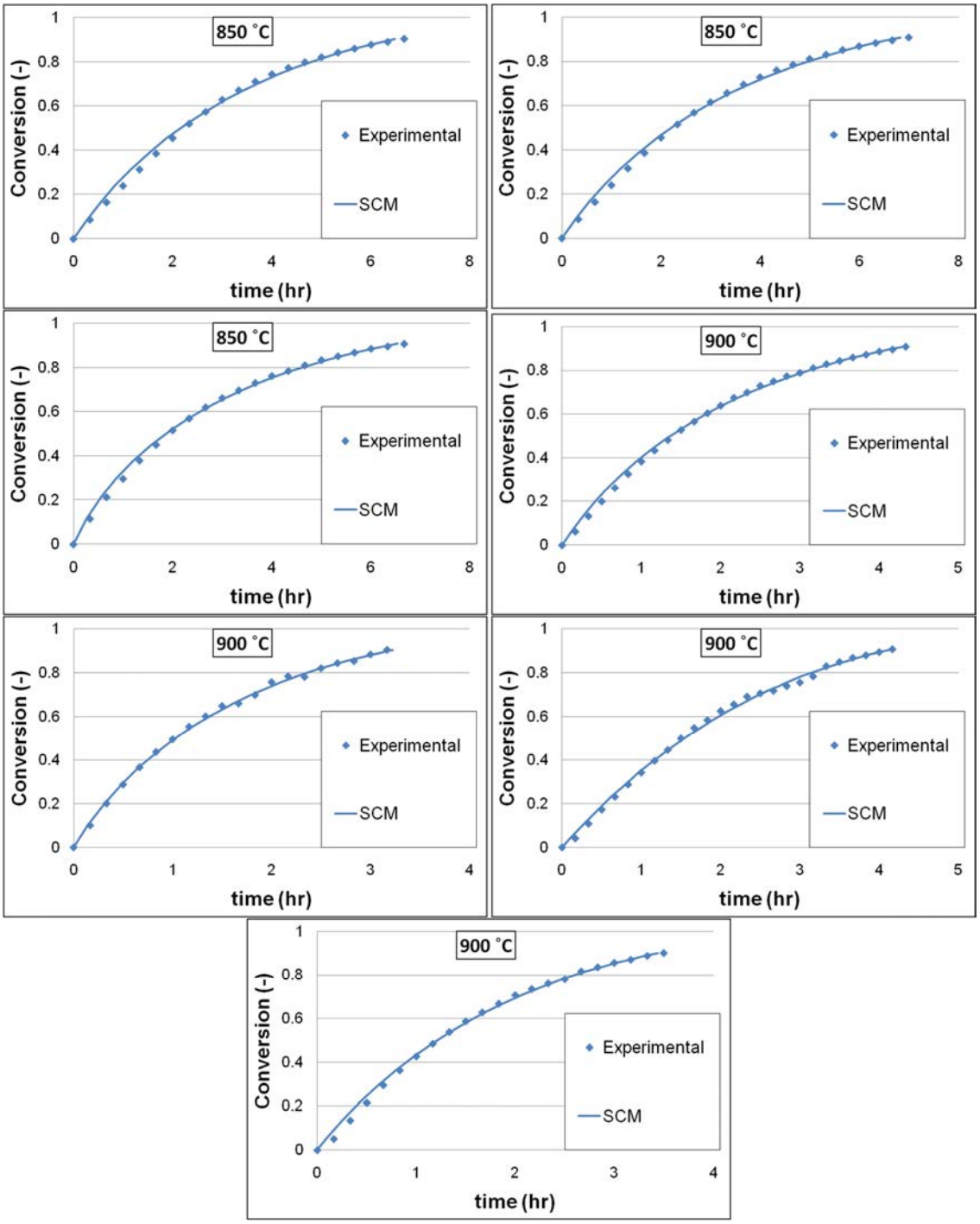

Figure B.8: Shrinking core model prediction of experimental results for the 20 mm particles.

Combined chemical reaction and ash diffusion controlled shrinking core model prediction of the 30 mm particles experimental results:

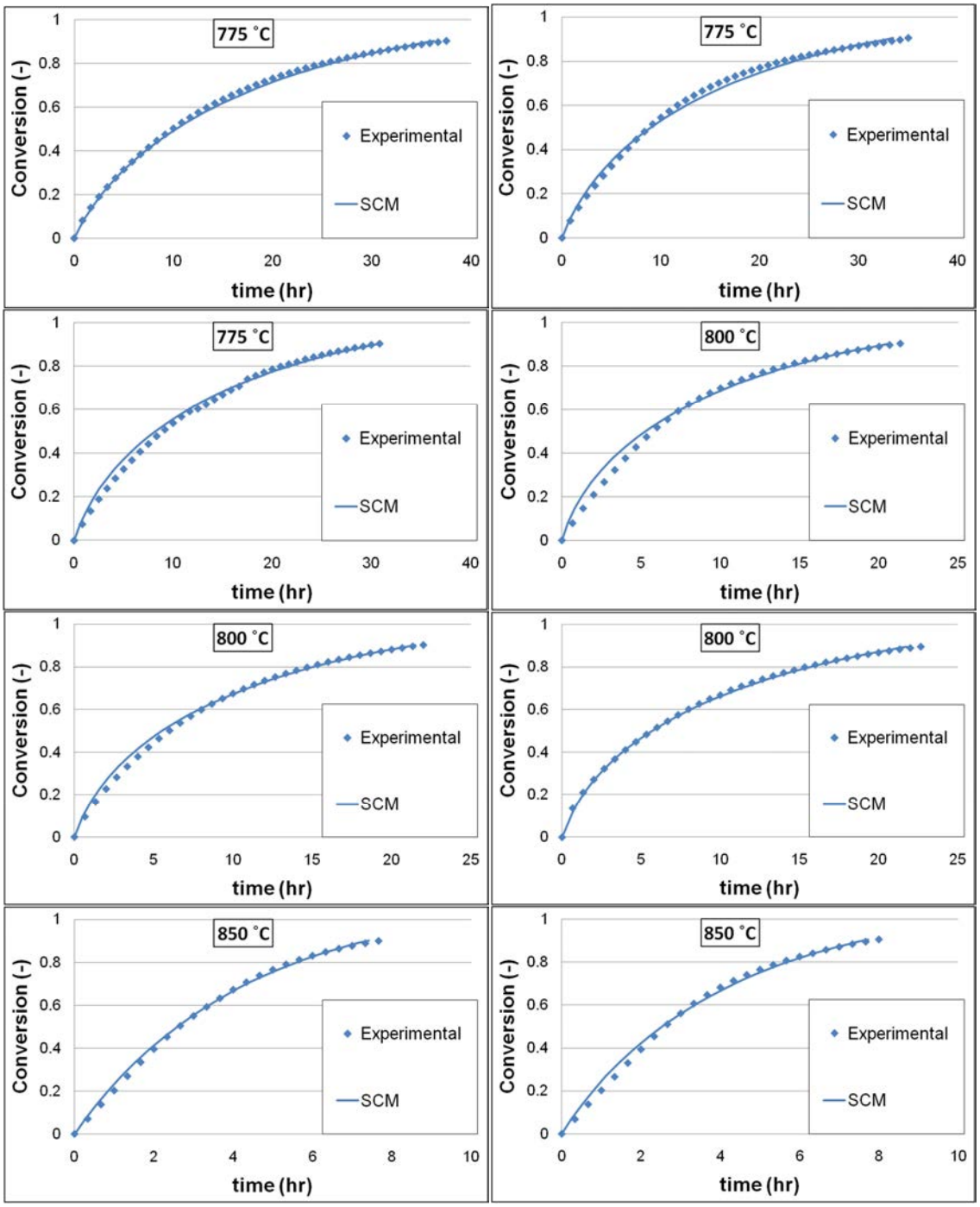
775 °C
Conversion (-)
time (hr)
Experimental
SCM
775 °C
Conversion (-)
time (hr)
Experimental
SCM
775 °C
Conversion (-)
time (hr)
Experimental
SCM
800 °C
Conversion (-)
time (hr)
Experimental
SCM
800 °C
Conversion (-)
time (hr)
Experimental
SCM
800 °C
Conversion (-)
time (hr)
Experimental
SCM
850 °C
Conversion (-)
time (hr)
Experimental
SCM
850 °C
Conversion (-)
time (hr)
Experimental
SCM

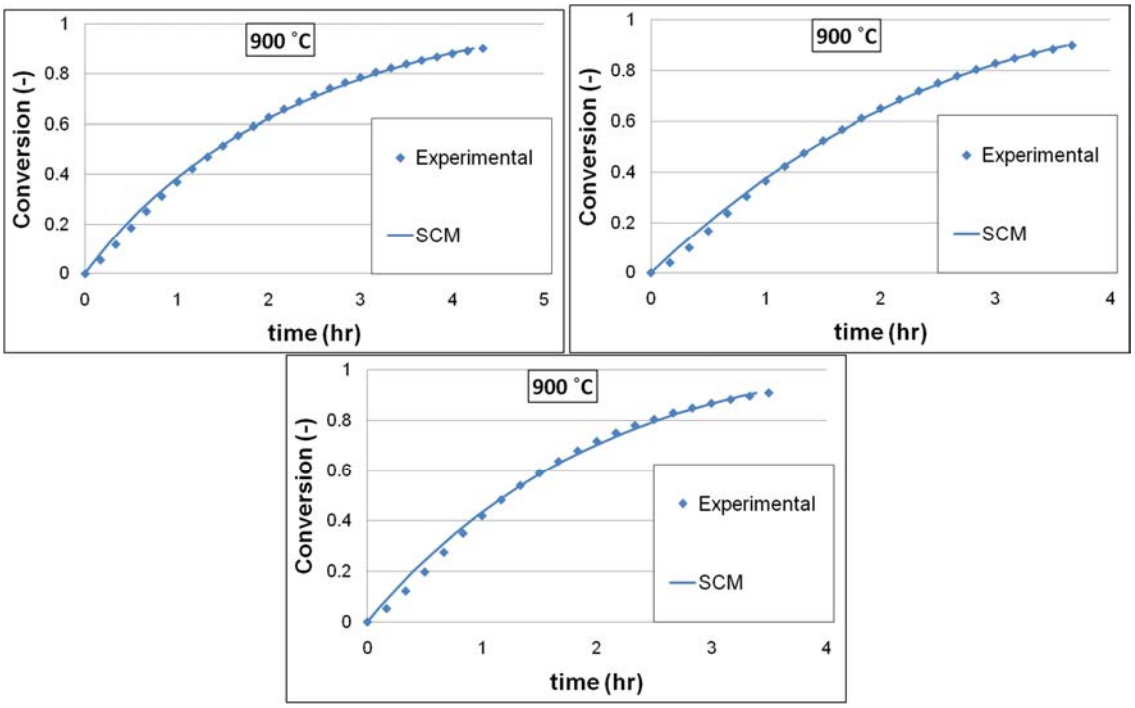

Figure B.9: Shrinking core model prediction of experimental results for the 30 mm particles.

B.1.3 Random pore model

The rate and the normalised time equations of the chemical reaction controlled random pore model is shown in Equation 4.13 and 4.14, respectively (Bhatia and Perlmutter, 1980; Everson et al., 2011).

$$\frac{dX}{dt} = \frac{r_s S_0 (1-X)}{1-\varepsilon_0}\sqrt{1-\psi \ln(1-X)} \qquad \text{Eq B.10}$$

$$\frac{t}{t_{90}} = \frac{\sqrt{1-\psi \ln(1-X)}-1}{\sqrt{1-\psi \ln(1-0.9)}-1} \qquad \text{Eq. B.11}$$

$$\psi = \frac{4\pi L_0 (1-\varepsilon_0)}{S_0^2} \qquad \text{Eq. B.12}$$

The normalised time random pore models (with structural parameter ψ→0, ψ=1 and ψ=6) prediction of carbon conversion is compared to the experimental carbon conversion and shown in Figure B.10.

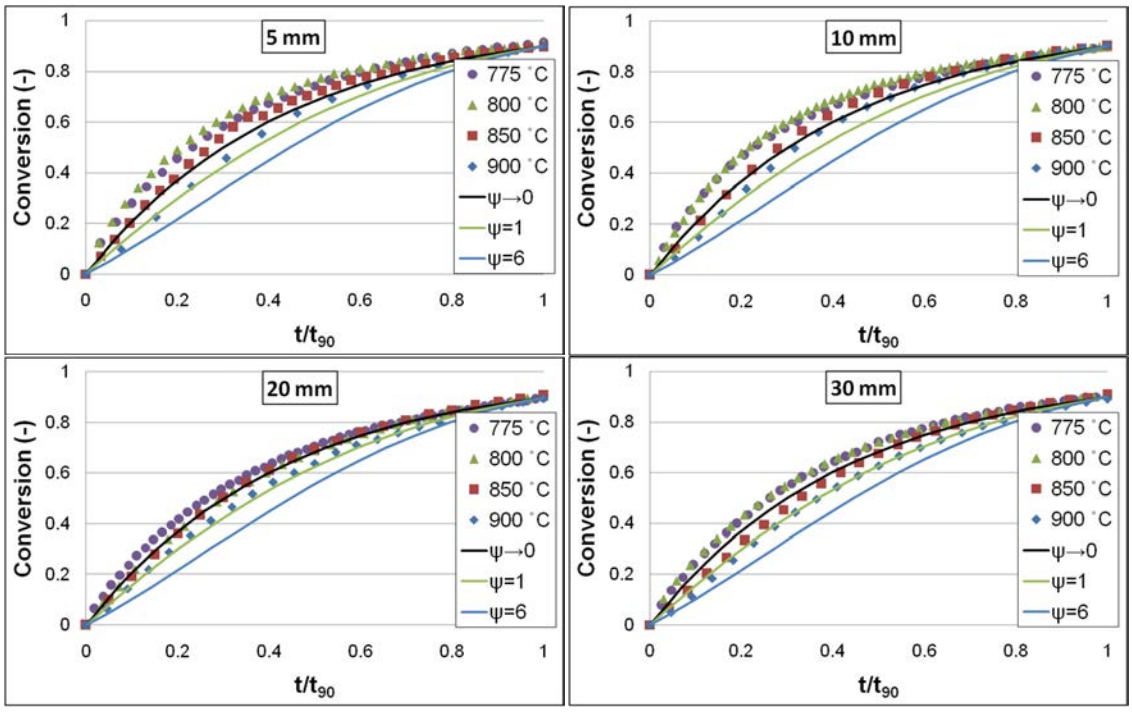

Figure B.10: Normalised time random pore model comparison with experimental data.

The structural parameters obtained for the different particle sizes at 850 and 900 ˚C are shown in Table B.3.

Table B.3: Structural parameter obtained for the 20 and 30 mm coal particles.

	850 ˚C	900 ˚C
20 mm	0.2	0.1
	0.1	0.4
	-	1.1
		0.6
30 mm	0.4	0.3
	0.1	1.6
		0.3

Random pore model prediction of the 20 mm reactivity experiments

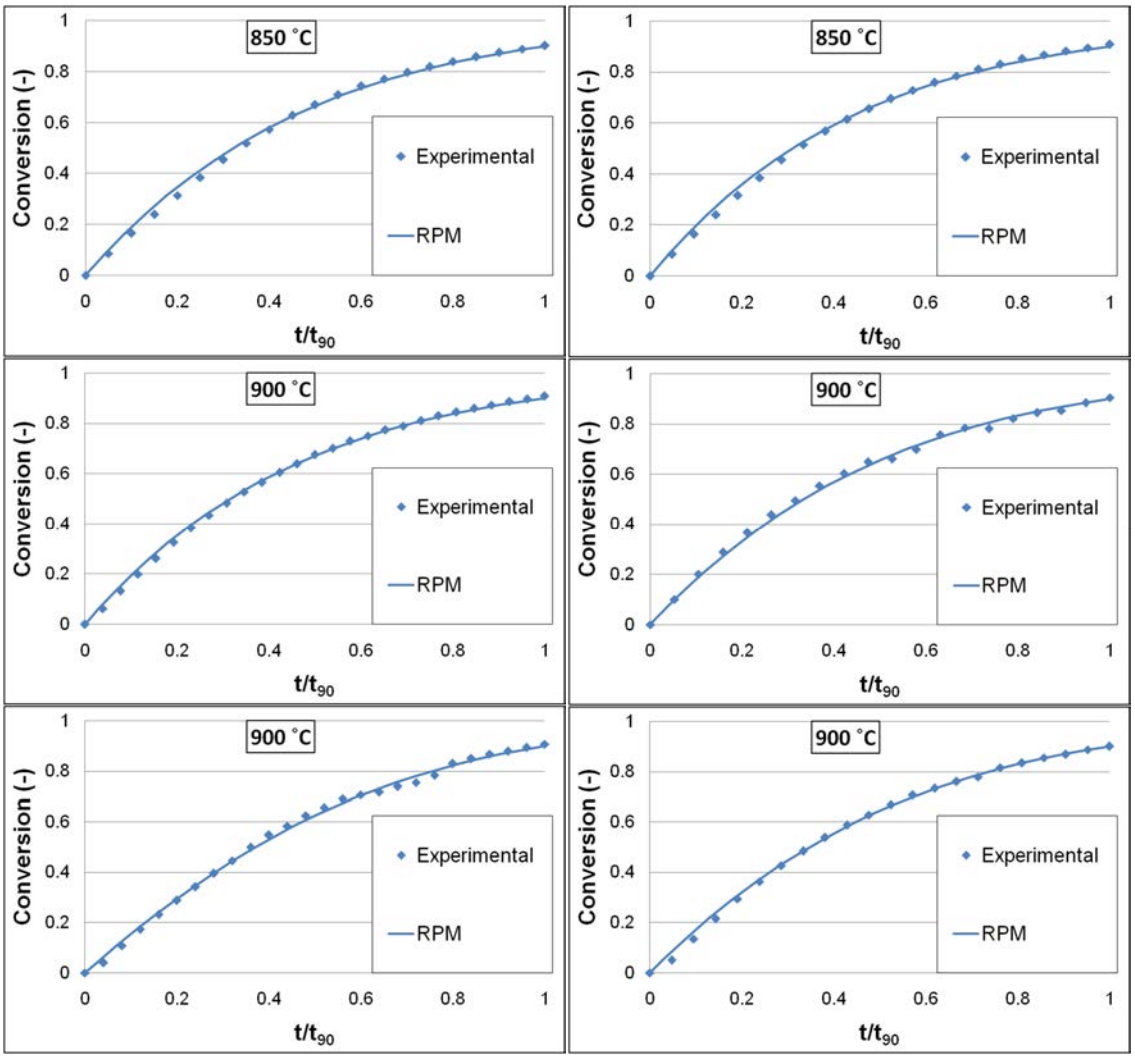

Figure B.11: Random pore model prediction of the 20 mm reactivity experiments.

Random pore model prediction of the 30 mm reactivity experiments

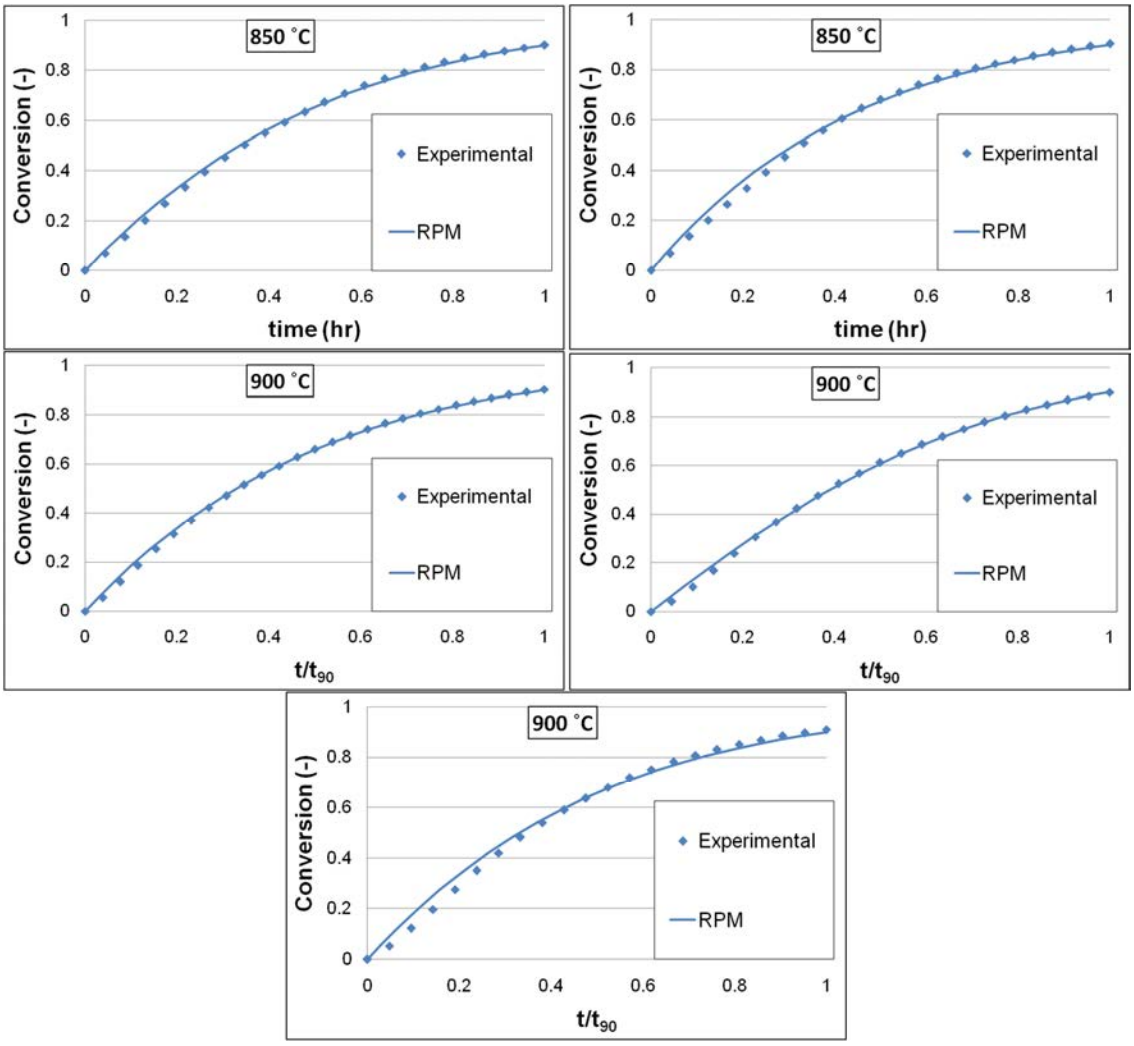

Figure B.12: Random pore model prediction of the 20 mm reactivity experiments.

B.1.4 Wen model

Wen model prediction of the 5 mm particles experimental results:

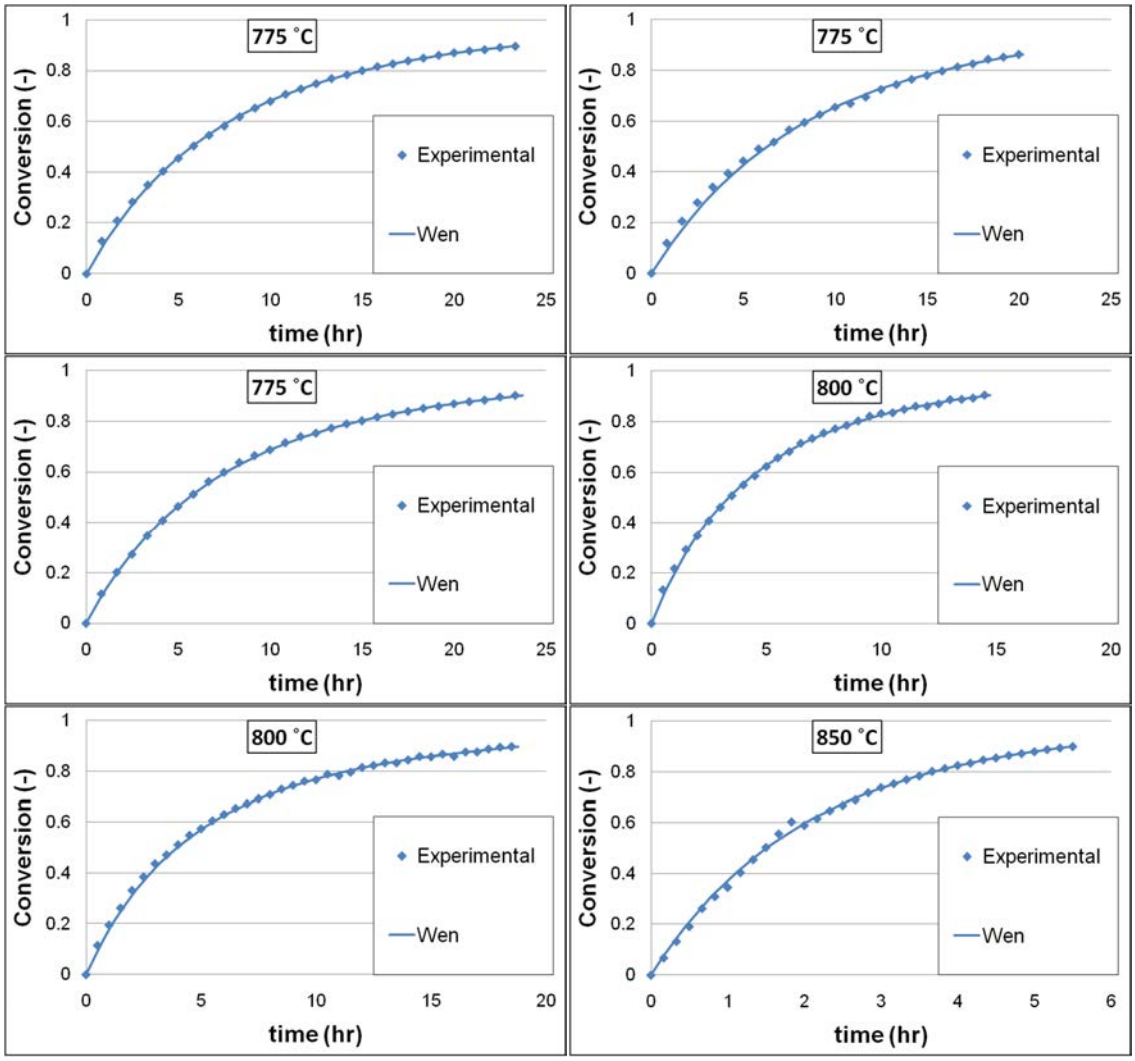

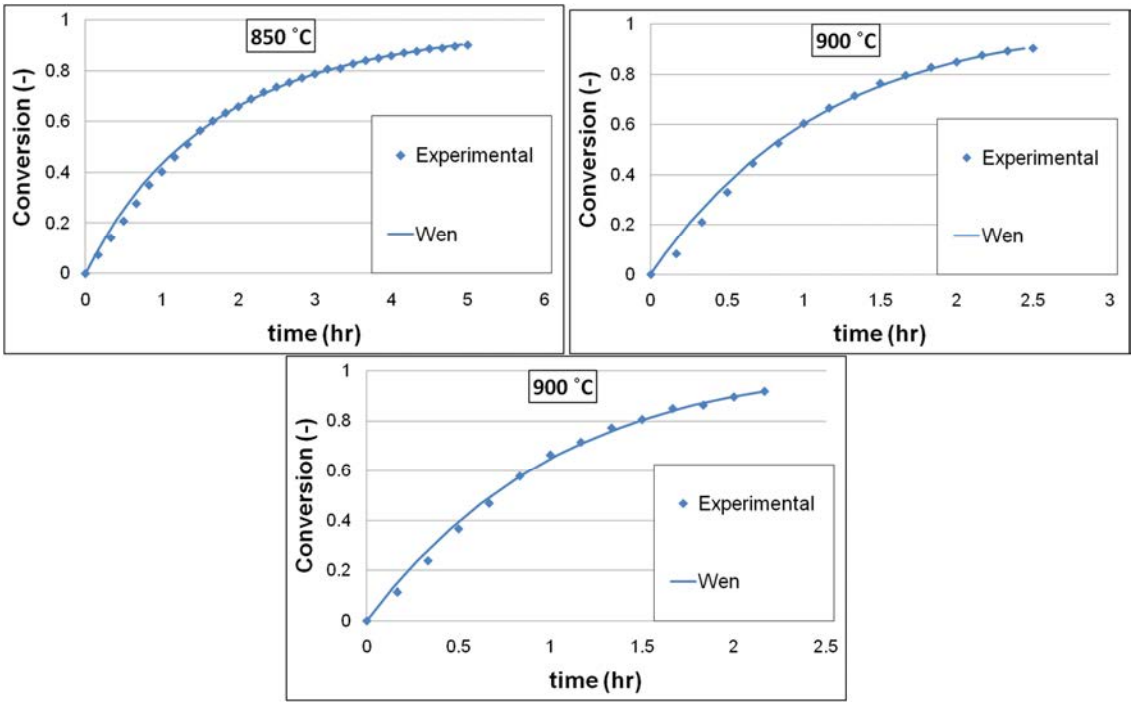

Figure B.13: Wen model prediction of experimental results for the 5 mm particles.

Wen model prediction of the 10 mm particles experimental results:

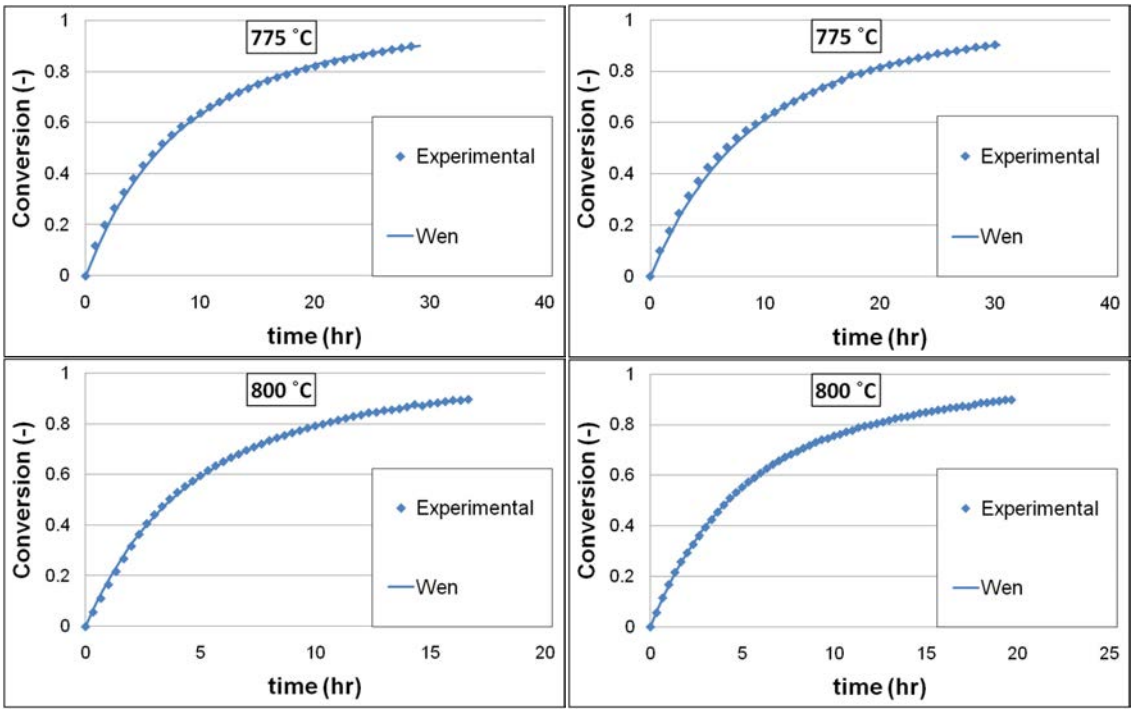

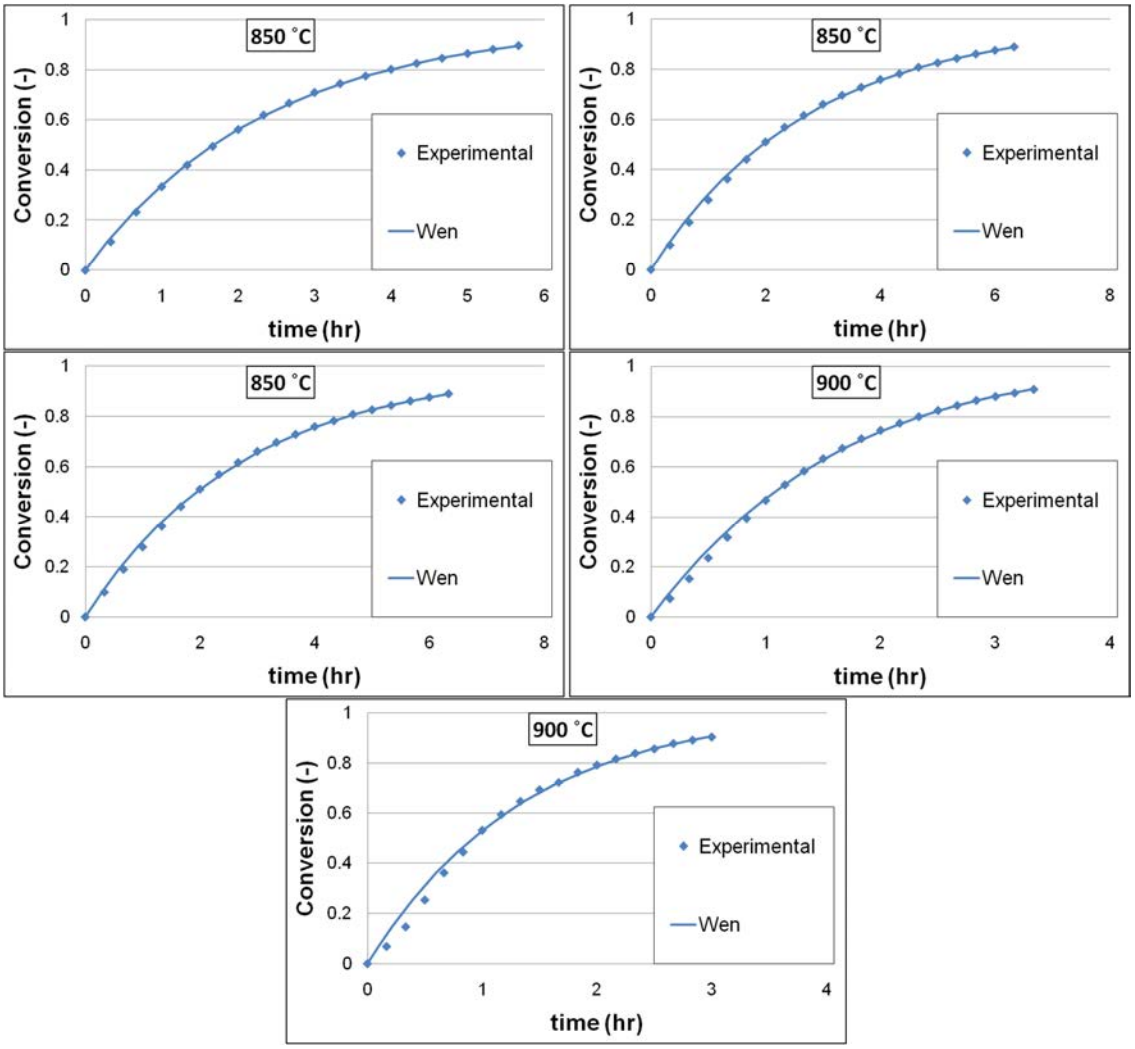

Figure B.14: Wen model prediction of experimental results for the 10 mm particles.

Wen model prediction of the 20 mm particles experimental results:

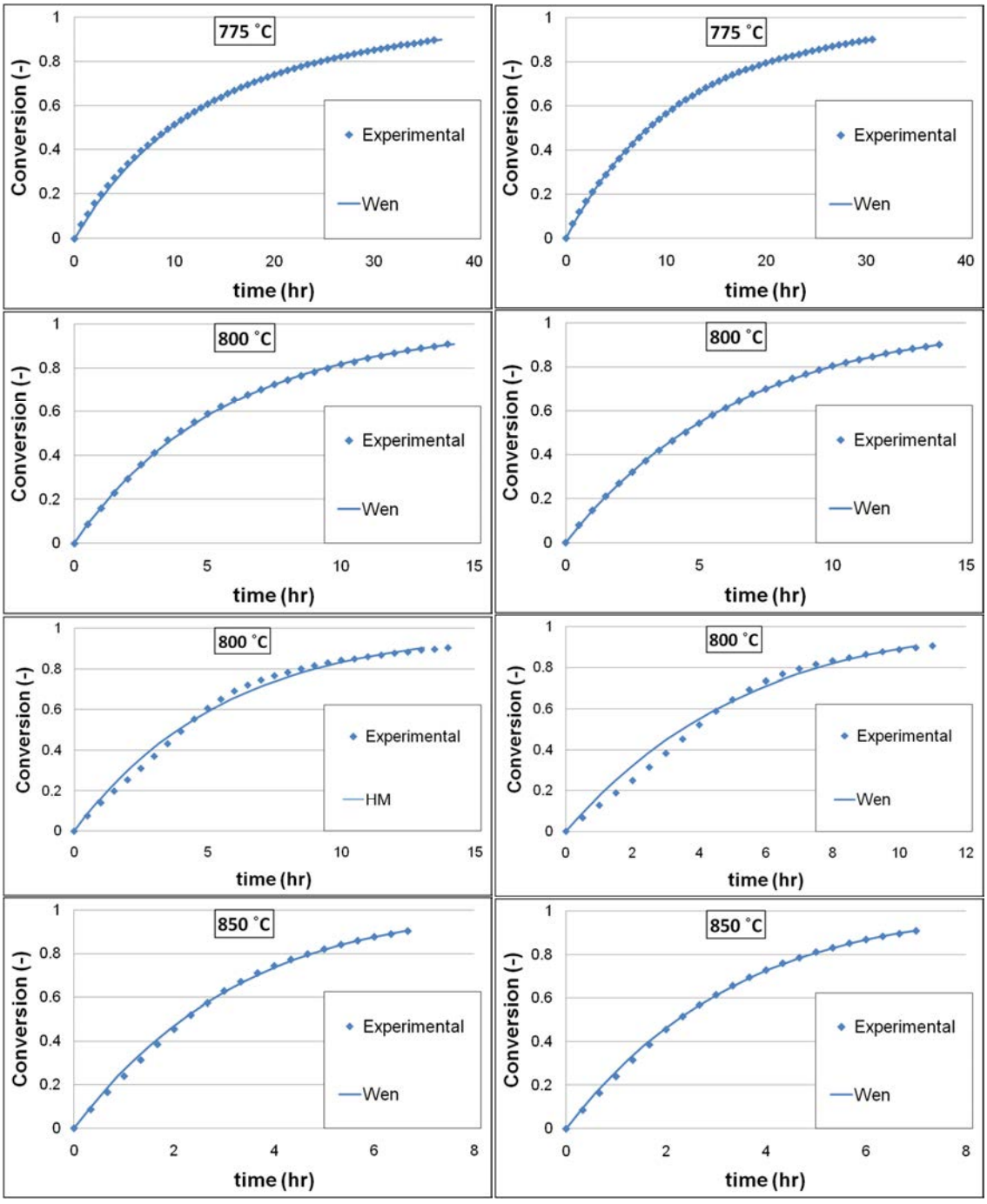

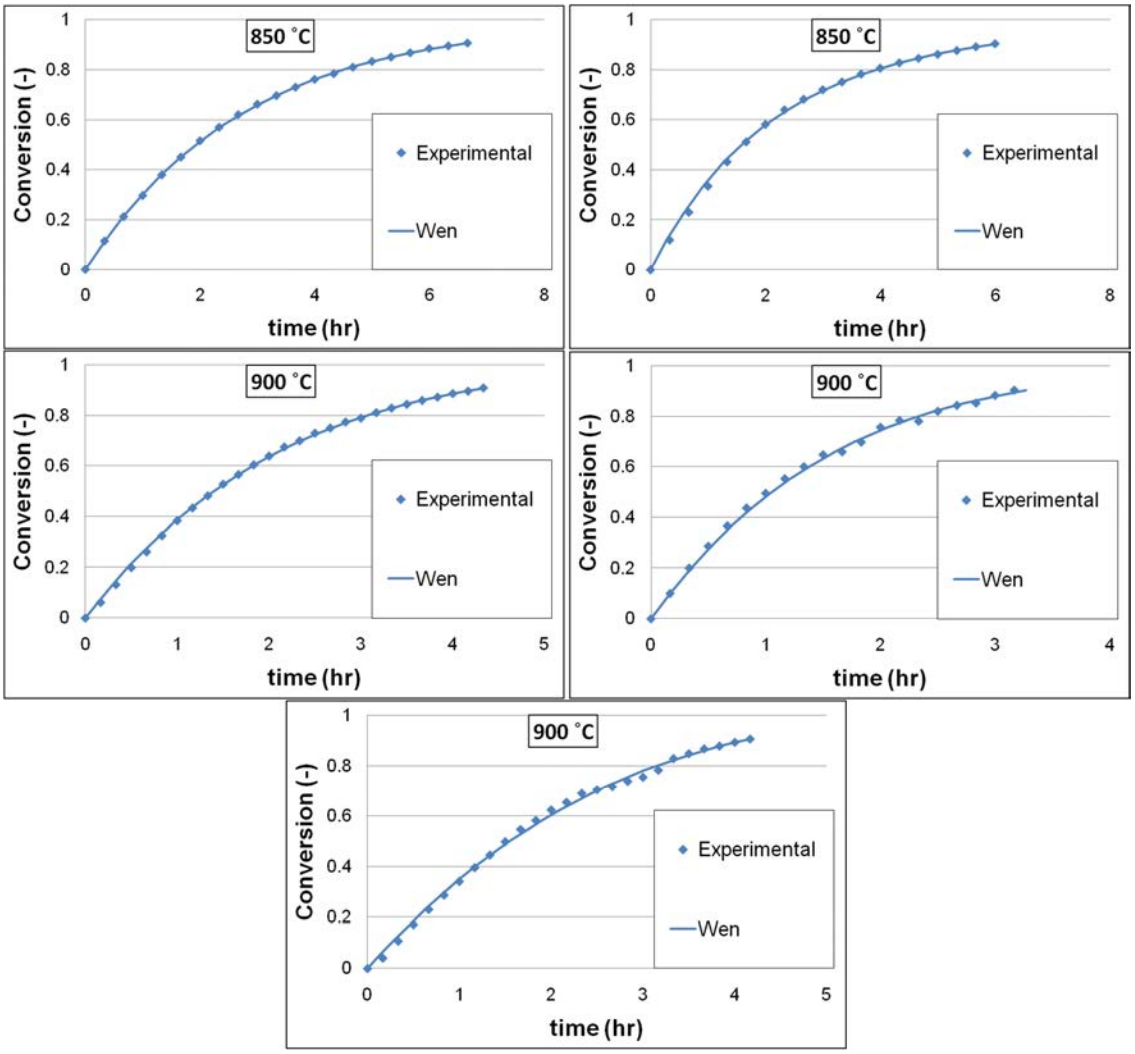

Figure B.15: Wen model prediction of experimental results for the 20 mm particles.

Wen model prediction of the 30 mm particles experimental results:

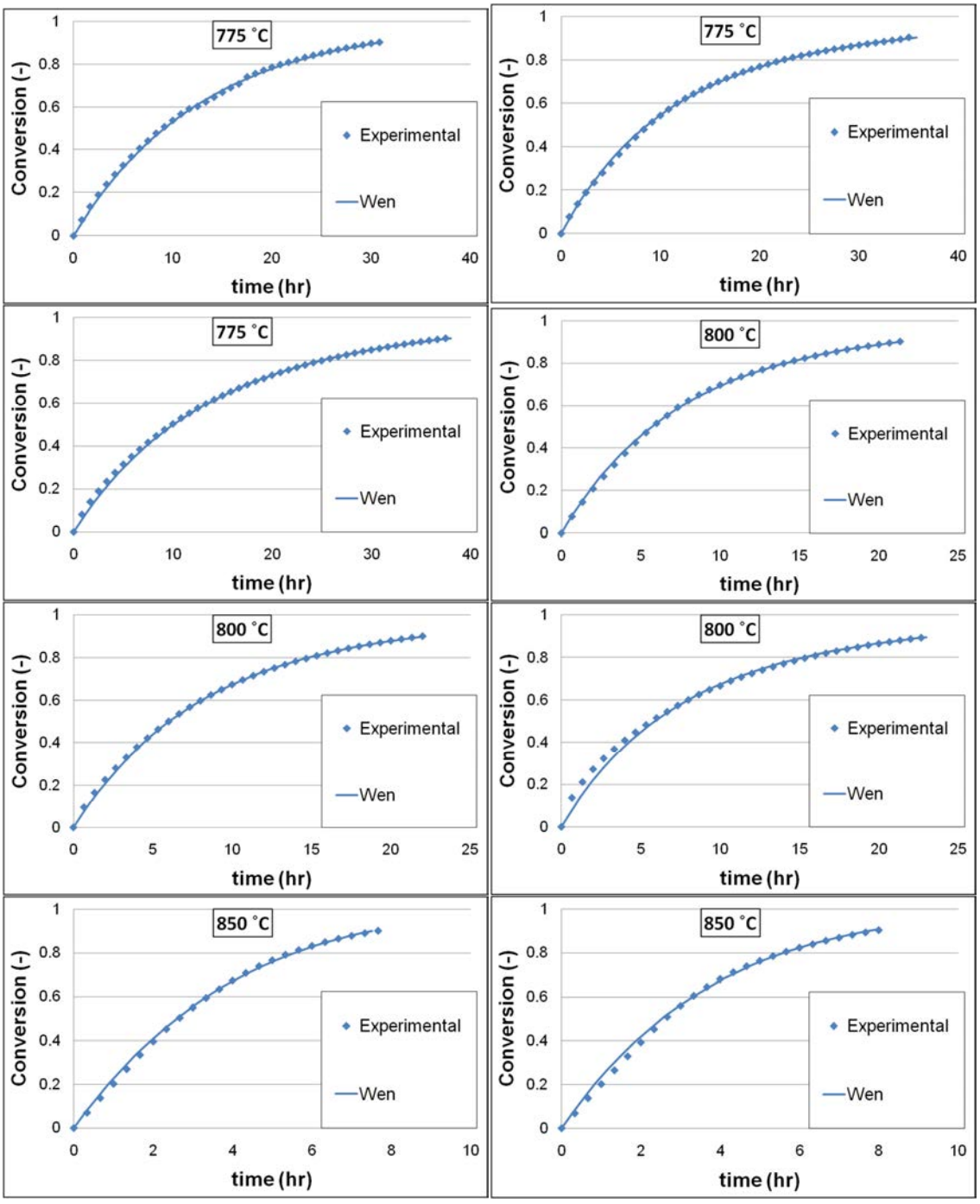

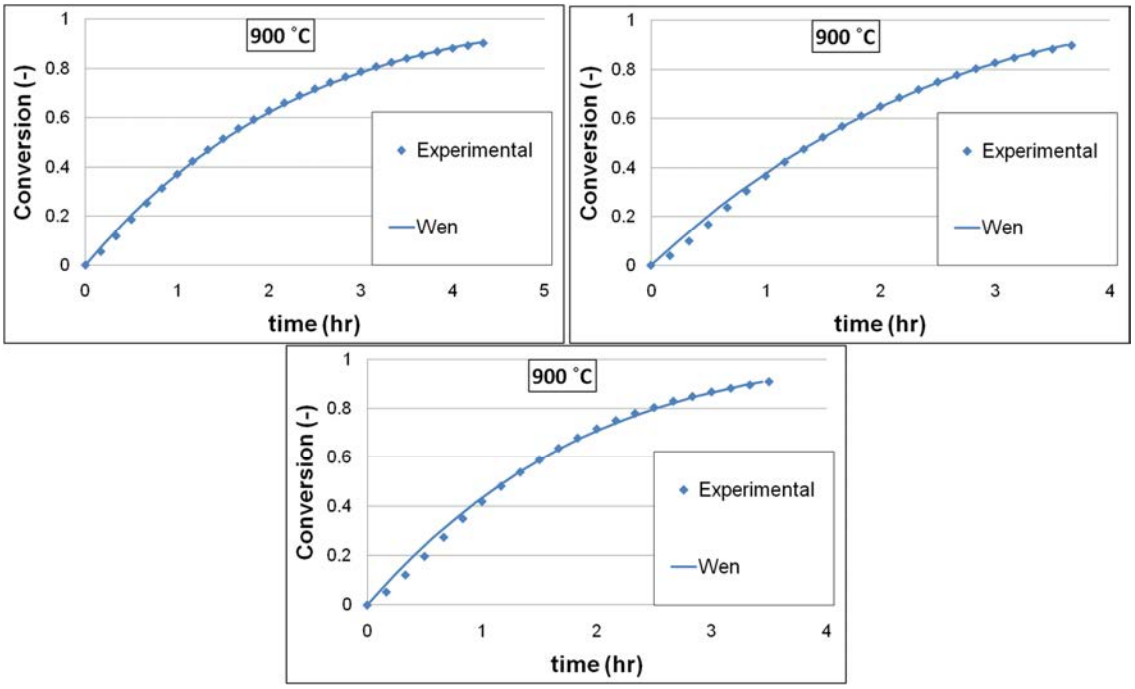

Figure B.16: Wen model prediction of experimental results for the 30 mm particles.